Identifying and interpreting geoarchaeological sites with high prospecting potential using aerial LIDAR, GIS and sedimentological analysis

by

Alexandra Lausanne
B.A, Western University, 2014

A Thesis Submitted in Partial Fulfillment
of the Requirements for the Degree of

MASTER OF SCIENCE

in the Department of Geography

Supervisory Committee

Identifying and interpreting geoarchaeological sites with high prospecting potential using aerial LIDAR imaging, GIS and sedimentological analysis

by

Alexandra Lausanne
B.A, Western University, 2014

Supervisory Committee

Dr. Ian Walker, (Department of Geography, University of Victoria)
Co-Supervisor

Mr. Daryl Fedje, (Department of Anthropology, University of Victoria)
Co-Supervisor

Dr. Olav Lian, (Department of Geography, University of Victoria)
Departmental Member

Abstract

Supervisory Committee
[Dr. Ian Walker, Department of Geography, University of Victoria]
Co-Supervisor

[Dr. Daryl Fedje, Department of Anthropology, University of Victoria]
Co-Supervisor

[Dr. Olav Lian, Department of Geography, University of Victoria]
Outside Member

The dynamic environmental history and relative sea level (RSL) changes experienced on the Pacific Northwest Coast of North America during the early post-glacial period and the early Holocene resulted in significant visibility challenges for prospection of early coastal archaeological sites. Archaeological visibility is the degree to which cultural material survives post-depositional processes and is detectable on the landscape today. It is influenced by environmental factors such as localized differences in relative sea level change, the rainforest canopy and dynamic post-glacial activity. This study offers an integrated methodological approach for locating palaeo-coastal sites by combining: i) geomorphic interpretation of landscape attributes captured by LIDAR (Light Detection and Ranging) mapping, ii) GIS-based archaeological site potential mapping, and iii) local RSL history. The RSL history for the study site (Quadra Island, British Columbia, Canada) shows notable regression over the past 14 500 years from a highstand of at least 195 m resulting from post-glacial isostatic rebound. Late Pleistocene and early Holocene palaeo-shorelines are found inland from, and elevated above, modern sea level and represent key areas for archaeological prospecting. Bare-earth Digital Terrain Models (DTMs) derived from the LIDAR dataset were interpreted to identify palaeo-shorelines at 10 m and 30 m above modern mean sea level. A GIS-derived map was created to identify regions of high archaeological potential using a decision tree method with variables including distance to palaeo-shoreline, low slope and a coastal complexity parameter. Select geoarchaeological sites were examined in terms of sedimentology, stratigraphy, microfossil content and geochronology as site-specific examples of sea level regression stillstands. Field validation results suggest that this integrated methodology provides a promising approach for archaeological prospection that could be applied to other post-glacial coastal settings.

Table of Contents

List of Tables

List of Figures

Acknowledgments

This research is part of the Discovery Islands Landscape Archaeology (DILA) project funded by the Hakai Research Institute. I would like to express appreciation to the Hakai Institute, part of the Tula Foundation, for their integral support for this project. Thank you to my supervisory committee Ian Walker (co-supervisor), Daryl Fedje (co-supervisor) and Olav Lian for support and guidance. Thanks to Quentin Mackie for his guidance and expertise on potential modeling and GIS. I would like to thank Christina Neudorf for processing of the optical dating samples, analyzing and interpreting the data, and for providing advice on the reliability and usefulness of the results. Thanks to Rob Vogt and Brian Menounos (UNBC) for the LIDAR data acquisition and processing, and also Derek Heathfield (Hakai) for LIDAR post-processing and Keith Holmes (Hakai) for GIS assistance. Thank you to Shahin Dashtgard and the Applied Research in Ichnology and Sedimentology lab for use of the laser granulometer. Thanks also to Morley Eldridge and Alyssa Parker (Millennia Research Limited) for predictive modeling input and to the DILA field crew. Thank you to Travis Gingerich and Jordan Bryce for field and lab support. I would also like to recognize SSHRC for the Canada Graduate Scholarship Master's Program funding, the NSERC Discovery grants for fieldwork and analytical support to Drs. Lian and Walker and the Canada Foundation for Innovation Leaders Opportunity Fund to Dr. Walker's Coastal Erosion & Dune Dynamics Programs, which provided logistical and analytical infrastructure support for this work. Thanks to family and friends for the continual support throughout this process.

1 Introduction and Research Objectives

On the Pacific Northwest (PNW) coast of North America, prospection for early post-glacial to early Holocene coastal archaeological sites is hindered by post-glacial landscape change and archaeological visibility. Archaeological visibility can be defined as the degree to which cultural material survives post-depositional processes and is detectable on the landscape today (Carson 2014; Fedje et al. 2011b; Schiffer 1987). In the Pacific Northwest, archaeological visibility is influenced by environmental factors such as localized differences in relative sea level change and dynamic post-glacial activity (Mackie et al. 2011). Changes in relative sea level (RSL) and subsequent landscape and ecosystem evolution often make modern landscape configurations very different from those of the past (Barrie and Conway 1998; Mackie et al. 2011). This is confounded by other local factors, including dense tree canopy and understory coverage, thick humic layers and sedimentation processes (Fedje et al. 2004; Lake and Woodman 2003), which make it difficult to visualize the (past and present) terrain and predict areas of high potential for prospection of archaeological materials. This study aims to provide a practical approach to improve archaeological prospection techniques for palaeo-shoreline sites by using: i) LIDAR (Light Detection and Ranging) derived Digital Terrain Models (DTM) and related geomorphic interpretation data, ii) GIS-based archaeological potential maps, iii) local RSL history and iv) sedimentology.

Using traditional survey methods, late Pleistocene to early Holocene (ca. pre-7000 year old) sites are often discovered through fortuitous means like surface exposures and tree throws and photogrammetry-based modeling (e.g., Fedje and Christensen 1999). For the purpose of this research, the late Pleistocene to early Holocene broadly refers to the regional start of the post-

glacial period (ca. 14 000 to 10 000 cal a BP)(Clague et al. 1982) to approximately 7 000 cal a BP (calendar annum before present). Some researchers assert that the limited number of known early Holocene coastal occupation sites in the PNW coast might be primarily due to methodological constraints and the obscured nature of these sites, rather than to an absence of archaeological evidence (e.g., Mackie et al. 2011). Quadra Island in southern British Columbia (B.C.B), Canada represents one such site and was selected for this study, given rich archaeological evidence in the region and baseline knowledge of RSL history (Fedje et al. in review).

The purpose of this research is to present an integrated methodological approach for identifying coastal archaeological sites based on LIDAR-derived bare-earth models, geomorphic interpretation, and baseline archaeological information. The objectives of this study are to: i) develop and demonstrate an integrated methodological approach to identify sites of high geoarchaeological potential useful for site prospecting coastal settings, ii) prospect for archaeological sites using a case study in an area that experienced appreciable RSL regression (Quadra Island, B.C., Canada), and iii) interpret the depositional context at select geoarchaeological sites in terms of late Pleistocene to early Holocene sea level change. The proposed methodology uses a high-resolution, LIDAR-derived bare earth DTM combined with landscape variables and elevations identified from a newly refined local RSL history (Fedje et al. 2018 in press) to create an archaeological potential map of sites of high potential using GIS. This study offers an integrated methodological approach that combines archaeological investigation with geomorphological landscape examination that could be adapted and applied in other coastal settings to improve archaeological site discovery. The archaeological potential map was tested through field survey. Several sites of high potential were found using this approach, with many

more such sites possible on Quadra Island through further investigation using this methodology as only limited areas were tested.

2 Study Sites

Quadra Island is part of the Discovery Islands group in the northern Strait of Georgia, or the northern portion of the Salish Sea, between Vancouver Island and mainland of British Columbia in western Canada (Figure 1). The mainland is characterized by deep fjords and islands. Quadra Island has many embayments and small associated islands including the Octopus Islands to the northeast. The surficial geology of Quadra Island composed of large areas of exposed bedrock and shallow colluvium, mixed marine and glaciomarine deposits, and some terrestrial deposits and landforms from glacial advances (e.g. Quadra Sand) and recessions (e.g. moraines) (Guthrie 2005) that result from the relatively recent glacial occupation of the area until ca. 16 000 cal a BP (Clague and James 2002; Shugar et al. 2014). Unpublished results from a broader study suggest that Quadra Island was deglaciated by at least 14 300 cal a BP (Daryl Fedje pers. comm. Nov. 24, 2017). The modern landscape of Quadra Island is diverse and includes active coastal landforms (embayed beaches, spits, and bluffs), deeply incised river valleys, mountain peaks up to 620 m above mean sea level (amsl), and many inland lakes, bogs and marshes.

Detailed sedimentological work was conducted on three study sites: Crescent channel Right of Way (CROW), Lactarius, and Kellerhals Gravel Pit (KGP). The locations of these sites are shown in Figure 2.

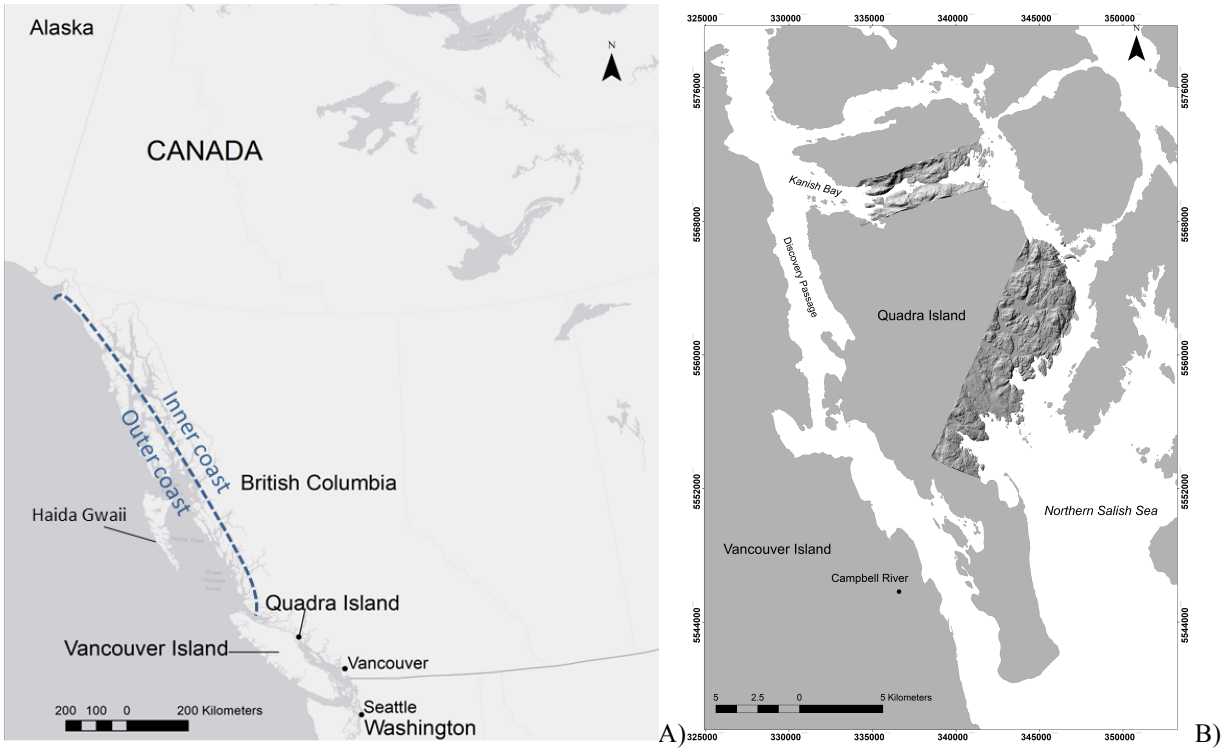

Figure 1: A) Map of the Pacific Northwest Coast of North America showing the location of Quadra Island, B.C., Canada and inner and outer coastal regions (as defined by Shugar et al. 2014) B) Map showing the locations of the LIDAR surveys collected for this research

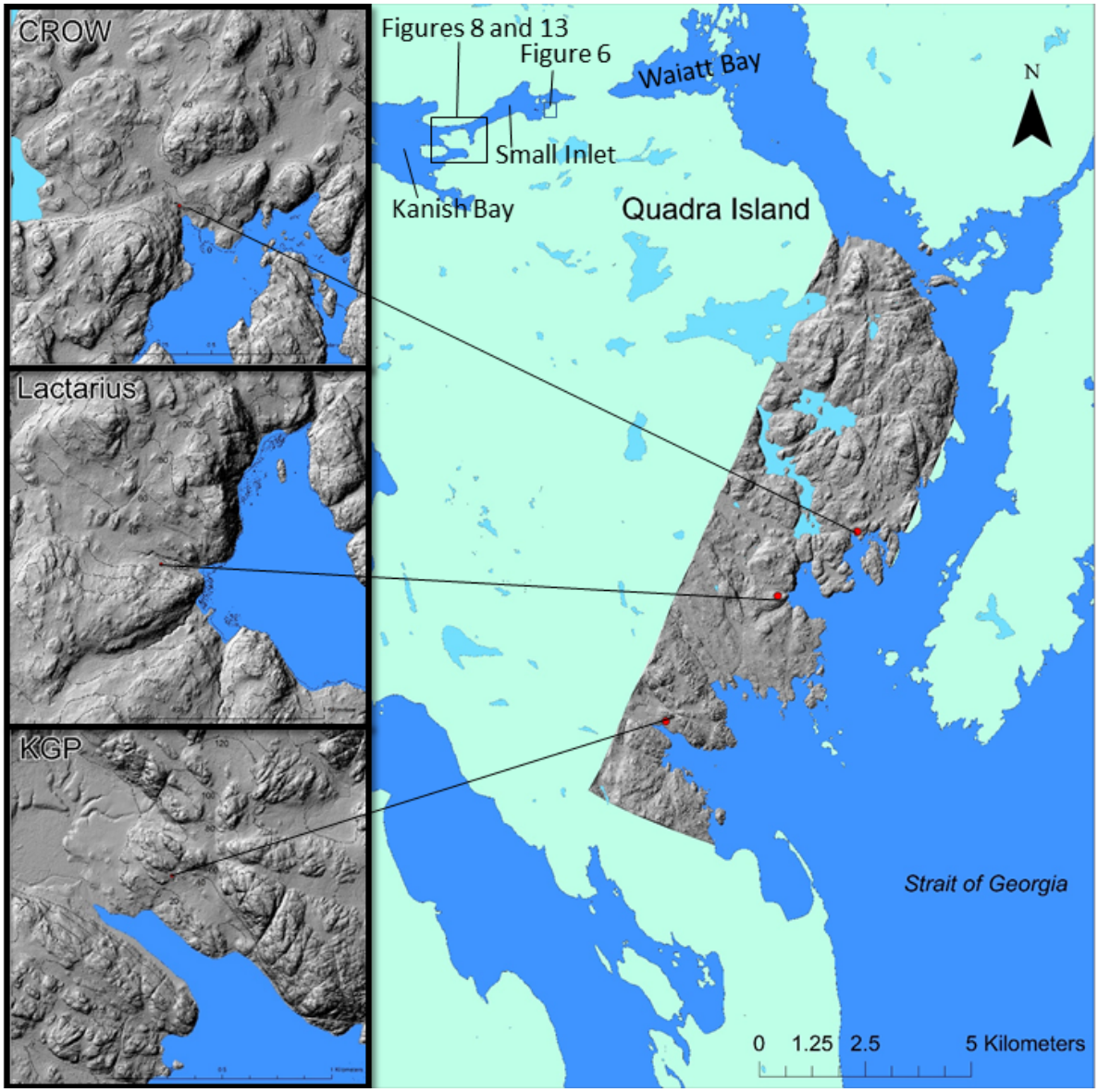

Figure 2: Location of CROW, Lactarius and KGP with DTM of south LIDAR survey area. Locations of Figures 6, 8 and 13.

2.1 CROW

The Crescent Road Right of Way (CROW) site (EbSh-81) sits on a terrace just northeast of a creek cut and 80 m inland from the present shoreline. Its elevation is 12 -14 m amsl. The site was first identified in 2013 through local knowledge. Two shovel tests to search for the presence of archaeological material (approximately 30 cm in diameter) were done in 2014 followed by

excavations including those conducted in 2014 and 2015 (i.e. EU3 or CROW3) (the focus of this research) and more recent excavations conducted in 2017.

2.2 Lactarius

The Lactarius site (EaSh-81) is located on a terrace south of a creek and approximately 180 m inland of the present shoreline. It is at 25 - 33 m amsl with the main excavation unit (EU1) at 26 m amsl. The site was first identified through shovel testing in August 2015 and the excavation unit was later opened in June 2016 and again in September 2016 for further analyses used in this study.

2.3 KGP

Kellerhals gravel pit is located 160 m inland of an embayment. The property owner has excavated a large portion of the area using a backhoe to create a gravel pit. The toe of the gravel pit is cut-off by a gravel road. There are small exposed bedrock cliffs to the north and east. The top of the gravel pit feature is flat to gently undulating topography and drops down steeply to the south. The top of the feature is at 33 m amsl while the bottom it around 26 m amsl.

3 Background

3.1 Local Sea Level History and Isostatic Rebound

On the Pacific Northwest coast of North America, local relative sea level (RSL) histories are the result of tectonic activity (vertical tectonic plate motions), global eustatic sea level changes and isostatic uplift or subsidence of the land in response to glacial activities (James et al. 2009; Shugar et al. 2014). Variations in these factors result in distinct RSL histories at a regional scale, which make localized studies of post-glacial landscape evolution imperative (Shugar et al. 2014).

The outer coast of B.C. (Figure 1) was on a glacial forebulge during the Last Glacial Maximum (LGM) (Shugar et al. 2014). As a result, sea level was as low as 150 m below modern sea level in areas such as Haida Gwaii, making the areas with highest archaeological potential presently underwater. However, regional isostatic and tectonic plate motions in some areas of the B.C. and Alaska coastlines have resulted in relatively stable RSL histories, leaving many potential archaeological sites likely still remaining on the PNW coast (Mackie et al. 2011, Mclaren et al. 2014, Shugar et al. 2014). Parts of the inner coast represent locations with high archaeological potential.

During the LGM, the inner PNW coast of British Columbia was isostatically depressed. On the south coast, the western fringe of the Juan de Fuca lobe of the Cordilleran Ice Sheet occupied Vancouver Island and the Salish Sea (Figure 1). This created late glacial shorelines (before 13 500 cal a BP) that are now stranded up to 200 m above modern sea level in some areas of south-coastal B.C. (Clague 1981; Clague and James 2002). Elsewhere along the B.C.coast, RSL histories on Vancouver Island and in the northern Salish Sea near Quadra Island are highly varied due to sub-regional differences in glacio-isostatic trends and tectonic plate

motions (Figure 3). Following deglaciation, isostatic uplift of the inner coast occurred rapidly, which caused RSL to drop into the early Holocene (Clague et al. 1982; Shugar et al. 2014). These trends are highlighted by regional research in the northern Salish Sea (Hutchinson et al. 2004; James et al. 2005; Fedje et al. in press). On Quadra Island, RSL fell from at least 195 m amsl at 14 500 cal a BP to about 5 m amsl by 12 000 cal a BP and then dropped more gradually to modern levels (Figure 4). This RSL curve corresponds well with one derived earlier by Shugar et al. (2014) using a dataset from within the broader North Strait of Georgia region (Figure 3). This RSL history indicates that inland and elevated locations on Quadra Island are potential locations for early to middle Holocene palaeo-shorelines and associated archaeological sites.

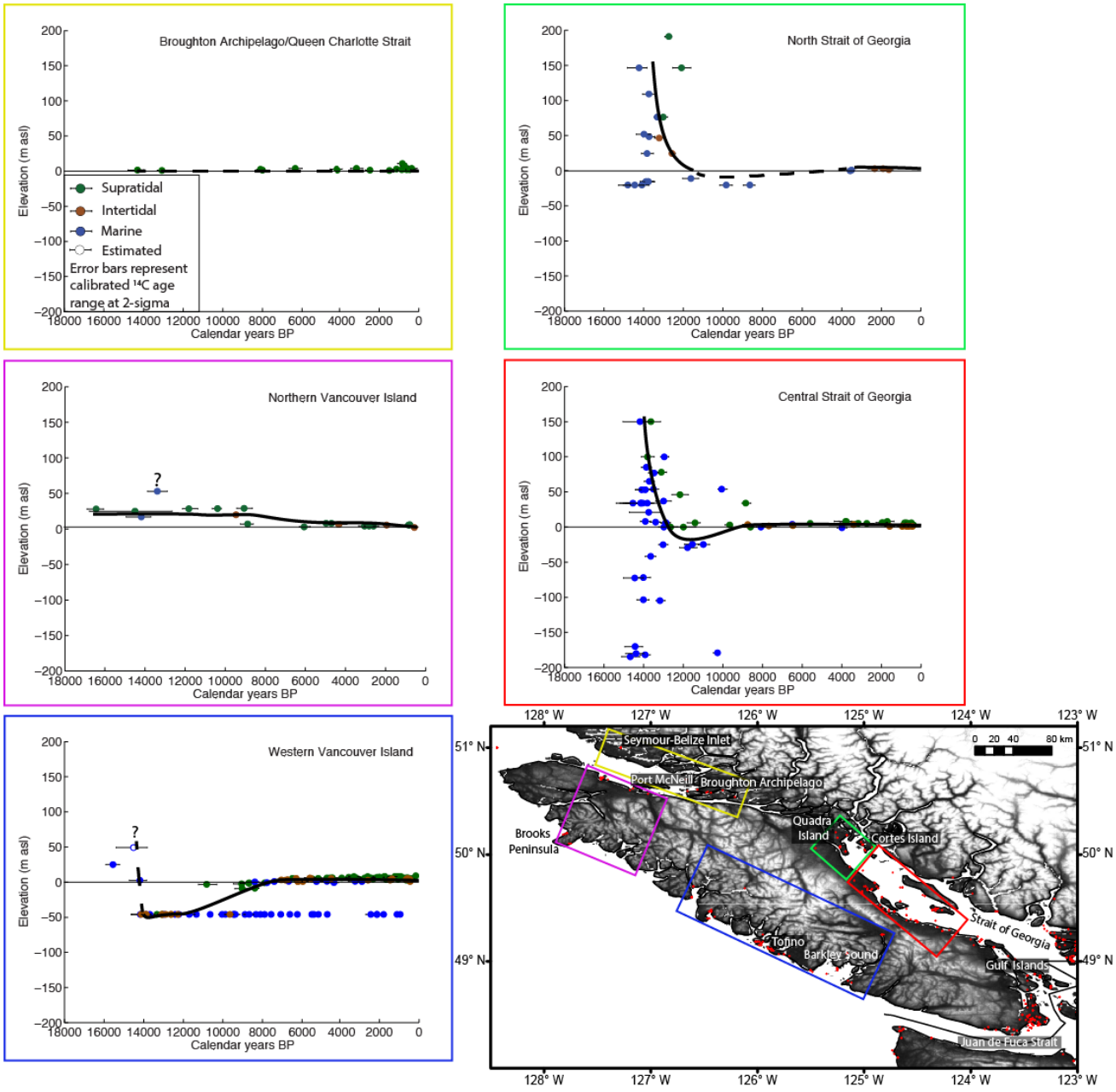

Figure 3: Relative sea level curves for various locations on Vancouver Island and the northern Salish Sea/Strait of Georgia. Reproduced from "Post-glacial sea-level change along the Pacific coast of North America," by Shugar, D., Walker, I., Lian, O., Eamer, J., Neudorf, C., McLaren, D., and D. Fedje, 2014 in *Quaternary Science Reviews*, 97, p. 197. Copyright 2014 by Elsevier Ltd.

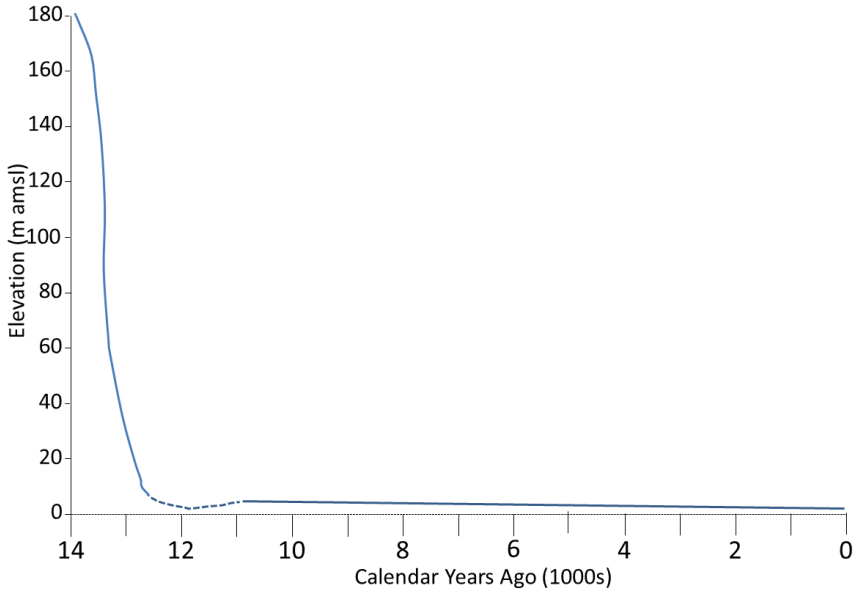

Figure 4: Relative sea level history for Quadra Island (palaeo-shoreline elevation in relation to modern sea level over the past 14 500 years) (adapted from Fedje et al. in press)

3.2 Archaeological Prospection: Using LIDAR to identify Palaeo-shorelines

Archaeological potential is the likelihood of an archaeological site to be found at a certain location and incorporates the likelihood of a location to have been used (e.g. camp, resource procurement site) by past peoples *in addition to* the degree that cultural material is detectable on the modern landscape (Carson 2014; Fedje et al. 2011b). Examples of features with high archaeological potential for early human occupation on the PNW coast include raised (or submerged) palaeo-shorelines, tombolos, berms, spits, terrestrial promontories (e.g., look-out points), and sheltered embayments (Mackie 2011).

Detailed geomorphic maps are necessary for efficient archaeological prospection. Many topographic maps lack sufficient elevational resolution for identifying subtle geomorphic or cultural features. LIDAR-derived bare earth digital elevation models (DEMs) and visually enhanced digital terrain models (DTMs) can be used, for example, to identify and interpret relic landforms that are otherwise concealed by dense forest cover in aerial photography (e.g., Challis

2012; Mackie et al. 2011). Palaeo-shorelines often manifest as raised, subtly sloping terraces that represent periods of RSL stability. This stability allowed for either greater accumulation of sediments or stabilization of landforms, as well as increased suitability for human occupation. In turn, cultural evidence is often deposited and preserved within sedimentary deposits in a more concentrated way, compared to deposits that have been reworked and redistributed by littoral processes during marine transgressions that have been spread thinly across the landscape during rapid shoreline regression (Fedje and Christensen 1999; McLaren et al. 2014). Archaeological prospection techniques that use a combination of LIDAR and/or aerial photographic interpretation of RSL change have been conducted on Haida Gwaii (Fedje et al. 2011a; Sanders 2009; Wolfe et al., 2008) and southern Alaska (Carlson and Baichtal 2015). As far as the author is aware, no such studies have been conducted along the southern British Columbia coast prior to this project.

3.3 Pacific Northwest Coast Archaeological Setting

The timing and routes of early First Peoples expansion into North America have been debated for decades (e.g., Erlandson and Deslauriers 2008; Fladmark 1979). Many researchers now believe that earliest human access to lands south of the late Wisconsinan Ice Sheets at the LGM may have been along the PNW coast as opposed to a migration via an ice-free corridor east of the Rocky Mountains (Erlandson and Deslauriers 2008; Fedje and Christensen 1999; Fedje et al. 2004). There is now strong support for a coastal human presence by at least the late Pleistocene, ca. 13 000 – 11 500 cal a BP (e.g., Davis 2011; Fedje et al., 2005a; Goebel et al. 2008; Josenhans et al. 1995; Mackie et al. 2013; McLaren et al. 2011; McLaren et al. 2018).

To date, a very limited number of late Pleistocene/early Holocene archaeological sites have been identified and recorded on the PNW coast (Mackie et al. 2011). Sites dating earlier than 10,000 years ago span from Alaska to Washington. These sites include On-Your-Knees cave in Southeast Alaska (with the earliest cultural layer dating to ca. 12 300 cal a BP)(Dixon et al. 1997), Gaadu Din Cave 1 and Gaadu Din Cave 2 (12 500 cal a BP) and K1 cave (12 600 cal a BP) in southern Haida Gwaii (Fedje et al. 2011b); Pruth Bay/EjTa-4 (ca. 13 300 cal a BP)(McLaren et al. 2018), Triquet Island (14 000 cal a BP)(Gauvreau and McLaren 2017), Bear Cove I (ca. 14 000 cal a BP)(McLaren 2008), Manis Mastodon (13 800 cal a BP)(Waters et al. 2011; Haynes 2011) and Ayer Pond (ca. 13 800 cal a BP)(Kenady et al. 2010) in the southern Salish Sea.

The cultural history sequence is relatively well established for the southern Salish Sea, however, comparatively less knowledge exists for areas further north along the inner coast of Vancouver Island, north of Campbell River through the Discovery Passage and the Johnstone Strait region (Engisch et al. 2004; Millennia Research Limited Research Ltd. 2007; Mitchell 1990). Unlike the southern and northern coasts of British Columbia, there had been no previous investigations of middle to early Holocene archaeological sites on Quadra Island prior to 2014 (Fedje et al. 2016).

3.4 Archaeological Predictive Modeling

Archaeological prospection using GIS-based predictive modeling was first developed in the 1970s by U.S. government agencies (Wheatley and Gillings 2002). Archaeological predictive modeling is becoming widely used, not only in academic research, but also in government mandated heritage management assessments, both in North America (e.g., Hudak et al. 2002; Kvamme 1995, 2006) and abroad (e.g., Allen et al. 1990; Canning 2005; Espa et al. 2006;

Kamermans et al. 2009; van Leusen and Kamermans 2005; Verhagen et al. 2007). Many archaeologists assert that predictive modeling is best used as a site discovery tool in the Cultural Resource Management (CRM) sector to identify and protect archaeological heritage, rather than as an explanatory tool for site location (Conolly and Lake 2006; Lake and Woodman 2003; Verhagen et al. 2009).

Predictive modeling uses a set of key physical/locational parameters commonly associated with archaeological sites, expressed as layers within a GIS system, to develop a model able to identify areas of high site potential. Physical environmental characteristics are most commonly used because relevant data are more easily obtained from GIS (Wheatley and Gillings 2002; Woodman and Woodward 2002). These layers can include landform derivatives and/or morphometric variables, such as: slope, aspect, local relief, elevation, proximity to fresh water, as well as nominal classifications of landscape features, such as terraces (e.g., Altschul 1990; Conolly and Lake 2006; Graves 2011; Kvamme 1985; Warren 1990;). A common end product combines landscape variables into an archaeological potential map that codes areas of the landscape on ordinal scales such as low, medium or high archaeological potential (e.g., Arcas Consulting Ltd 2002).

In B.C., recent provincial guidelines have incorporated archaeological predictive modeling into initial local government project planning stages for development through Archaeological Overview Assessments (B.C. Ministry of Forests 2009). Both high and low potential areas are targeted for survey, and planners are warned in advance of anticipated Archaeological Impact Assessment (AIA) mitigation costs at different locations. During archaeological surveys, sampling can be intensified in areas of high archaeological potential to maximize site location efforts (Verhagen and Whitley 2012).

Some potential modeling has previously been conducted for CRM purposes in the Quadra Island area (e.g., Arcas Consulting Ltd 2002; 2005; Millennia Research Limited 2007). Millennia Research Limited (2007) carried out an extensive modeling analysis for the northernmost part of the northern Salish Sea and southern Johnstone Strait, which included Quadra Island but no archaeological testing was done on the island. Through regional data compilation and analysis, they derived location variables for sites such as shell middens. These studies offer useful modeling variables and approaches, however, they were only applied to the modern coastline and do not incorporate highly localized RSL histories or specifically model for inland palaeo-coastal sites.

4 Methods and Data

4.1 LIDAR Data, DTM Development and Geomorphic Mapping

In August 2014, aerial LIDAR surveys were flown over Quadra Island from a fixed-wing aircraft equipped with a Riegl VQ-580 laser scanner. One survey swath was focused on the north of the island (14.35 km^2) and another was on the south east side (47.71 km^2) (Figure 1). The average LIDAR point cloud density from these surveys was 19 points/m^2 and the dataset was referenced to the NAD83 geodetic datum and UTM zone 10. To produce a bare-earth DEM, post-processing was done using the Merrick Advanced Remote Sensing (MARS®) 7 GeoCalc tool in order to re-classify ground points and remove the vegetation layer within the LIDAR dataset. Ellipsoidal heights of the vertical datum for remaining ground points were converted to CGVD28 using the HTv2.0 geoid. The data were then imported into the QT Modeler (version 8.0.6.0) software and gridded using adaptive triangulation to finally produce a DEM at 1 m^2 grid cell resolution (Fernandez et al. 2007). In contrast, most archaeological predictive models typically use a horizontal resolution of 5 m^2 or coarser (e.g. Duncan and Beckman 2000; Millennia Research Limited Research Ltd 2007). The vertical accuracy for the LIDAR-derived model is 16 cm on average, estimated through averaging of 15 static surveyed GNSS occupation points using a Differential Global Positioning System (DGPS).

Principal components analysis (PCA) was used to enhance the visualization of the topography with various hillshade angles applied to the DEM to create a DTM following the method of Devereux et al. (2008) and Challis et al. (2011). Sun illumination angles were trialed from 16 different directional azimuths in 22.5 degree increments, with the zenith angle held constant at 30 degrees above the horizon. Three dominant sun azimuth angles identified from the

PCA statistics captured the most topographic information through shading geomorphic features within the dataset and provided the most effective visualization of topographic features, such as palaeo-shorelines, river valleys and ravines. A more in-depth account of the procedure is described by Davis (2002) and Mather (2004). The DTM was than visually analyzed for potential palaeo-shoreline features such as beach ridges or terraces.

Potential palaeo-shorelines were identified from the DTM using a moving window of 500 x 500 m and then 1000 x 1000 m across the terrain in Quick Terrain (QT) Modeler (see section 4.3.1.1). In addition, a series of shoreline cross sections were drawn (at intervals less than 50 m apart) across the entire survey area to help visualize the elevation and character of these features in relation to the surrounding topography. Beach ridges (explained below) were often used to identify shoreline positions and were manually identified in the shoreline cross sections, typically by shore-parallel, continuous breaks in slope in sediment rich areas that reoccur at a constant elevation across the landscape (i.e., shore-parallel lines) (Kelsey 2015) (See Figure 6). Contour lines were then generated at two elevations (10 and 30 m amsl), which were the most obvious and reoccurring ridges. The lowest elevation break in slope of a series of potential beach ridges was considered the start of a potential regressional sequence of palaeo-shorelines. Each ridge has an indicative meaning associated with an individual RSL position, so a series of ridges indicates change in RSL over some time period (see section 4.3.1.1 for further information).

4.2 Geomorphic Interpretation

Various geomorphic features were identified through visual inspection of the DTM, including beach ridges, alluvial fans, deltas, valleys and ravines. These features were identified through visual analysis of the PCA-derived DTM by looking at 3D form, from various hillshade

shading angles and by using QT Modeller to flood the DTM to the elevation of each feature. Each of these features can be interpreted in terms of indicative meaning for past RSL and possible changes in RSL.

Beach ridges can develop through various processes and commonly develop on progradational or regressive shorelines (Davidson-Arnott 2010; Tamura 2012). Otvos (2000) defines beach ridges as semi-parallel intertidal and supratidal landforms formed though wave processes. Beach ridges and shoreline platforms have a similar indicative meaning (i.e., position relative to mean sea level and considering tidal variations)(Shennan 1982; 1986), but the former is dominated by depositional processes and the latter is influenced and defined by wave action (Kelsey 2015). Shore platforms are shore-parallel features that extend landward from a former shoreline position to form marine terraces (Kelsey 2015). They are commonly composed of basal bedrock or resistant sedimentary deposits that may be overlain by contemporaneous (if relic) or modern littoral sediments. Beach ridges are generally supratidal or indicative of positions between the average high tide (Otvos 2000) and the spring tide elevation (Kelsey 2015). Beach ridges can be composed of gravel to fine grained sand, depending on source materials. A series of beach ridges and their subsurface deposits can be examined to interpret changes in shoreline positions and RSL with shoreline regression or progradation.

Alluvial fans, or low angle depositional cones (Owen & Matthews 2014), are also common in the study region and are derived mostly from fluvial deposition of alluvium at the foot of steep terrain or outlet of a narrow valley. Interpretation of these features in a coastal context can provide evidence of environmental change. In some cases, alluvial fans may drape over beach ridges and platforms and conceal them.

Deltas are river-fed clinoforms that can prograde or retreat during sea level fluctuations (Porebski and Steel 2006). Whether a river forms a delta at the river-ocean interface depends on sea level and the energy of ocean waves and currents (Pratson et al. 2007). If sea level rise outpaces the sediment supply rate, then delta maintenance and/or formation is not possible (Pratson et al. 2007). Other important factors controlling delta progradation include: depositional slope within the receiving shoreline, land subsidence or emergence rate, receiving basin size and shape, and tidal dynamics (Bianchi 2016).There are usually two phases of delta formation: the construction phase and the abandonment phase (Bianchi 2016). Traditionally, deltas are characterized in terms of being wave, tide, or river dominated. Gilbert-type deltas are characterized by steep subaqueous slopes and have a three-part geometry (i.e., topset, foreset and bottomset beds)(Colella and Proir 1990). If an alluvial fan gets drowned by RSL transgression, it becomes a fan delta. Conversely, a fan delta can be stranded by RSL regression and become an alluvial fan. A fan delta is comprised of alluvial fan sediments that are at the interface of an active fan and a standing body of water (Nemec and Steel 1988).

4.3 Development of the Archaeological Potential Map

Archaeological potential modeling is a form of additive GIS-based mapping of spatial variables that are overlain to reveal areas of varying, cumulative degrees of archaeological potential (e.g., low, medium and high) across the landscape (Arcas Consulting Ltd. 2002). The goal with this approach is to focus efforts on limited, higher potential survey areas so as to optimize time spent and costs incurred during field surveys. Efforts were focused toward a final map that identifies areas of *highest* archaeological potential for palaeo-shoreline occupation sites based on a set of variables, such as distance to palaeo-shoreline, low degree of slope, and a

coastal complexity parameter. All other locations were not included in the high potential category (i.e., not given a potential rating) of the model. The rationale for the above variables is explained below in section 4.4.

A deductive modeling approach is useful where limited archaeological studies have been conducted (Dalla Bona 2000; Kamermans 2000; Verhagen and Whitley 2012). Deductive models are theory-driven and chose variables based on the literature for the study region, instead of using a set of input training site data to select variables and create a model. Compared to inductive/data-driven approaches, deductive/theory-driven approaches also have the flexibility of being applied to other settings (Moon 1993). According to Millennia Research Ltd (2007), a very high proportion of the provincial archaeological site data (i.e., within the Remote Access to Archaeological Data – RAAD system) are either inaccurately geographically positioned, in some cases by up to 1 km, and/or are incorrectly sized. In the Quadra Island area, these RAAD recorded sites are predominantly clam garden and shell midden sites located along the modern shoreline and, therefore, are not representative of inland palaeo-coastal site types. Inductive modeling requires training data that are representative of the target site type (e.g. a set of palaeo-coastal sites). RAAD data were not used to build or test the model as there were insufficient site data to fit the statistical assumptions (i.e., lack of representative training data) used to build an inductive model. Given the objectives of this study, and the limitations of the data, a deductive approach was implemented.

A weighted value method is commonly used for CRM purposes and was originally trialed then refined with the decision tree approach for the Quadra Island data. The weighted value method multiplies landscape variables (e.g., degrees of slope, metres from palaeo-shoreline and a coastal complexity value by a proportional weight (0-1), depending on importance to locating

archaeological sites (Dalla Bona 2000; Millennia Research Limited 2007). Lack of sufficient local archaeological site data of inland palaeo-coastal sites (e.g., less than 30) to make statistical correlations of the importance of each variable on archaeological site location, means the model requires a level of subjective decision making. Therefore, to reduce subjective assumptions, a decision tree approach was used to create the final potential map.

The decision tree (Figure 5) incorporates both categorical and numeric data (Espa et al. 2006) in a logic structure. Each level denotes a binary (yes or no) test on a landscape variable at a 1 m^2 raster cell level. The cells that "pass" all of the tests make up the resulting high potential map, which was executed using the Raster Calculator in ArcGIS 10.2. For example, if the location is < 5 m away from a potential palaeo-shoreline (e.g., at 10 or 30 m amsl), then the cell is positive for the proximity to palaeo-shoreline parameter and continues down the tree. If a location proves positive for all three tiers of questions, it is included in the model as having high archaeological potential. If a location fails any one of the tests, it is excluded from the model and not given an archaeological potential value. Each variable will be expanded upon below in terms of rationale for selection and the selection for the 10 m and 30 m amsl parameters will be explained.

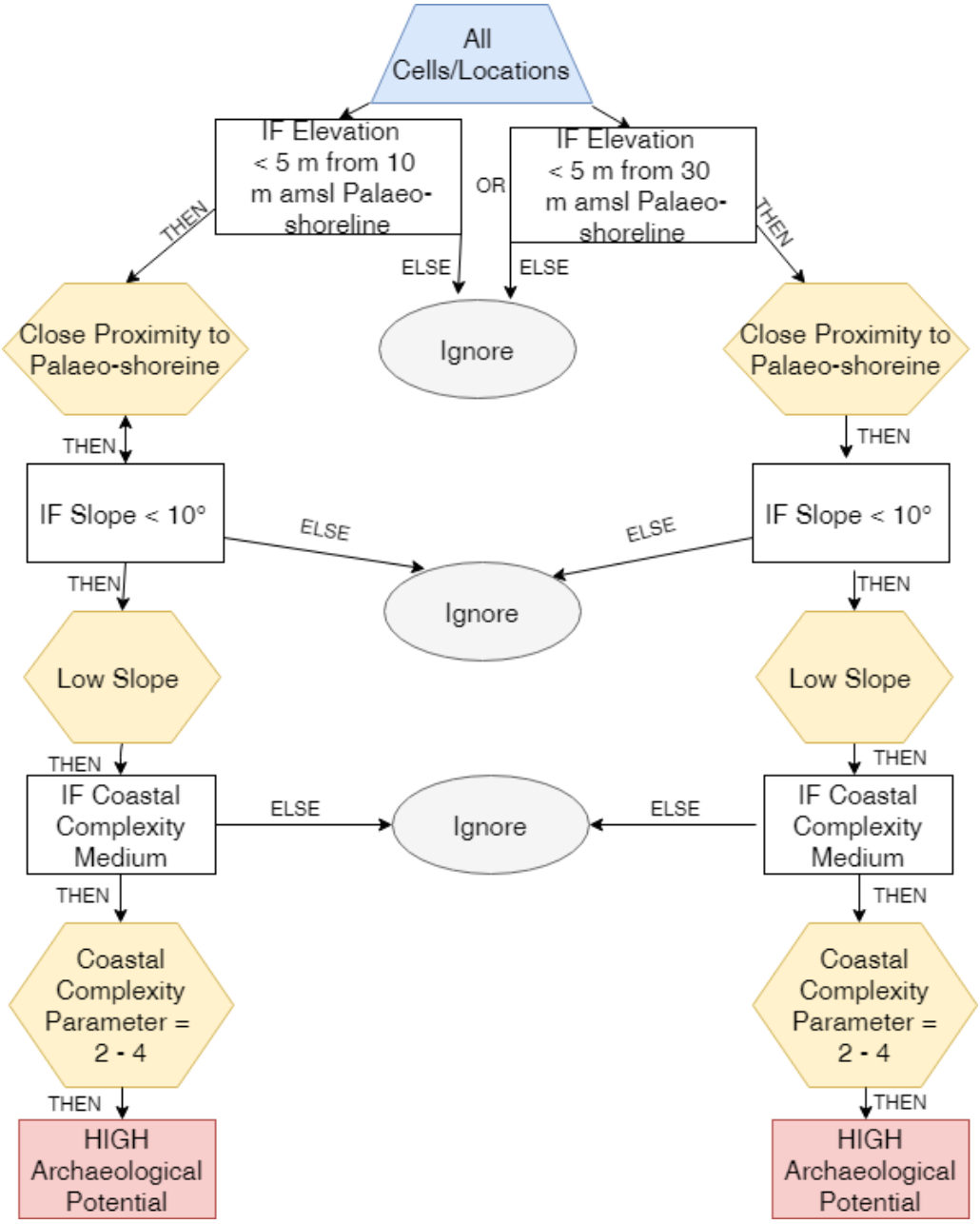

Figure 5: Potential map decision tree with landscape variables (yellow). Raster cells are filtered down through binary tests if/then statements so only areas that represent high archaeological potential remain (red); these are used to create the potential map. Values of 2-4 were considered medium coastal complexity. High archaeological potential indicates high potential locations of finding late Pleistocene/early Holocene palaeo-coastal archaeological sites.

4.3.1 Variable Selection

Landscape variables are the primary basis for the decision tree process that identifies locations ideal for past human activities and, thus, archaeological potential (i.e. proxies for

human decision-making and use patterns) (Dalla Bona 2000). Common variables for archaeological modeling include: slope, elevation, aspect and distance to freshwater (Altschul 1990; Conolly and Lake 2006; Graves 2011; Kvamme 1985; Warren 1990). Various combinations of variables were trialed. The final variables for the potential map were chosen based on concepts of site location from the regional archaeological prospection literature (e.g. Grier et al. 2009; Millennia Research Limited 2007) and in consultation with a panel of academic and professional archaeologists and coastal geomorphologists with local expertise.

Each landscape variable holds a degree of uncertainty because they are defined largely by attributes of the modern landscape that are used to interpret the palaeo-landscape at past sea levels. Uncertainties are compounded when variables are combined in a potential map. Based on trials of different variable combinations (e.g., distance to freshwater, presence of embayment) and, to keep uncertainties to a minimum, only three variables were included in the potential map: i) elevation relative to palaeo-shorelines, ii) slope, and iii) coastal complexity.

4.3.1.1 Elevation Relative to Identified Palaeo-shorelines

Identifying palaeo-shorelines is important for discovering new archaeological sites on the PNW coast (e.g., Carlson and Baichtal 2015; Fedje and Christensen 1999; McLaren et al. 2011; Mackie et al. 2011) and abroad (e.g., Breivik 2014; Carson 2014). Previous studies of the locational patterns of habitation sites (most often represented by shell middens) show that these are commonly located in close proximity to palaeo-shorelines (Carlson and Baichtal 2015; Stein 2008). Because of this relationship, many studies credit elevation relative to modern sea level to be the most important parameter for archaeological prospecting of raised terrace regions (Carlson and Baichtal 2015; Schmaltz et al. 2014). It should be noted, however, that there is evidence

supporting significant differences in coastal archaeological site distribution in PNW coast locations between early and late Holocene time (Mackie and Sumpter 2005). Thus, the possibility of non-analogous use of the coastline should be considered during the process of establishing high potential site prediction. The government of British Columbia has developed a protocol for archaeological potential modeling under their Archaeological Overview Assessment (AOA) guidelines, which states that accurate existing site location and DEMs are the most important components to modeling (B.C. Ministry of Forests 2009). By integrating high-resolution (vertical) bare-earth DEMs with the local sea level history, archaeologists can associate specific elevations as potential palaeo-shorelines for a specific age range.

Depositional landforms can often be identified initially by their external 3D morphology (Gilbertson 1995). To this end, the DTM was visually examined to identify locations with possible sedimentary palaeo-shorelines, with features such as beach ridges or terraces as priority targets. Beach ridges were identified by breaks in slope or low mounds in sediment rich areas that reoccur at a constant elevation across the landscape (i.e., shore-parallel lines)(Kelsey 2015). Obvious breaks in slope beneath a series of potential beach ridges (as defined by Otvos 2000) were considered evidence of the minimum elevation for a potential unit of palaeo-shorelines. Beach ridges, including storm berms, are indicative of the upper swash zone of either spring high tides or less frequent storms (Kelsey 2015). Concurrent work on RSL history in the region (Fedje et al. 2018 in review, Figure 9) indicates phases of sea level regression and associated possible stillstand elevations at 5 – 7 m, 10 – 14 m, and 28 – 32 m amsl. For instance, at about 12 000 cal a BP, RSL had fallen to approximately 5 m amsl. The shorelines along the most recurrent elevations were then converted into a contour line at the select elevation and incorporated as a variable into the potential model.

Potential palaeo-shorelines were identified from the DTM in ArcGIS using moving windows of 500 x 500 m and 1000 x 1000 m to obtain different scales of perspective. The DTM was then flooded virtually in QT Modeler and viewed from various 3D perspectives to more closely examine the terrain and to identify breaks in slope in sedimentary deposits (versus bedrock), to the nearest metre of elevation. A series of shoreline cross-sections were extracted from the DEM and the elevations of ridges were recorded (e.g. Figure 6). The shoreline migrates between the foreshore (intertidal) limit and backshore limit with tides and storms.

From this GIS-based analysis, as well as from knowledge of the landscape acquired during a reconnaissance field season, other elevations (10 and 30 m amsl) with low slope surfaces also stood out as likely candidates for relatively stable early post-glacial palaeo-shorelines (Fedje et al. 2016). These elevations stood out as the most obvious breaks in slope. Although there were many other subtle potential palaeo-shorelines at other elevations, for the model to be useful, and not classify the entire landscape, only these two elevations were selected as inputs for the model. These contours were given a minimal uncertainty (or buffer) of +5 m horizontal distance (inland) from each contour, following work in other areas. Other studies on the early Holocene site prospection on the PNW coast suggested that early peoples would usually camp within 1-5 m in elevation from a shoreline (Carlson and Baichtal 2015). A maximum uncertainty value of +5 m encompasses the tidal zone and the immediately adjacent supratidal zone or backshore.

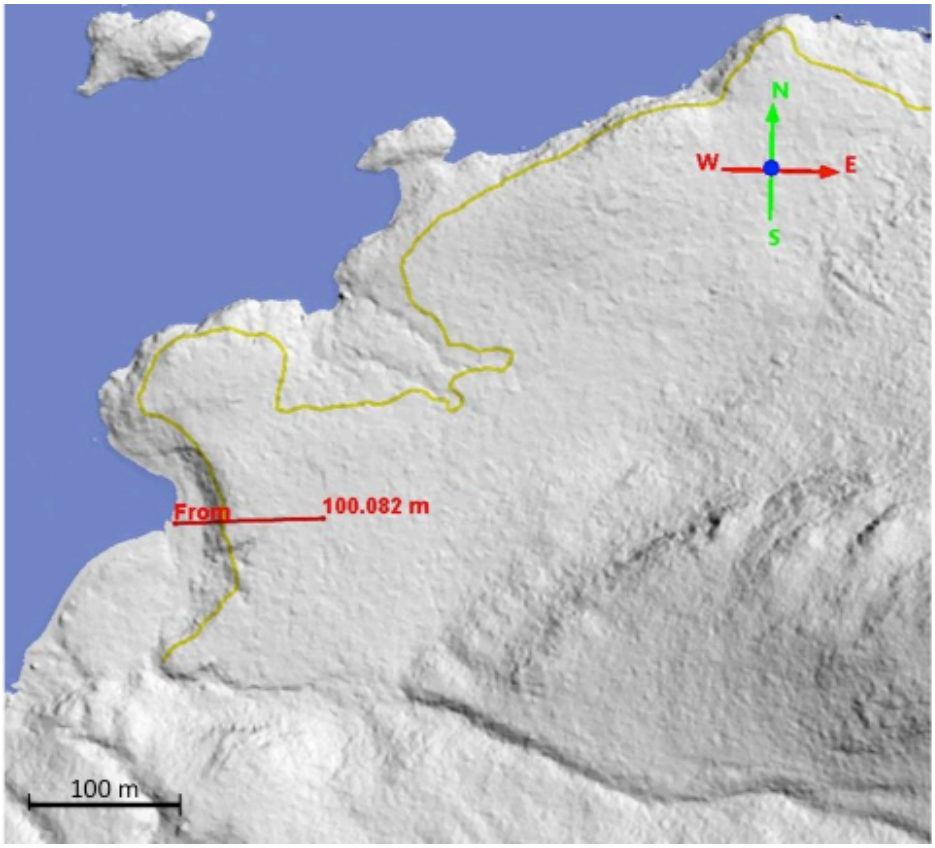

A)

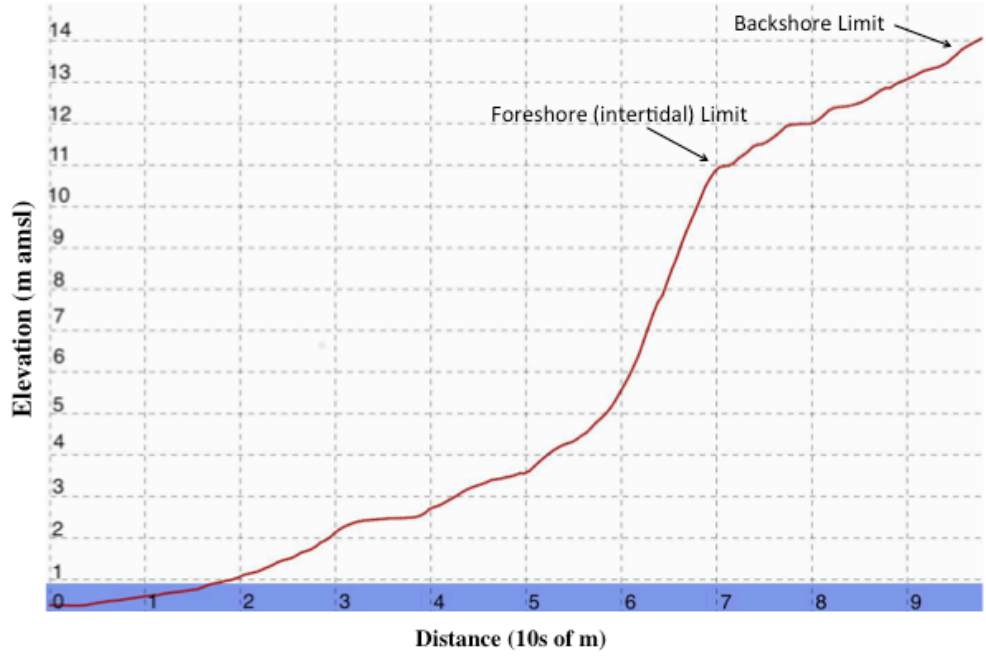

B) Figure 6: A) DTM showing the 10 m amsl terrace contour (yellow) and location of the shoreline cross-section shown in B) (red line). B) Example of shoreline cross-section from red line in A. Blue is the modern ocean level at 1 m amsl. This area is in the north LIDAR swath just to the west of the Small Inlet and Waiatt Bay land divide (Figure 2)

4.3.1.2 Slope

In many archaeological prospection studies, slope is a key variable, in that flat areas are thought to be a more desirable living surface than sloped surfaces and thus are more likely to attract settlement and the accumulation of archaeological material (Conolly and Lake 2006; Maschner and Stein 1995; Punke 2002; Verhagen and Whitley 2012). Low slope angle is shown to be a significant variable in archaeological locations in other areas of the PNW coast (e.g., Maschner and Stein 1995). Slope was calculated based on the maximum change in elevation between a cell and its neighbours within a 3 x 3 m moving window. A slope of less than 5° is commonly considered ideal (Maschner and Stein 1995; Wescott and Kuiper 2000). Due to the fine resolution of the DEM data (1 m^2), a filter that only included cells in the model with less than 5° slope produced a very fragmented and pixelated slope coverage. Therefore, 10° was set as the maximum slope for the high archaeological potential class (Figure 8). This captured more continuous areas and a greater proportion of low-sloping regions of landscape. In the final model, the total percent area captured by this variable is constrained by the limited area captured by the other variables (i.e., 5 m horizontal distance within each palaeo-shoreline).

4.3.1.3 Coastal Complexity Parameter

The coastal complexity parameter is a relative measure of the planview shape or curvature of the shoreline. Palaeo-shorelines with a higher degree of coastal complexity are considered more desirable living locations for past peoples than linear palaeo-shorelines. Complex coastlines typically offer: 1) limited fetch and protection from adverse weather; 2) higher biodiversity for resource procurement; 3) more shoreline area per unit width of open ocean available for use; 4) improved ability to land a boat (Arcas Consulting Archeologists Ltd. 2002,

2005; Mackie 2001; Mackie and Sumpter 2005; Maschner and Stein 1995; Millennia Research Limited 2007; Monteleone et al. 2012).

The coastal complexity parameter was generated based on methods by Millennia Research Limited Research Ltd (2007) in their study in the Strait of Georgia region, wherein they found this parameter to be effective in predictive modeling of island-dominated regions. The method consists of the following steps. First, the palaeo-shorelines at 10 m and 30 m amsl contours were converted to points spaced at 50 m apart (Figure **7**). Then buffers of 250 m radius were created around each point and a point count within each buffer was assigned to the centroid shoreline point. Points were then buffered by 25 m to create a continuous layer of complexity values and, then, clipped to a 5 m inland buffer to match the bounds of the palaeo-shoreline variable. These values were normalized following a method similar to that of Monteleone et al. (2012). All values were normalized to the value of a completely linear shoreline. To scale the results, buffer point count values were divided by 10 such that a completely linear shoreline within the 500 m diameter buffer would therefore equal 10 points.

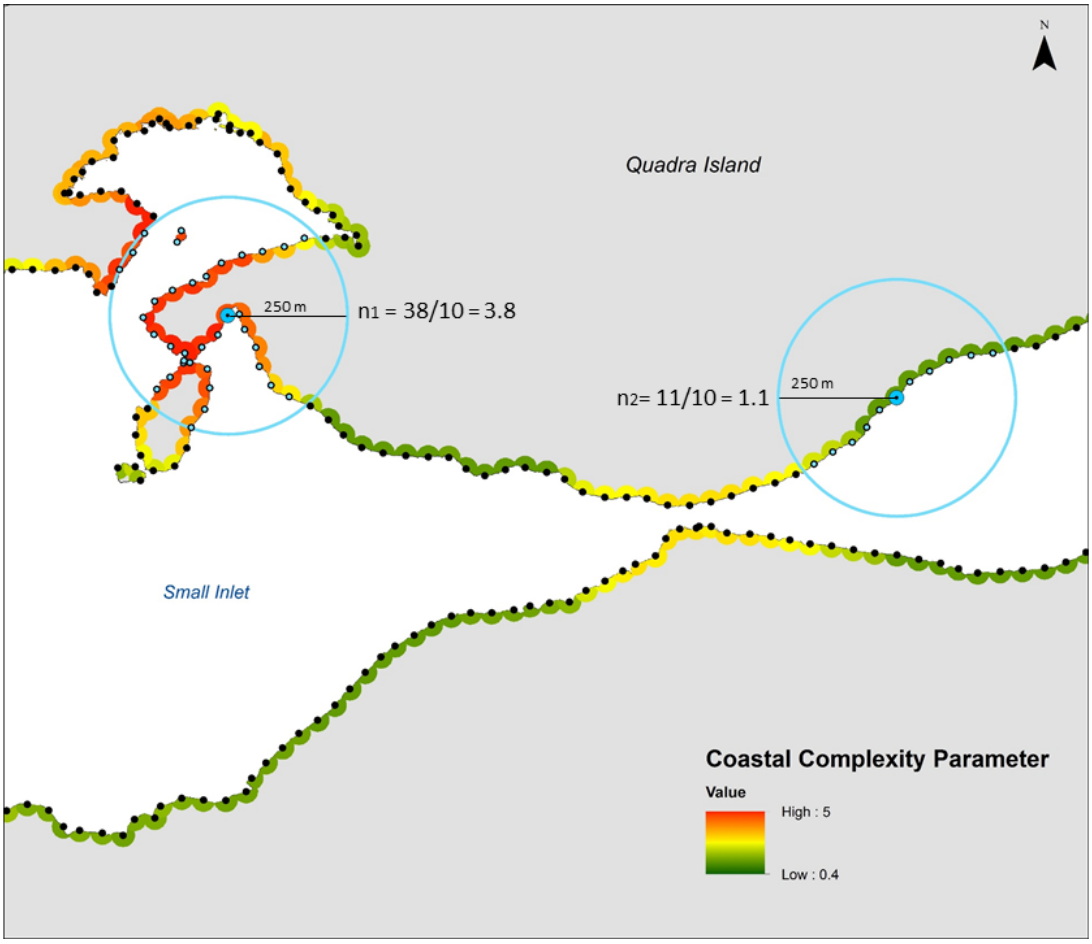

Figure 7: Example of coastal complexity value calculations along a section of the +30m palaeo-shoreline, north LIDAR survey, Quadra Island. Higher values indicate greater shoreline convolution (n1) and more sheltered locations while lower values (n2) indicate more exposed locations. Waiatt Bay is to the east, where n_2 is located (see Figure 2)

Research studies using similar coastal complexity indices have shown that early Holocene sites on the PNW coast tend to be associated with moderate or medium coastal complexity (e.g., Mackie and Sumpter 2005; Monteleone et al. 2012). Through trialing various moderate coastal complexity value ranges (e.g. 2-3, 2.5-3.5) for the dataset, a range of 2-4 captured contiguous stretches of shoreline with moderate complexity values and enough shoreline to make the potential map pragmatic. Therefore, only coastline segments with moderate complexity values of 2-4 were considered as areas of high archaeological potential to target archaeological sites on focal palaeo-shorelines in the final map (Figure 8B).

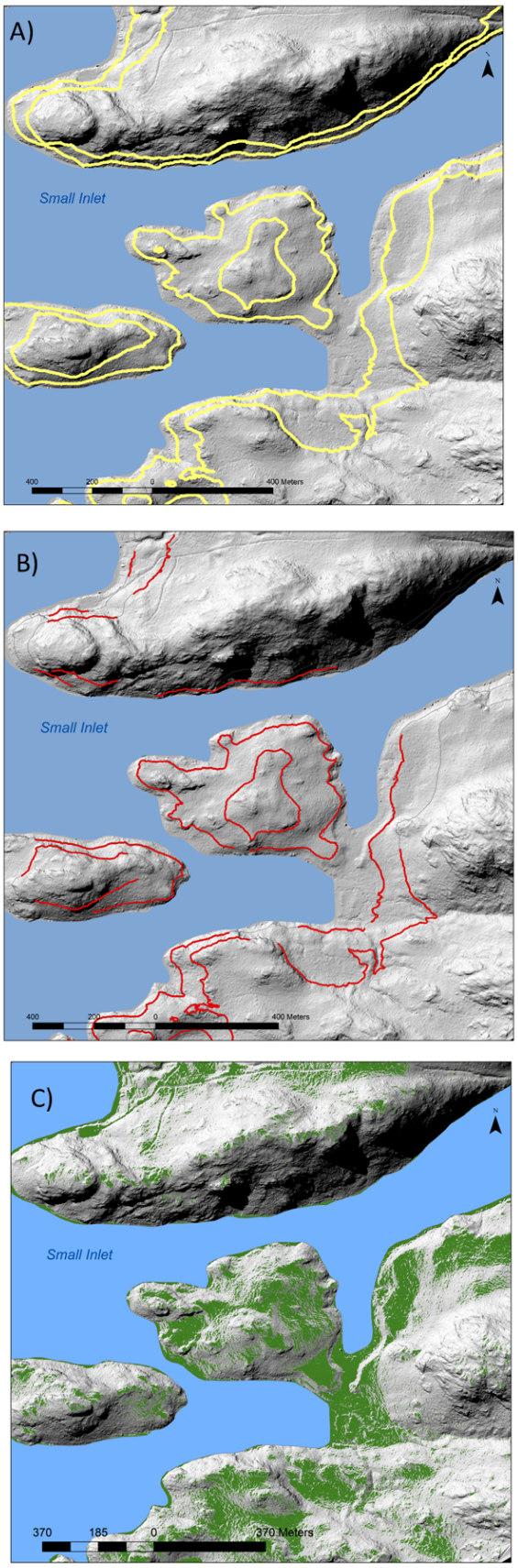

Figure 8: Proof of concept model output for each variable used to identify areas of high archaeological potential: A) Palaeo-shoreline: 10m and 30m amsl (+5m uncertainty) (yellow); B) Coastal complexity: values 2- 4 for 10m and 30m amsl palaeo-shoreline (red); C) Slope: under 10° (green). The location of this demonstration site is indicated in Figure 2.

4.4 Analyses of Three Sediment Sections

Sites at select elevations were selected for detailed examination of the sedimentology for evidence of the origin of sediments, age of sediments, presence of beach sediments and presence of sea level regression. These sites included: CROW (14 m amsl), Lactarius (27 m amsl) and KGP (32 m amsl). Analysis techniques used to interpret each of the three selected sites included: lithostratigraphic and sedimentological analysis; radiocarbon dating, optical dating and dating by association with the established RSL curve; and analyses of microfossils and macrofossils. The rationale and purpose for each of these techniques will be discussed, followed by the sampling and analysis procedures.

4.4.1 Lithostratigraphic and Sedimentological Analysis

Lithostratigraphic analysis was done in the field for all three sites (CROW, Lactarius and KGP). Lithostratigraphy is the classification of strata (or depositional units of rocks or sediments) based upon their lithologic properties and the position of each unit relative other units (Weerts and Westerhoff 2007). By describing and interpreting lithostratigraphic units, it is possible to understand the depositional environments and processes that created the units.

Stratigraphic profiles were drawn in the field from exposed sections or excavation pits for all three sites. On site descriptions of sediment units were recorded for the gravel pit exposure at KGP and for the 1 m^2 archaeological excavations (CROW and Lactarius). Sediment samples were also collected, sieved and processed through a laser granulometer in the laboratory and characterized for grain size distributions. For each site, a datum was established next to the unit using a piece of rebar. Measurements were taken from top to bottom of the excavation unit and

recorded as depth below the archaeological site datum (dbd), then later converted to depth below surface (dbs) as needed. At CROW, the datum was 10 cm above the surface level and at Lactarius it was 20 cm below the surface level. The thickness of each sedimentary unit was recorded with a measuring tape and line level. Photographs of the deposits were also taken.

Sedimentological analysis was performed in the laboratory to help further define lithostratigraphic units in terms of sediment composition and to understand the environmental changes as evidenced in differences between depositional units. For example, differences in particle size distributions can help differentiate beach sediments from aeolian and marine deposits (e.g., Eamer et al., 2017a). The primary purpose was to determine which units represented terrestrial, coastal or marine depositional environments.

Samples for grain size analysis were selected from beneath the archaeological/cultural layers at CROW and Lactarius and were mechanically sieved and/or analyzed through a laser granulometer (MasterSizer 5000). All samples were first dried in an oven at 105 ºC for 24 hours then each was split mechanically with a splitter to get a representative sample. The samples that were processed in the MasterSizer were first sieved using a 500 µm sieve to prepare them for the machine. The laser granulometer was used to analyse the grain size of sediments <500 µm in diameter (samples CROW3: S10, SED1, SED2, SED4; KGP: SED9, SED1) and particles >500 µm diameter were further sieved (samples LRA2, LRA 4). Laser granulometry was used for finer samples because dry sieving is not useful for particles <50 µm (Gee and Bauder 1986). The laser granulomter uses laser diffraction to get the particle size distribution (PSD) by measuring the intensity and variation of angles of diffracted light as the laser passes through a particulate sample suspended in fluid (Rodrigquez and Uriarte 2009). Samples with a wide range of

particles sizes were both sieved and put through the laser granulometer (samples LRA 1, LRA7, LRA8).

The MasterSizer produces particle size measurements based on the average of three measurements for each sample. The obscuration is the measure of the intensity of the light that is absorbed by the sediments (Storti and Balsamo 2010). The obscuration rate ranged from 12-35%, which was considered high, but still within acceptable bounds (Shahin Dashtgard pers. Comm. Nov 22. 2017). The upper measuring limit of the granulometer is 500 µm so the granulometer and dry sieving data were normalized and combined at 355 µm for applicable samples. The laser granulometer amounts of the <355 µm fractions were converted to be out of a percentage of the whole sample, which was determined through sieving. Statistical parameters derived from the PSD were calculated using the software GRADISTAT version 4.0 (Blott 2000).

Sieving is commonly used to determine PSD for sandy sediments (Rodriguez and Uriarte 2009). Samples were dry sieved at a ¼ phi interval (from 355 µm to 2000 µm) and then converted to percent of the total sample to make results comparable across samples. The conversion formula to phi units is: phi = -log2(D), where D is the grain size diameter in millimeters. For some samples with larger grain size variation 4000, 6700, and 13200 µm sieves were also used. Samples were sieved in a dry shaking apparatus (ELE rotasift) for 15 minutes each, then the amount remaining in each sieve was weighed and entered in to gradistat to derive the PSD.

4.4.2 Dating Techniques – Radiocarbon, Optical and Relative Sea Level Dating

Three methods were employed for constraining the chronological age of the sediment record. Radiocarbon (^{14}C) dating was used to obtain ages from the cultural components where

suitable organic materials were present. Samples were identified and collected in the field using a trowel and small vials with care taken to avoid contamination. They were then stored in a freezer and examined under the microscope to remove any attached sediment before being sent to Keck laboratory for accelerated mass spectrometer (AMS) dating. Ages are reported with two-sigma uncertainties. From the non-cultural sediments at sites KGP, CROW, and Lactarius, sediment samples were brought to the lab and wet sieved through nested 1000 μm and 250 μm fine screens. More than 1000 g of sediment was processed for each site and examined for organic material at 8x magnification. In some deposits, rare small fragments of charcoal (< 1000 μm diameter) were found. After several attempts, material submitted for ^{14}C dating was found to be insufficient (i.e., submitted material failed to survive pre-treatment or modern ages were obtained). Some attempted radiocarbon ages were from unsuitable materials like burned roots. ^{14}C dating was therefore abandoned for these sediments. Subsequent to completing this analysis a radiocarbon age was obtained from deltaic sediment at CROW (Fedje et al. 2018).

4.4.3 Optical Dating

As the non-cultural sediments were largely void of organic material and primarily comprised of medium sand to silt, optical dating was attempted in order to date when the sand grains were last exposed to sunlight, and thus to indicate their burial age (i.e., the age of stabilization for some landforms). The procedure for acquiring optical ages is described in, for example, Lian and Roberts (2006), Lian (2013), and Roberts et al. (2015). Optical dating samples were carefully extracted by inserting opaque brass or aluminum tubes into cleaned section faces from the C horizon of the lithostratigraphic sequence at CROW3 at 1.90 m dbs (samples OSL-3 or CROW-3) and 1.15 m dbs (samples OSL-1 or CROW-1) and from KGP at

4.24 m dbs (sample KGP-1). Samples were also collected at these depths for grain size analysis (e.g. CROW3 SED1 from 1.90 m dbs and SED3 from 1.15 m dbs).

Optical dating samples were prepared and analyzed at the Luminescence Dating Laboratory at University of the Fraser Valley. The samples were prepared following laboratory procedures outlined Wintle (1997) and Neudorf (2015). In the laboratory, under dim orange light, the sample tubes were opened and the outer light-exposed surfaces were removed. A portion of these outer scrappings were dried and milled to a fine powder, and sent to a commercial laboratory (Maxxam Analytics) to determine U, Th, ^{40}K, and Rb concentrations. The concentrations of these radioisotopes are needed to determine the environmental dose rates at each sample site. Portions of the remaining sample were treated with HCl acid and H_2O_2 to remove any carbonates and organic material, respectively. Samples were then rinsed and wet-sieved, isolating the 180 – 250 μm sized grains for dating. Quartz and feldspar were separated from heavy minerals, and from each other, by settling in a 'heavy liquid', lithium metatungstate (LMT) at densities of 2.69 g/ml and 2.58 g/ml. This procedure is not perfect, and as such, it results in K-feldspar and quartz concentrates. Grains were then treated with HF acid to remove feldspar contamination from the quartz extracts, and the outer surfaces of both quartz and feldspar grains that had been affected by alpha radiation (see Neudorf et al. 2015 for details), and this was followed by a rinse in dilute HCl acid to remove fluoride precipitates. The grains were then rinsed and dried, and finally placed on ~1 cm diameter aluminum disks using silicon oil as an adhesive. Each aliquot contained ~ 100 grains, and was measured using a Risø TL-OSL DA-20 reader. A modified version (Neudorf et al. 2015) of the standard single-aliquot regenerative-dose (SAR) method (Murray and Wintle 2000, 2003) was used to estimate the equivalent dose of each aliquot (Figure 9). For each aliquot, fading rates were determined using the SAR method

described by Auclair et al. (2003), and these were used to correct age values using the method of Huntley and Lamothe 2001. The central age model (CAM) is typically used to find the equivalent dose for the age calculation for deposits that have experienced complete bleaching before deposition and burial, whereas the minimum age model (MAM) is typically used in the case where grains have experienced incomplete bleaching, or consist grains with different bleaching histories (Galbraith and Roberts 2012). For each sample, a weighted mean fading rate was used to correct for anomalous fading. All optical ages are reported in calendar years.

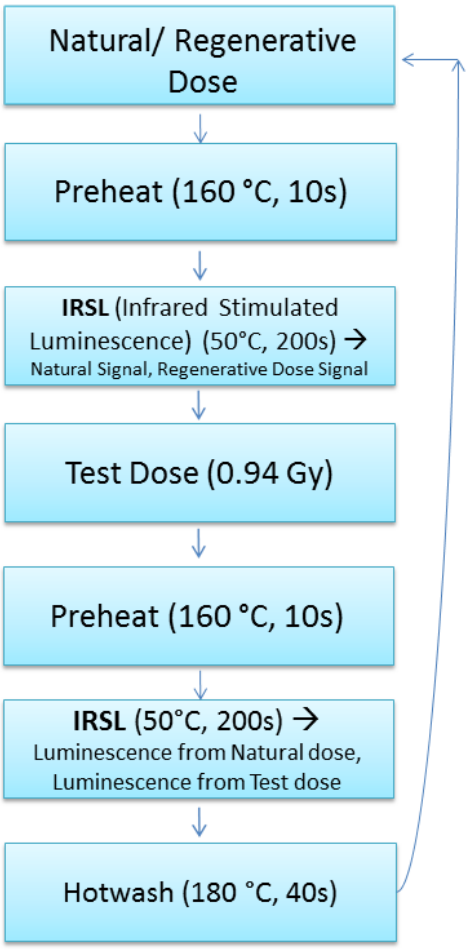

Figure 9: SAR protocol applied to samples (adapted from Neudorf et al. 2015)

4.4.4 Use of the RSL Curve for Providing Age Estimates

The RSL curve established for Quadra Island (Figure 4) was used to date some sites where radiocarbon or optical dating was not conclusive or possible. By determining the elevation of each site accurately from the LIDAR DEM, and referring it to the RSL curve, approximate age ranges could be acquired, as done in other studies on the PNW coast (e.g., McLaren 2008) and elsewhere (e.g., Breivik 2014; Svendsen and Mangerud 1987). In some cases, this was used to provide corroborating evidence to further confirm the radiocarbon and optical ages.

4.4.5 Diatom Analysis & Marine Shell Casts

The study of in situ intertidal organisms, like protists, diatoms and marine shell casts or fossils, preserved in ancient coastal sediments, gives information that can be used to more precisely identify and date sea level positions than the study of geomorphic features alone (i.e. beach ridges, coastal dunal and estuarine features) (Flood and Frankel 1989; Baker & Haworth 1997). High energy-depositional features such as beach ridges can often only construct the sea level curve to a resolution of ± 1 m (Flood and Frankel 1989), whereas diatom analysis of isolation basins can be more precise.

The presence of marine macrofossils, in the form of shell casts, was recorded in the field. Photographs and samples were taken, with further photographs taken in the lab. Some shell casts were carefully excavated and gently stored in bubble wrap inside plastic containers and taken back to the lab. Photographs were then sent to local shellfish experts to identify the species of bivalves. Select sediment samples were examined for microfossils to identify diatoms and testate amoebae indicative of freshwater, brackish water or marine settings. Diatoms and some testate amoebae taxa are siliceous types of protists. Diatoms are unicellur algae that commonly live in

aquatic environments, and species composition varies depending on the salinity, temperature and nutrient level of the water (Zang and Sawai 2015). These samples included: LRA7, LRA5, LRA4, LRA2, LRA1, KGP SED3, KGP 460-470, KGP 478-480, KGP 480-482, CROW3 SED3, CROW3 SED1, and CROW3 SS10. Samples were kept at 4 ºC until preparation. There were few to no organics in the bulk samples so H_2O_2 treatment was deemed to be not necessary. Diatom slide preparation followed the method describe by Battarbee et al. (2006) along with a clay decantation procedure where necessary. Samples were prepared by first putting 20-30 ml of sediment and ~30 ml of distilled water into capped test tubes. The test tubes were then agitated and let sit for 2-5 minutes. The sediment-water mixture was then poured off and saved, and the coarse material (sand and silt) was poured off. The tube was then filled with more distilled water, shaken and left to settle for ~ 2 hours. The samples were then decanted with 5 ml glass pipettes to remove the excess water then shaken and let sit for another ~ 2 hours. This procedure was repeated 2-3 more times, until the turbid water became completely translucent. The water was then pipetted off until ~ < 5 ml of water and sample remained. The sample was then shaken to create a slurry and extracted into small vials. The slides were made by putting 3-4 drops of the sample onto a microscope cover slip and adding 3-4 drops of distilled water. The cover slips were left to dry overnight and the next day adhesive was added to the slide and the cover slip was mounted.

Slides were thoroughly examined using a Nikon Japan – 516406 light microscope at 400x to 1000x magnification. Reference guides were used to identify freshwater, brackish and marine dwelling protists (i.e. diatoms and testate amoebae) (Campeau et al. 1999; Charman 2015; Diatoms of the United States n.d.; Fallu et al. 2000; Meisterfeld 2001; Pientiz et al. 2003). Presence of species and approximate counts of each species present were recorded per sample.

The counts on each slide provide a measure of relative abundance. The specific habitat of these species was then used to determine depositional environment. Usually a count of 300 specimens is needed to determine environmental context, but due to the sandy nature of the substrate lower counts were expected. Counts ranged from 1-20 specimens, and occasionally up to 500 specimens.

5 Results:

5.1 Geomorphic Interpretation and Identification of Potential Palaeo-shoreline Elevations

Key elevation ranges emerged from this analysis and from field surveys for archaeological sites. The lower tier includes elevations from 10 to 14 m amsl, with 10 m representing the most common lowest elevation. The top tier ranged from 26 to 32 m with 30 m being the most common elevation. Both of these elevation levels had additional subtle potential palaeo-shoreline features (beach ridges or berms) above the most dominant break in slope. These elevations were recorded using the LIDAR-derived DTM with $1m^2$ resolution and approximately 20 cm vertical accuracy.

Sites at these elevations make prime areas for detailed examination of the sedimentology for evidence of the early Holocene history. Therefore, CROW (14 m amsl)(Figure 10), Lactarius (27 m amsl)(Figure 11) and KGP (32 m amsl)(Figure 12) were selected for site-specific sedimentological analysis. In each of the figures below, four panels were constructed to illustrate the geomorphic mapping process. Panels A) show the broad scale geographic location of each site on the DTM. Panels B) show a close-up geomorphic map representing the area defined by the black box in panel A). Features such as bedrock, relic alluvial fans, ravines and terraces were mapped. The red lines indicate the transects for the topographic profiles, which is shown in panels D). Panels C) show a ground photo taken to display the presence of terrace features and ravines. Panels D) show the topographic profile and examples of beach ridges and terraces used to identify potential palaeo-shorelines.

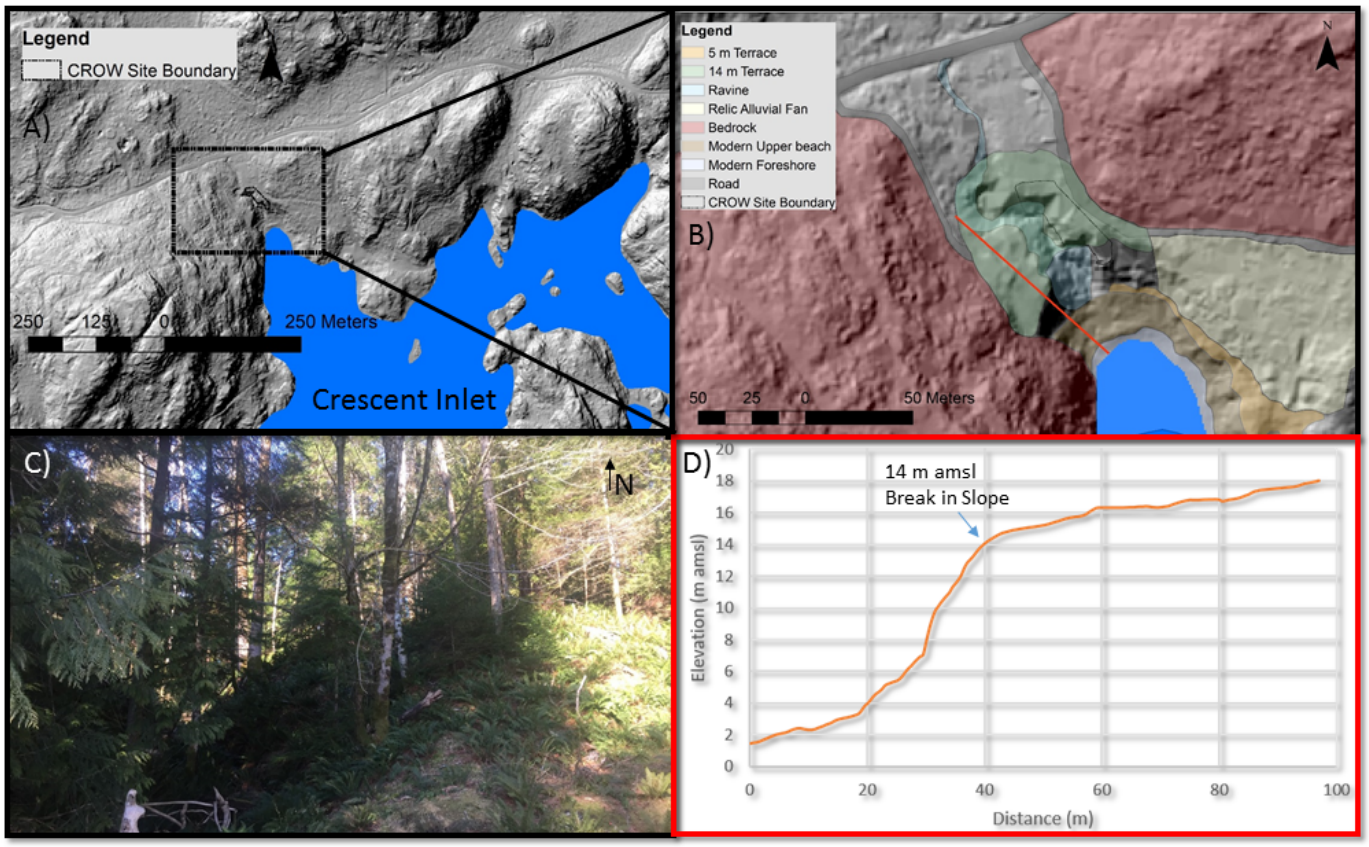

Figure 10: Geomorphic mapping of Crescent inlet Right of Way (CROW) site: A) Site location of CROW on bare earth model, B) Geomorphic mapping of CROW showing features and topographic profile location, C) Photo facing North and looking up slope at the terrace, D) Topographic profile of the 14 m amsl terrace. Location of profile shown above (red). Distance 0 m starts in the southeast and continues to 100 m in the northwest direction. Vertical exaggeration is 2.6 X.

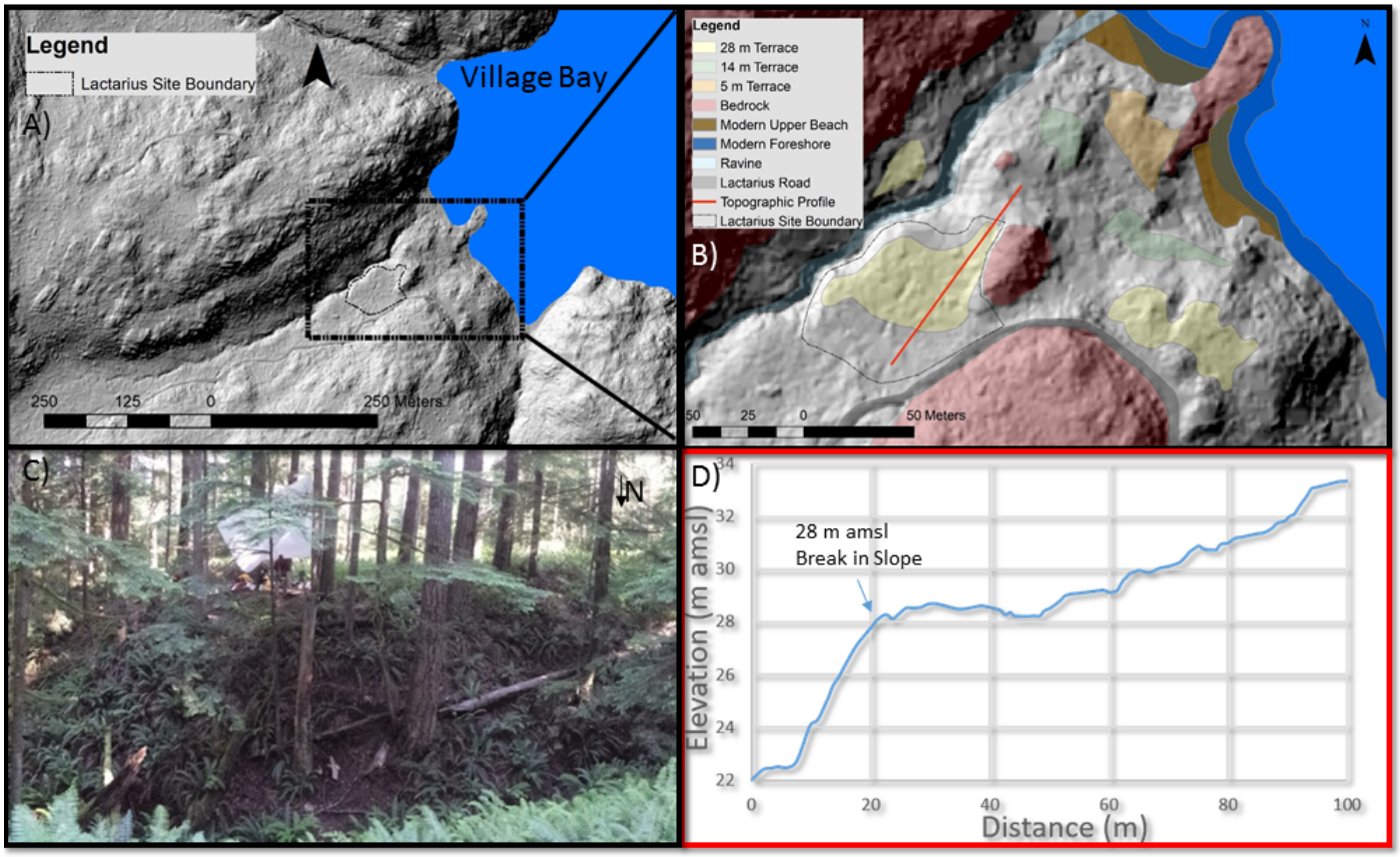

Figure 11: Geomorphic mapping of Lactarius site: A) Site location of Lactarius on bare earth model, B) Geomorphic mapping of Lactarius showing features and topographic profile location, C) Photo of the excavation unit from across the creek facing South D) Topographic profile of the 28 m amsl terrace. Location of profile shown above (red). Distance 0 m starts in the northeast and continues to 100 m in the southwest direction. Vertical exaggeration is 4.2 X.

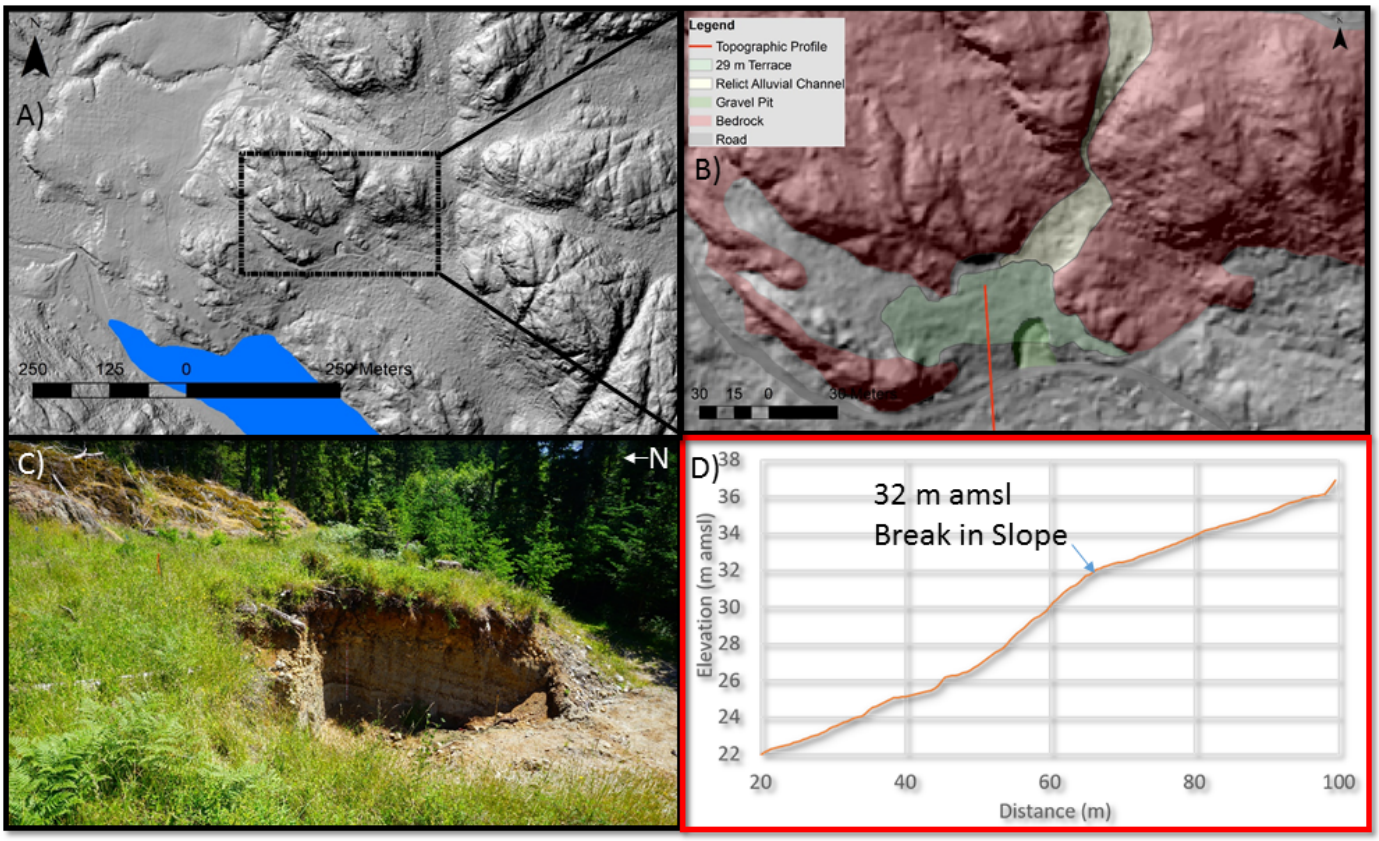

Figure 12: Geomorphic mapping of Kellerhals Gravel Pit (KGP) site: A) Site location of KGP on bare earth model, B) Geomorphic mapping of KGP showing features and topogrpahic profile location, C) Photo of the site facing East showing foreset bed exposure, D) Topographic profile of the palaeo-delta feature. Location of profile shown above (red). Distance 0 m starts in the south and continues to 100 m in the north direction. Vertical exaggeration is 2.5 X.

5.2 Archaeological Site Potential Map

An example of the final archaeological potential map can be seen in Figure 13. During the decision tree (logic filtering) process, each variable reduced the identification of areas of potential archaeological sites into smaller regions of high archaeological potential (m^2) that could be explored for further field survey. For instance, the high potential category of the slope variable represents 28.0% of the total LIDAR (DTM) area in both survey swaths (Figure 1), the palaeo-shoreline elevation (+5 m buffer) variable represents 5.6% and the coastal complexity

parameter (+5m buffer) represents 1.5% of the total area. The result of the combined filtering in the decision tree process then produced an overlapping area of all three variables of only approximately 0.3% of the area as high archaeological potential (Figure 13).

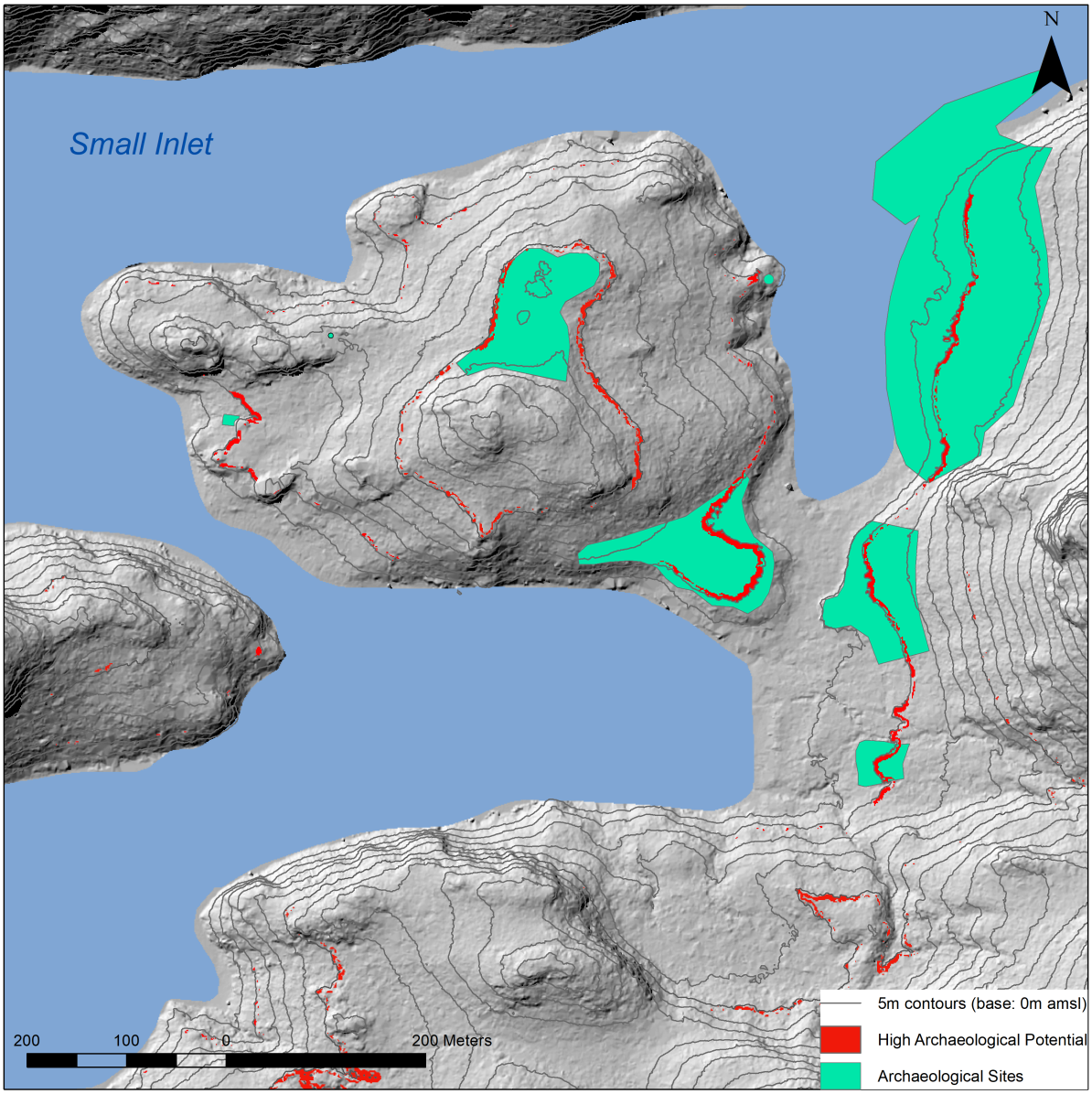

Figure 13: Shows the potential map results for Small Inlet (within the north survey swath of Quadra Island) overlain by newly recorded archaeological sites from the 2015 field survey (green).

Due to logistical restraints (i.e. time and resources), it was not possible to systematically test all identified areas of the landscape for presence or absence of archaeological material to the

degree necessary for complete validation of the potential map. However, existing sites and limited surveys identified many areas. The north LIDAR section was the primary focus as less work had been done in this area and many areas were only accessible by boat. The effectiveness of the potential map was evaluated against data gathered from fieldwork in 2014-2015. As shown in Figure 13, confirmed archaeological site locations occur within close proximity or overlap areas predicted to have archaeological material by the potential map.

5.3 Archaeological Survey

The potential 10 m and 30 m amsl palaeo-shorelines were used to guide the 2015 field survey (Figure 14). Using the software Avenza PDF Maps on digital tablets in the field allowed researchers to view their exact position (±5m) in relation to landscape features on the DTM, such as palaeo-shorelines. The potential map was also used to guide 2015 survey and helped to unearth many previously unknown archaeological sites. Using the palaeo-shoreline elevations and potential map as guides, 12 locations were tested in 2015 and 10 yielded archaeological materials (primarily stone tools) (Figure 13). These sites all occurred around approximately the 10 m or 30 m amsl elevations and information on these 10 sites is indicated in Table 1. At each of the positive targets, stone tools were usually found on the surface or in the first shovel test, and this demonstrates the effectiveness of the approach.

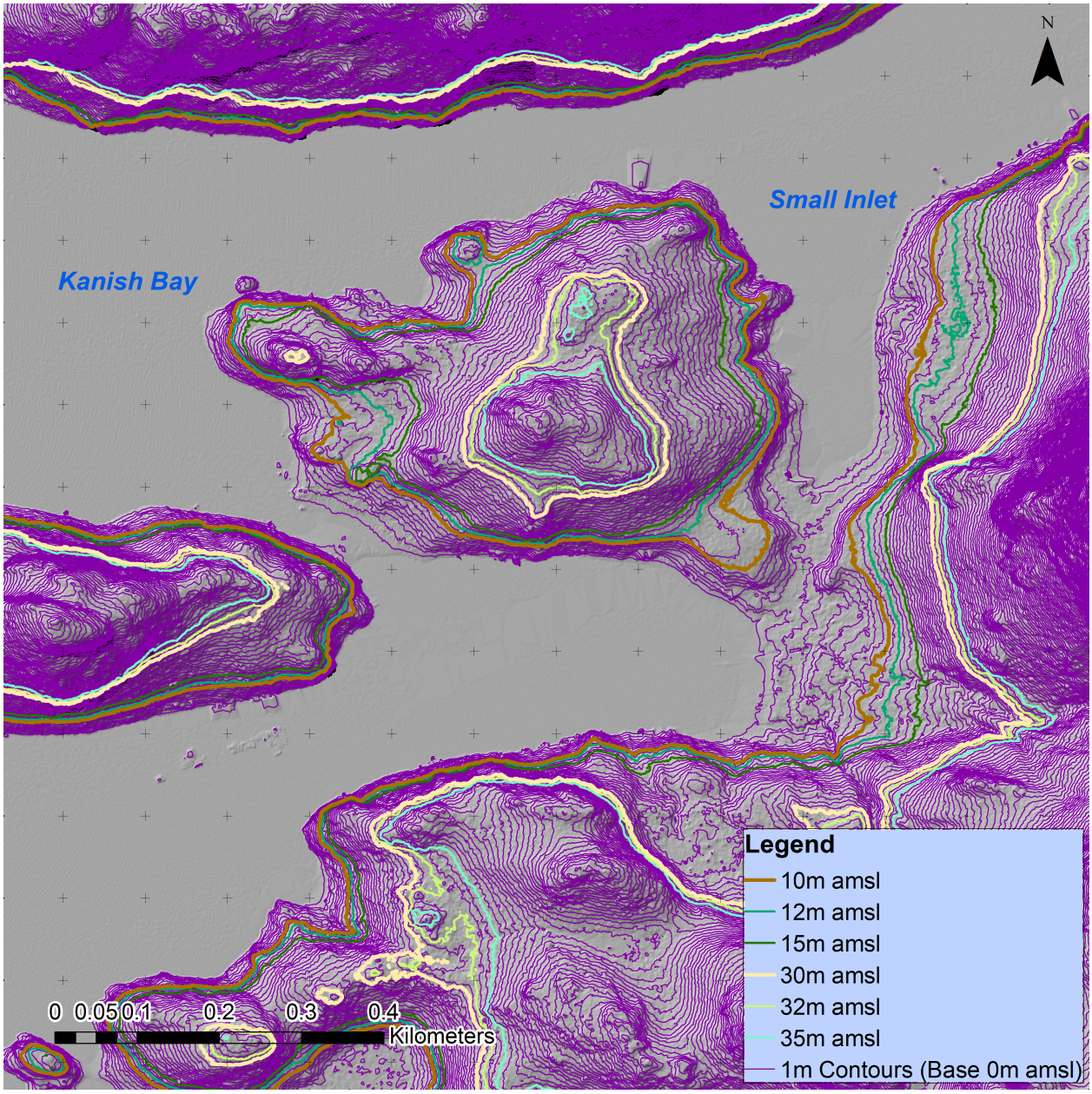

Figure 14: Example of map highlighting 10 m, 12 m, 15m and 30 m, 32 m, 35 m amsl palaeo-shorelines used in field survey

Table 1: Archaeological sites from 2015 within zone of high archaeological potential

Site Name	Elevation (m amsl)	Location	Radiocarbon Age (Cal a BP)	Presence of temporally or cultural diagnostic material	Context (Surface or subsurface)
EaSh-80 Kellerhals Terrace	25	LIDAR South, Hyacinthe Bay	N/A	Lithics	Subsurface
EaSh-81 Lactarius	27	LIDAR South, Village Bay	5180 +/- 15 5320 +/- 15 5360 +/- 15 8875 +/- 20 8820 ± 25 5375 ± 15 8800 ± 20 8855 ± 20 160 ± 15 5990 ± 15 2655 ± 15 5065 ± 15	Raised beach, lithics, possible Western Stemmed Tradition	Both
EbSg-26 Surge Terrace	28	LIDAR South, Surge Narrows	N/A	Raised beach, lithics	Both
EbSh-6 Small Inlet North Terrace	9	LIDAR North, Small Inlet	N/A	Raised beach, lithics, multidirectional core indicative of early period coastal lithic technology	Both
EbSh-93 Small Inlet Terrace 10m DF	9	LIDAR North, Small Inlet	N/A	Raised beach, lithics	Both
EbSh-94 Small Inlet Promontory 30m	28	LIDAR North, Small Inlet	N/A	Raised beach, lithics	Both
EbSh-95 Small Inlet Terrace 10m DM	9	LIDAR North, Small Inlet	5755 ± 20 5590 ± 20 6535 ± 15 6160 ± 15 6740 ± 20	Raised beach, lithics, may represent early to middle Holocene occupation,	Both
EbSh-96 QM Flake	6	LIDAR North, Small Inlet	N/A	Lithic	Surface

Site Name	Elevation (m amsl)	Location	Radiocarbon Age (Cal a BP)	Presence of temporally or cultural diagnostic material	Context (Surface or subsurface)
EbSh-97 Small Inlet-Waiatt Bay Divide	30	LIDAR North, Small Inlet-Waiatt Bay Divide	430 ± 20 6410 ± 20	Raised beach, lithics	Both
EbSh-23 Waiatt Bay Village Site	5	LIDAR North, Waiatt Bay	2940 ± 20 2035±15 5390±20	Clam garden, shell midden, raised beach, lithics, early period	Both

5.4 Site-Specific Interpretations

5.4.1 CROW

The surficial geomorphology at the CROW site is shown in Figure 10. The internal sediment profile and sample locations can be seen in Figure 15. A stylized version of the sediment lithostratigraphic log is shown in Figure 16 with radiocarbon ages. In total, 1,912 subsurface stone artifacts were found at the site (Cal Abbott, pers. Comm. May 2, 2017). Archaeological material was found in the upper palaeosols and throughout the unit to approximately 100 cm dbs (depth below surface). There were also three isolated finds of waterworn stone artifacts found at 200 cm dbs from the basal sandy silt unit.

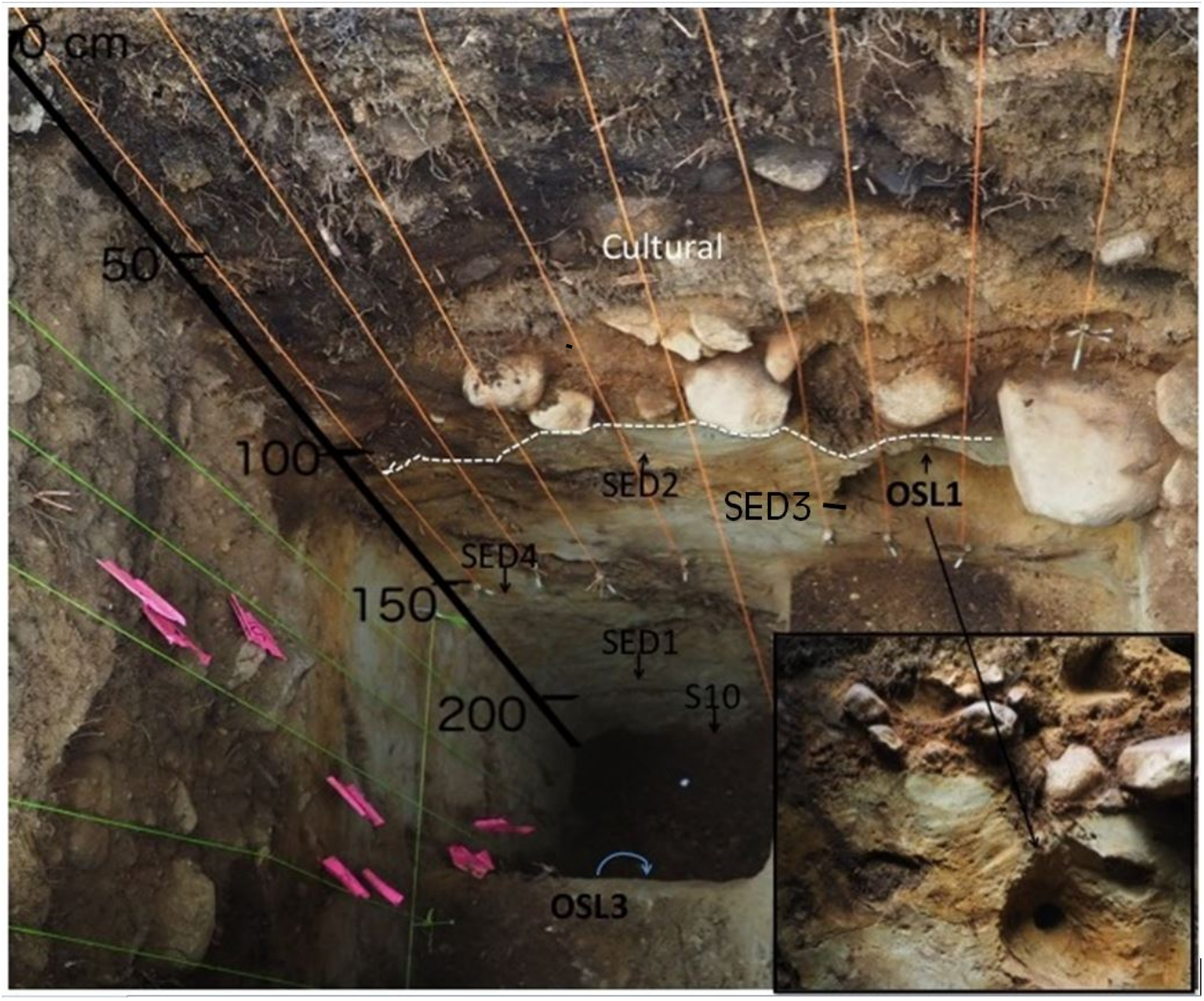

Figure 15: CROW North Wall sediment profile showing locations of sediment (SED or S) and optical dating (OSL) samples

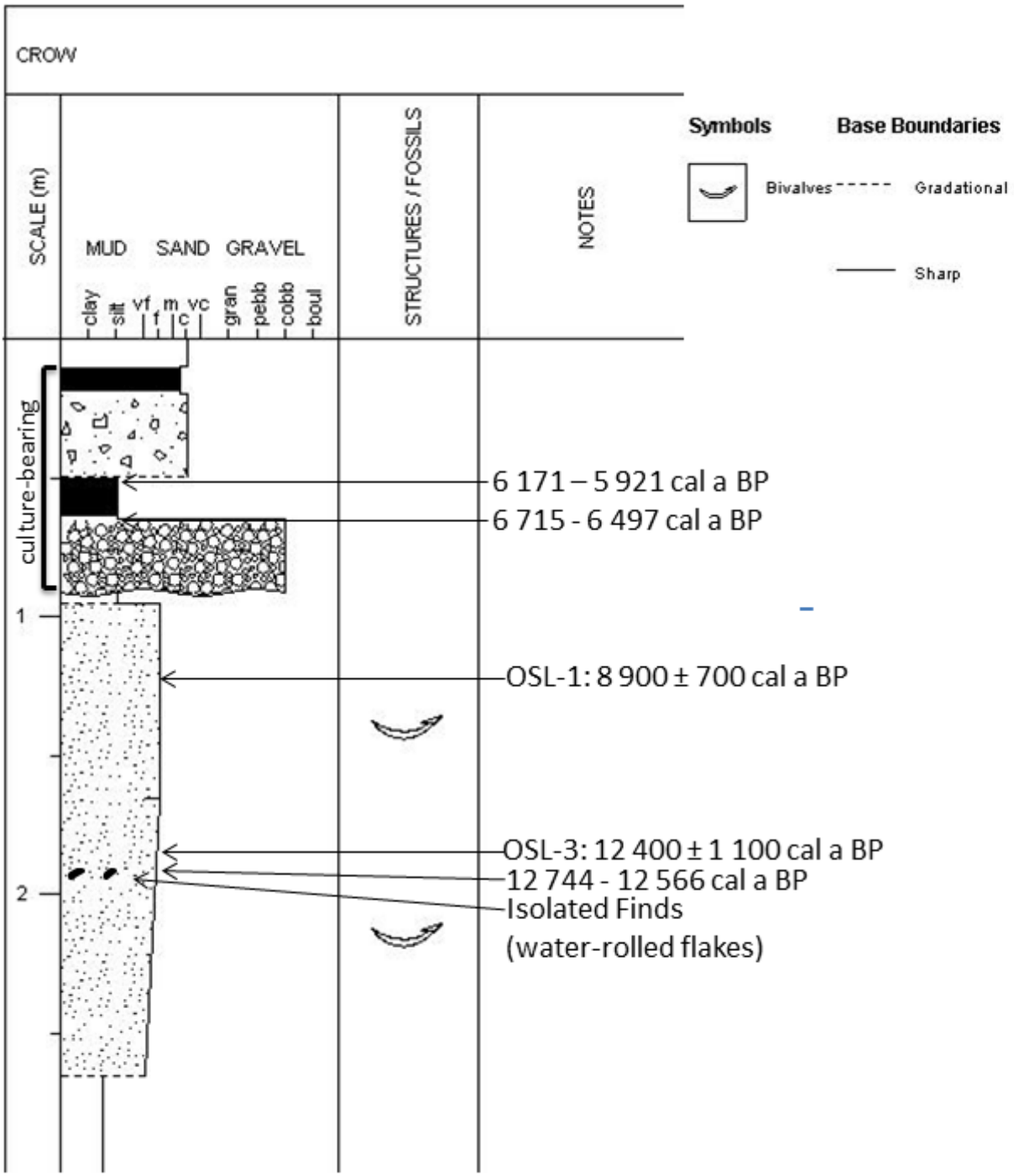

Figure 16: CROW Excavation Unit 3, lithostratigraphic log. Ages are ^{14}C ages, unless labeled otherwise.

The grain size distribution results are found in Appendix A and are summarized in Figure 17. The locations of samples collected for grain size analysis are shown in stratigraphic sequence from the top (surface level) to bottom (at depth). The associated statistics and distributions were

produced in GRADISTAT using the Folk & Ward (1957) method per Blott 2000. The mean, sorting, skewness and kurtosis of the grain size distributions can be seen in Figure 17. No bedding structures were present in any of the deposits.

Diatom results are shown in Table 2. The presence of shell casts in sand was noted at 125 cm dbs and continued to be found in the deposit until 260 cm dbs (from augering) (Figure 18 and Figure 19). Shell casts were identified by local experts including Andy Lamb, author of *Marine Life of the Pacific Northwest* (Lamb 2005*)*, Tom Cockburn, (PhD in marine biology) a Research Associate in palaeontology at the Royal BC Museum, and Rick Harbo, author of *Shells and Shellfish of the Pacific Northwest* (Harbo 1997) and Research Associate at the Royal BC Museum. All of the shell casts from all sites appear to be bivalves of late Pleistocene age that continue to exist in modern times (pers. Comm. Tom Cockburn Jan. 12, 2018). The shell casts in Figure 18 suggest that rock oysters (*Pododesmus macrochisma*) and butter clams (*Saxidomus gigantea*) are present. Figure 19 shows a bivalve species of scallop (*Chlamys* sp.) and of cockle (*Clinocardium* sp.) (pers. Comm. Andy Lamb Jan. 4, 2018 and Tom Cockburn Jan. 12, 2018).

A radiocarbon age of 12 744 – 12 566 cal a BP (UCI 193684) resulted from a sample at a depth of 105 cm dbs from unit 2017-1 was immediately adjacent to a cockleshell cast (Fedje et al. 2018). This date aligns with the RSL age of the site which is about 12 500 cal a BP. The optical dating results from samples CROW-1 and CROW-3 can be seen in Table 3. The depth for sample CROW-3 is 190 cm and the associated columns show the sample age in thousands of years (ka) based on the central age and minimum age models. The optical age for sample CROW-3 is 12 400 ± 1 100 cal a BP using the central age model (CAM). The optical age for

CROW-1, at 115 cm dbs, is 8 900 ± 700 cal a BP.

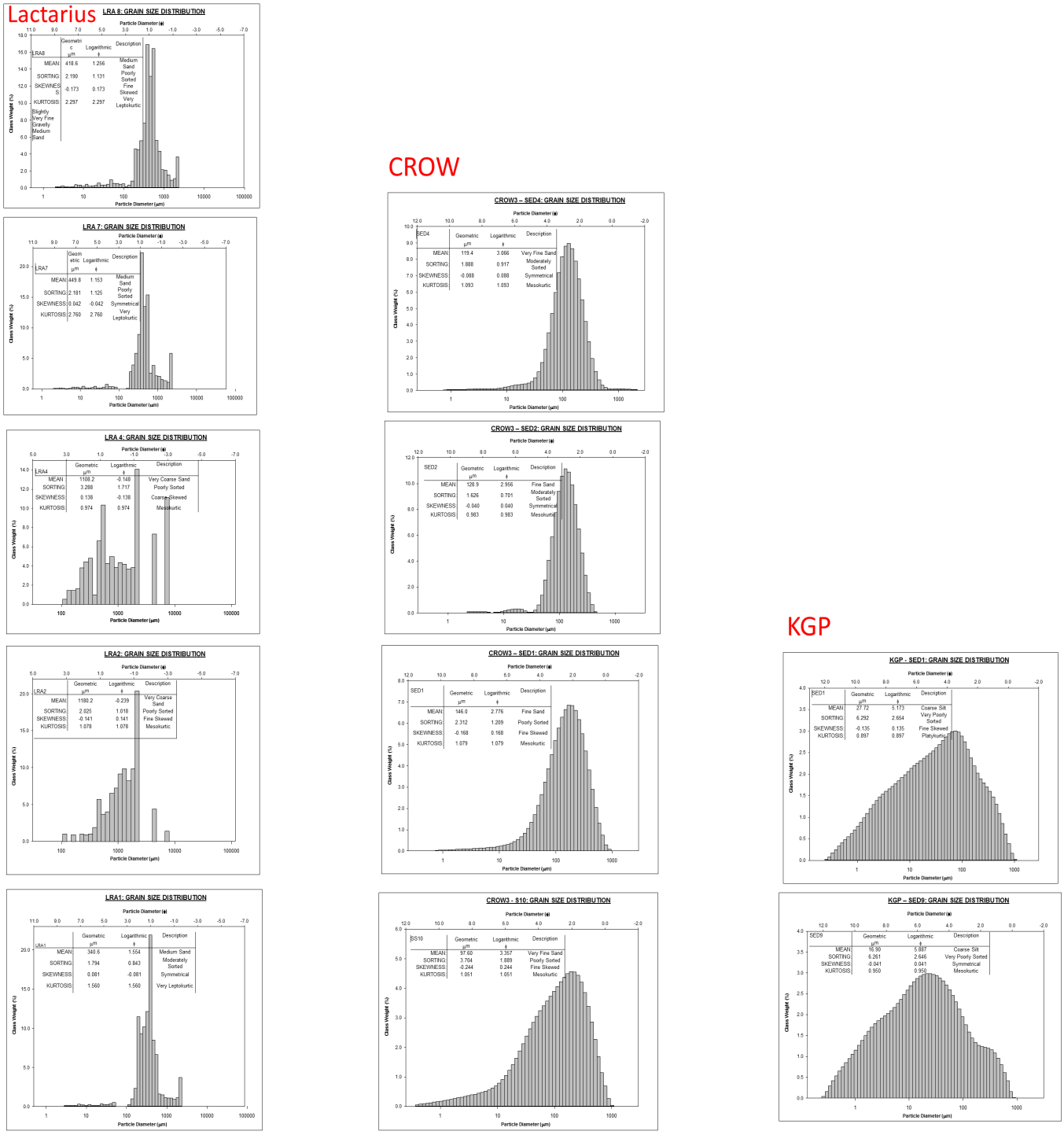

Figure 17: Grain size distributions and associated statistics calculated by the Folk & Ward method for CROW, Lactarius and KGP

Table 2: Microfossil analysis results showing species and abundance

Site Name	Sample ID	Depth (cm dbd)	Microfossil Type	Species	Abundance	Count	Proxy Indicator
Lactarius	LRA7	89-94	Chyrsophyte cysts		abundant	c. 200	Freshwater
			Amoebae - testat	*Euglypha rotunda*	present	1	Freshwater to Brackish
			Diatom	*Pinnularia maior*	present	1	Freshwater
			Sponge		common	c. 20	undefinitive
	LRA 5	99-106	Chrysophyte cysts		common	c.20	Fresh
			Amoebae - testat	*Euglypha rotunda*	present	4	Freshwater to Brackish
			Diatom		absent		
			Sponge		common	c. 30	Undefinitive
	LRA 4	100-107	Chrysophyte cysts		abundant	c. 50	Freshwater
			Diatom	*Diplaneis Interrupta*	Present	3	Brackish
				cf. Martyana Martyi	Present	1	Fresh/brackish
				Biremis circumtexta	Present	1	Coastal/marine
			Sponge		present		undefinitive
	LRA 2	139-147	Chrysophyte cysts		present	5	Freshwater
			Amoebae - testat	*Nebela*	present		Freshwater
			Diatom	*Dictyocha speculum*	present	1	Marine
				Quadrulella simetrica	present		Freshwater
	LRA1	148-155	Chrysophyte cyst		common	10	Freshwater
			Amoebae - testat	*Trinema enchelys*	present	1	Marine
				Quadrulella simetrica	present	1	Freshwater
				Euglypha rotunda	present	1	Freshwater to Brackish
			Diatom	*Dictyocha speculum*	present	1	Marine
				Navicula cf. pseudoten	present	1	Freshwater
				plagiograma Stauroph	present	1	Marine
				Nitzschia cf. claussii	present	1	Marine
				Diatomella Minuta	present	1	Marine
				Skeletonema costatum	present	1	Marine
				Thalassionema nitzsch	present	1	Marine
			Sponge		present		Undefinitive
KGP	SED3	390	Chrysophyte cysts		absent		
			Diatom	*Grammatophora ocear*	present	1	Marine
				Coscinodiscus	common	c. 40	Marine
				Plagiogramma staurop	present	4	Marine
				Unidentified		8	
			Sponge Spicule		common	8	
	460-470	460-470	Chrysophyte cysts		absent		
			Amoebae - testate		absent		
			Diatom	*Plagiogramma staurop*	common	15	Marine
				Plagiogramma pulchell	presnet	1	Marine
				grammatophera ocean	present	1	Marine
				Coscinodiscus	common	15	Marine
				Dictyocha speculum	present	1	Marine
				Unidentified		4	

Table 2: Microfossil analysis results showing species and abundance

Site Name	Sample ID	Depth (cm dbd)	Microfossil Type	Species	Abundance	Count	Proxy Indicator
KGP	478-480	478-480	Diatom	*Coscindosicus*	present	1	Marine
			Sponge	*cf. Clathria*	common	c. 100	
	480-482	480-482	Sponge	*Cladorhizadae (demospon*	present		
				Guitarridue	present		
CROW3	SED3	114-119	Chrysophyte Cysts		abundant	>500	Freshwater
			Amoebae- testate	*Nebela*	present	>3	Freshwater
			Diatom	*Plagiogramma staurophor*	present	3	Marine
				cf. pinnularia parva	present	1	Freshwater
				Aulacoseira distans	present	3	Freshwater
				Tabularia tabulata	present	1	Marine/Brackish
				Dictyocha speculum	present	1	Marine
				Fragilaria brevistriata	present	4	Freshwater/Brackish
				Fragileria constuens	present	4	Freshwater/Brackish
				cf. Pennato	present	1	
				Aulacoseira perglabra	present	1	Fresh
				cf. Cocconeis	present	1	Undefinitive
	SED1	180-190	Chrysophyte Cysts		absent		
			Amoebae - testate	*Euglypha rotunda*	present	2	Brackish
			Diatom	*Coscinodiscus*	present	1	Marine
				Achnanthes delicatula	present	1	Brackish
				Diploneis subcinta	present	1	Brackish/Marine
				Cocconeis californica	present	1	Marine
				Fragilaria cf. brevistriata	present	1	Freshwater/Brackish
			Sponge		present		
	S10	255	Chrysophyte Cysts		absent		
			Diatom	*Coscinodiscus*	abundant	8	Marine
				Dictyocha speculum	common	5	Marine
				Thalossionema nitzchiodid	present	1	Marine (deep)
				Plagiogramma stauropho	abundant	10	Marine
				Plagiogramma pulchellum	aresent	1	Marine
				Dictyocha fibula	present	1	Marine
				unidentified		4	Undefinitive
			Sponge		common		Undefinitive

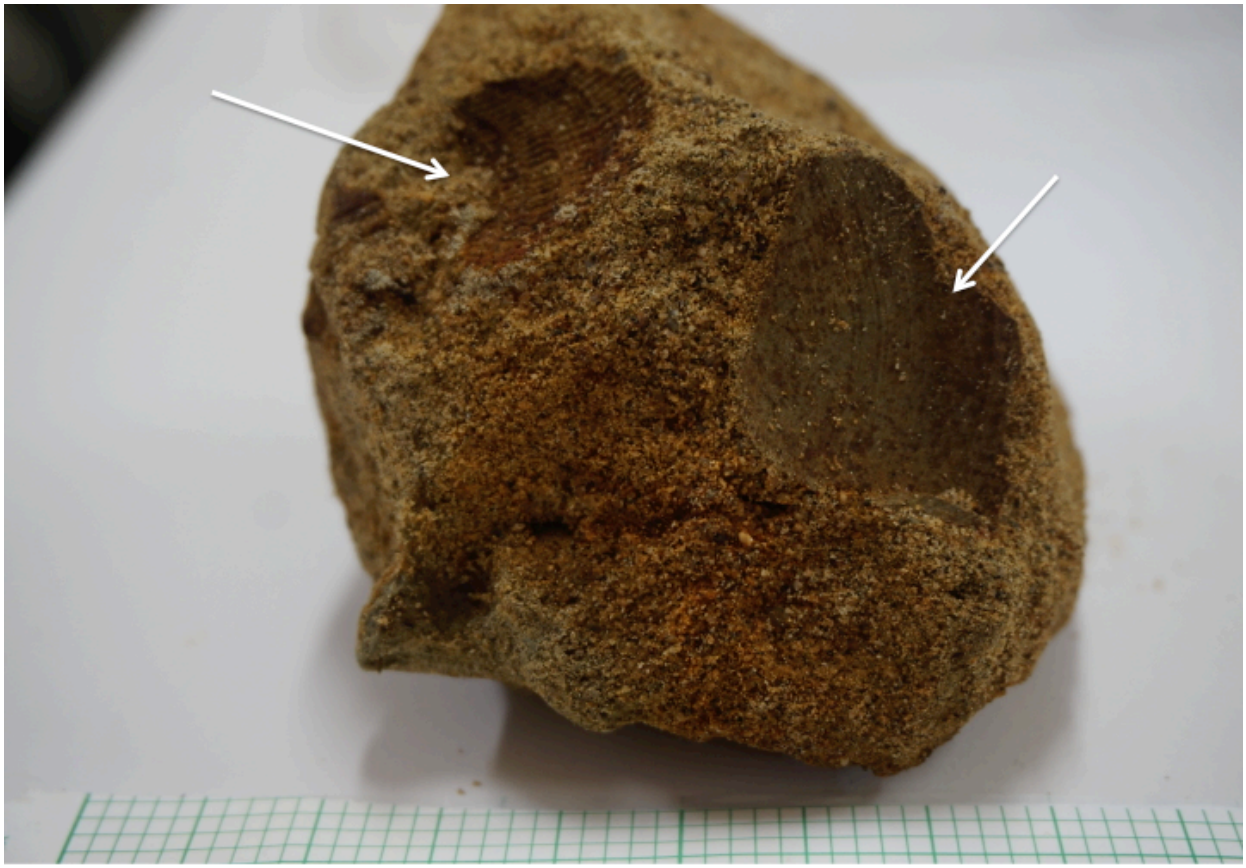

Figure 18: CROW shell casts in sandy sediments from 125 – 137 cm dbs likely showing oyster (left) and butter clam prints (right)(pers. Comm. Tom Cockburn Jan 12, 2018). The thick green bars on graph paper along bottom of image represent 1 cm spacing.

Figure 19: CROW Shell casts from 260 cm dbs likely showing species of scallop (left) and cockle (right) (pers. Comm. Andy Lamb Jan. 4, 2018 and Tom Cockburn Jan. 12, 2018). Scale bar on top of image in cm**.**

Table 3: Optical dating results (conducted and prepared by Christina Neurdorf, UFV).

OSL sample	Grain size (µm)	N1	Total Dose Rate (Gy/ka)	OD[2] (%)	Recuperation (%)	Fading rate3 (%/decade)	CAM[4] De (Gy)	CAM[4] age (ka)	MAM[4] *De* (Gy)	MAM[4] age (ka)
CROW-1	180-250	24/24	2.10 ± 0.12	22±3	0.6±0.1	4.34±0.12	12.4±0.6	8.9±0.7	12.0±0.3	8.7±0.6
CROW-3	180-250	24/24	2.01 ± 0.12	33±5	0.5±0.1	7.47±0.05	11.2±0.8	12.4±1.1	8.7±0.6	9.5±0.8
KGP-1	180-250	23/24	2.04 ± 0.15	30±4	0.6±0.1	4.77±0.07	13.9±0.9	10.7±1.0	12.8±0.4	9.9±0.8

[1] Reported as number of aliquots accepted / number of aliquots measured.
[2] 'Overdispersion' (OD) is the spread in De values remaining after all measurement uncertainties have been taken into account and can be the result of incomplete bleaching and sediment mixing, or, in complex depositional environments, differences in β doses received by individual grains due to their proximity to pore water, cemented grain clusters, rocks or organic material with different dosimetric characteristics.
[3] Fading rates have been measured multiple times on samples CROW-3 and KGP-1.
[4] CAM is the Central Age Model and MAM is the Minimum Age Model of (Galbraith et al. 1999). The age of CDS-1-1 was not calculated using the MAM because the fine-grain (4-11 µm) polymineral fraction was measured (i.e., the signal from each aliquot will be a combined signal from hundreds of grains) and consequently, the OD value is 0

5.4.2 Lactarius

The DTM with the landforms at the Lactarius site is shown in Figure 11. The sediment profile and collected samples can be seen in Figure 20. A stylized version of the sediment lithostratigraphic log is shown in Figure 21 with radiocarbon ages. Archaeological material was found in the upper palaeosols and throughout the unit until approximately 125 cm dbs. There are strong cultural lenses in the form of palaeosols from 40 – 50 cm dbs and from 75 – 80 cm dbs, but there are also artifacts in between these lenses. Some fire cracked rock was present until at least 80 cm dbs (e.g. 1.5 to 6 kg per 0.05 x 1 x 1 m area increments). Two artifacts were recorded from LRA2.

The grain size distribution results can be seen in Figure 17 (raw data in Appendix A). Due to a limitation in sieves, grain size samples LRA4 and LRA2 were only sieved at ¼ phi intervals up to -1 phi and then through -2, - 2.66, and -3.5 phi sieves. No bedding structures were present in any of the deposits.

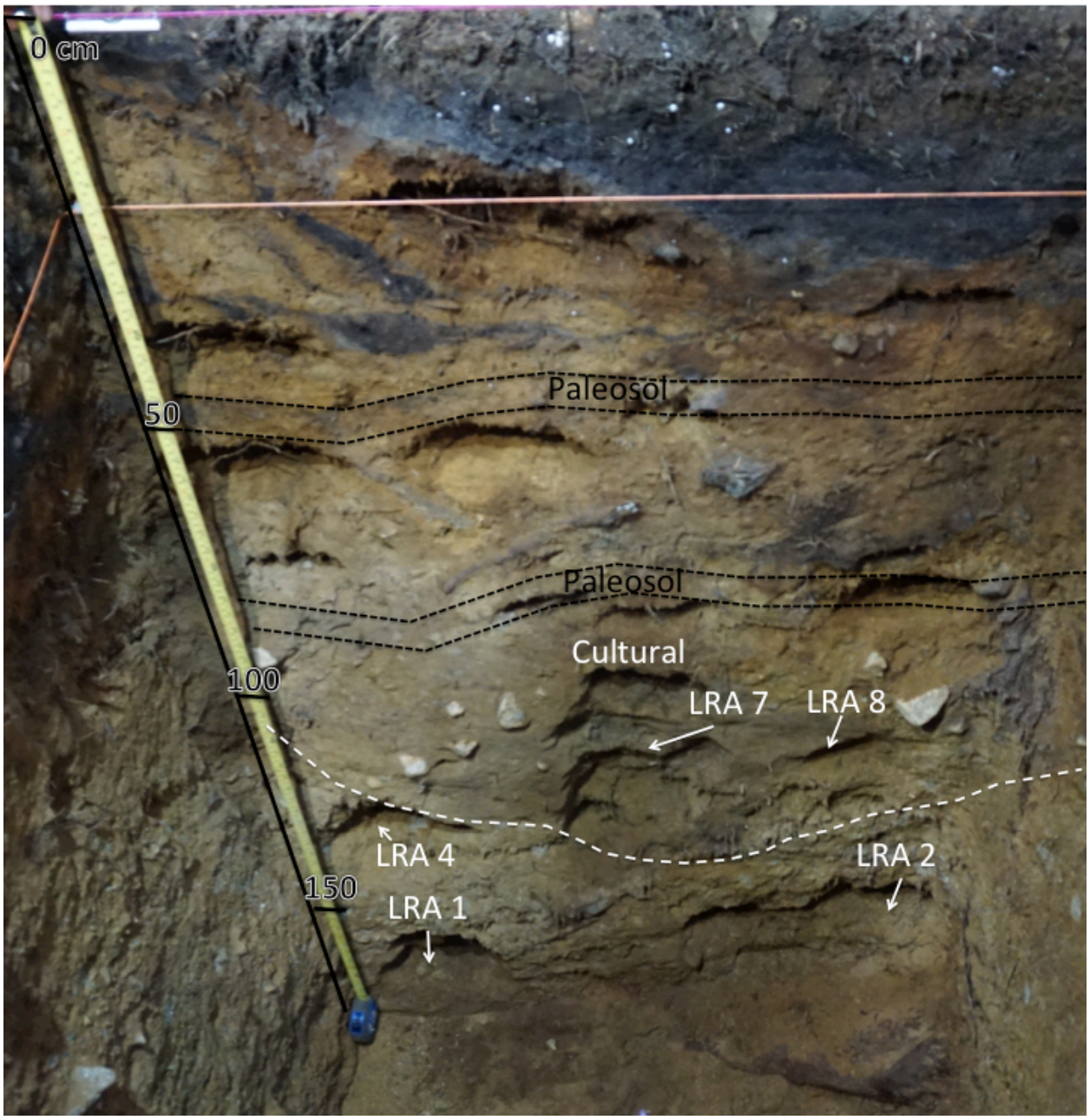

Figure 20: Lactarius east wall sediment profile showing positions of sediment samples (LRA). The measuring tape on the left shows 0 cm to 180 cm dbs.

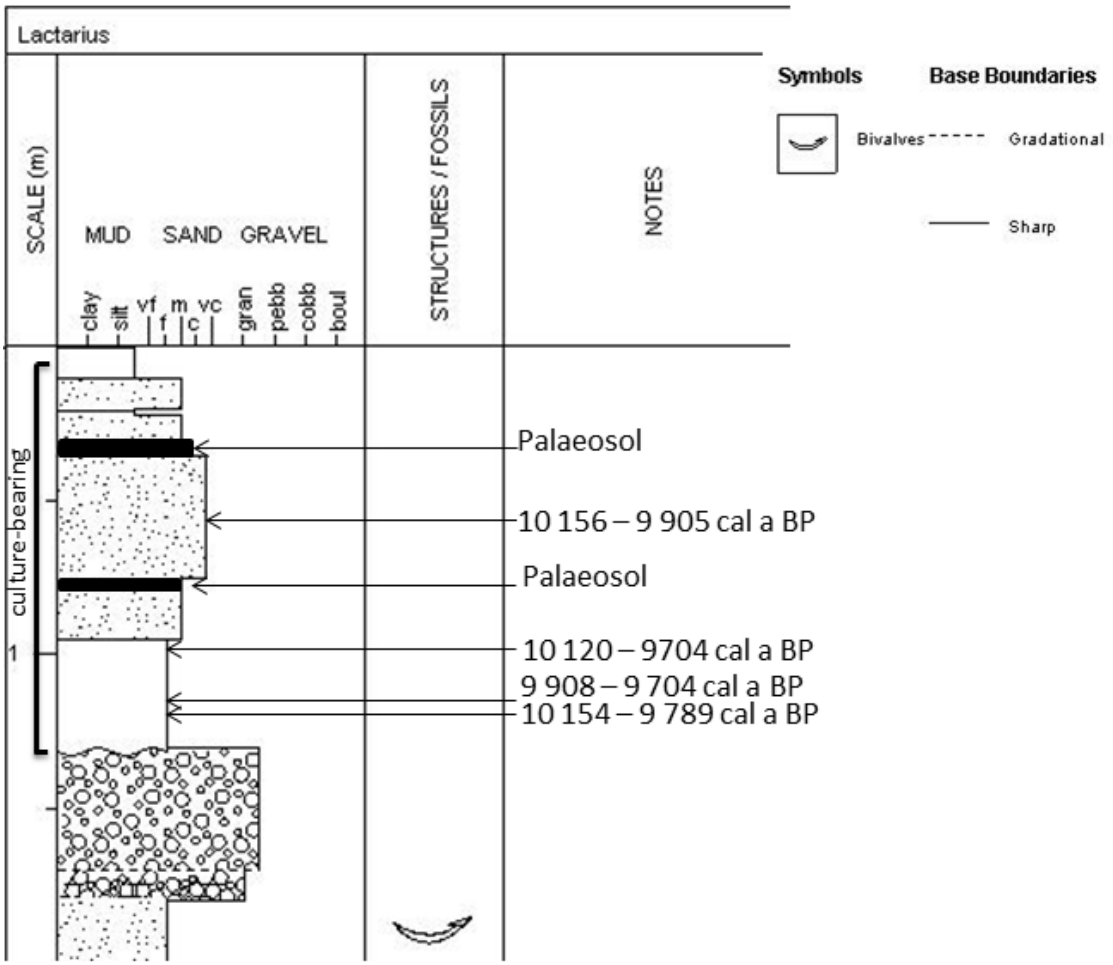

Figure 21: Lactarius EU1 lithstratigraphic log. All ages are ^{14}C ages.

Diatom results are shown in Table 2. Shell casts were only present from the basal sand layer from about 175-190 cm dbs (Figure 22). The far left and middle casts likely represent scallop shells (*Chlamys rubida*), which are subtidal, and the right is indeterminate (pers comm. Rick Harbo Jan. 4, 2018 and Tom Cockburn Jan. 12, 2018).

Figure 22: Lactarius shell casts from 175 – 190 cm dbs likely showing scallop shells (left and middle) (pers. Comm. Rick Harbo Jan. 4, 2018 and Tom Cockburn Jan. 12, 2018)

5.4.3 KGP

KGP and the landforms surrounding it are shown in Figure 12 and Figure 23. The sediment profile with a collected optical dating sample is shown in Figure 24. No archaeological material was found at this site. However, there is a rock shelter only 55 m away at an elevation of 39 – 41 m amsl.

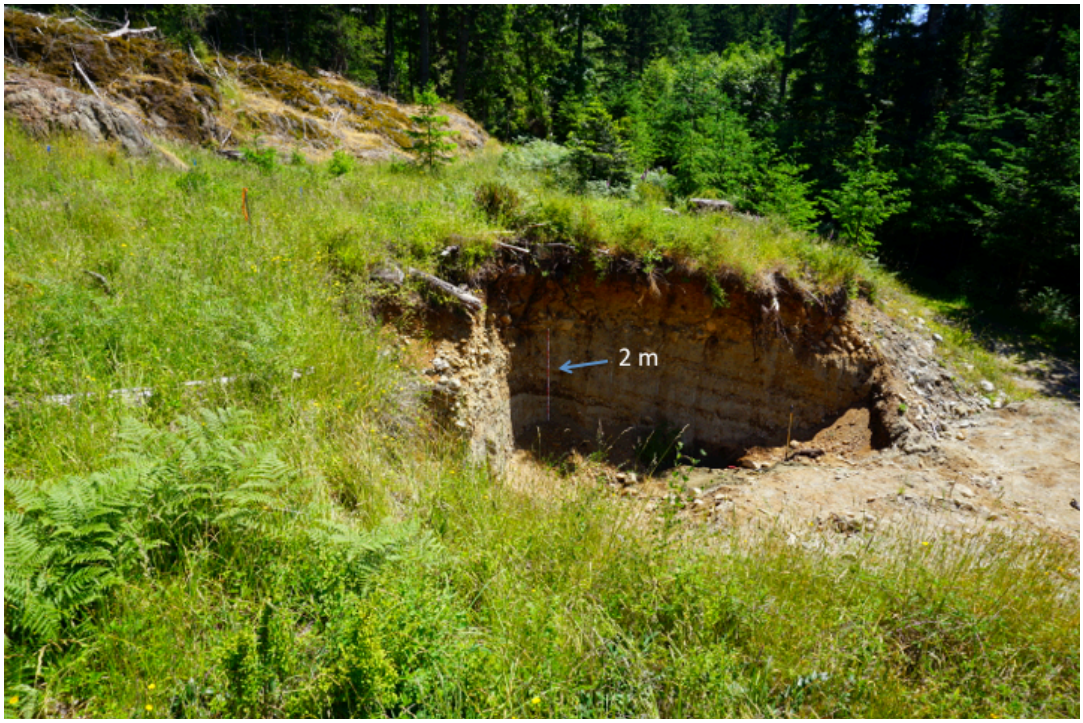

Figure 23: KGP Top view of gravel pit facing East with 2 m measuring stick for scale

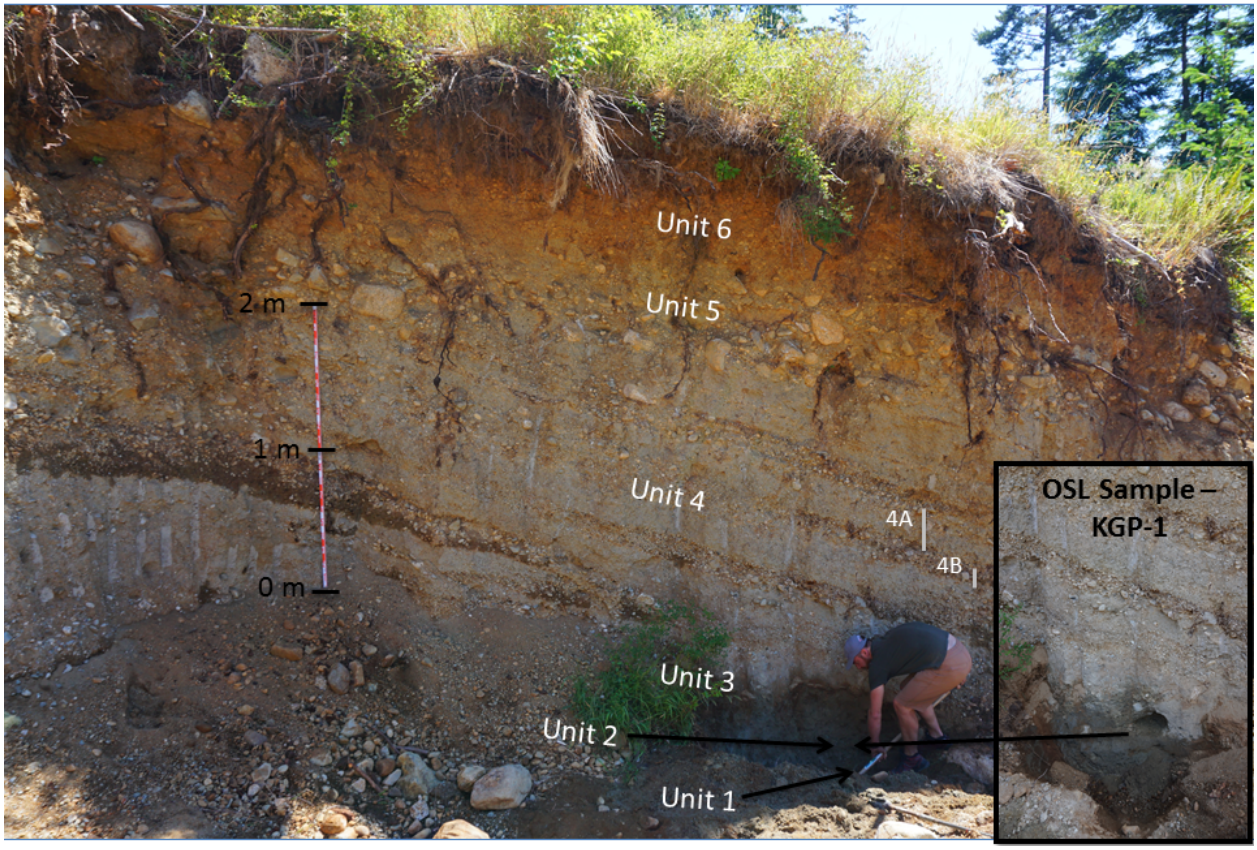

Figure 24: KGP profile of East wall showing distinct layers and optical dating sample location (KGP-1)

The sedimentological descriptions of each unit from the 7.30 m wide exposure of the east wall, as seen in Figure 24, are as follows. Unit 1 is composed primarily of massive blue-grey clay that is exposed for 20 cm and extends deep beyond the excavation depth. The contact between Unit 1 and Unit 2 is gradational. Unit 2 is a 40 cm thick, massive blue-grey sandy silt material with minor clay, minor sand and isolated pebbles less than 1 cm in diameter. The contact between Unit 2 and Unit 3 is gradational. Above, is Unit 3 – a 70 cm thick and brown medium sand, moderately sorted, with minor sub-rounded to sub-angular pebbles (1-3 cm in diameter). This is the unit from which the optical dating sample (KGP-1) was taken. Table shows the optical dating results for sample KGP-1. The optical age is 10 700 ± 1 000 cal a BP for sample KGP-1 using the CAM (Table 3).

Unit 4 is comprised of rhythmically crossbedded sand and gravel that can be divided into distinct subunits of: A) pebble rich sand that is poorly bedded and includes sub-rounded to sub-angular pebbles, and B) well sorted pebble-gravel that is partially matrix supported and partially open framework, and includes sub-rounded to rounded clasts (0.5 to 2 cm in diameter). Unit 4A is approximately 30 cm thick and 4B is approximately 10-20 cm thick. The crossbeds of Unit 4 have a strike of 53° NE and a dip of 143° SE. Unit 5 is 40 cm thick and contains clast-supported to matrix-supported cobbles. It is weakly horizontally bedded. The cobbles are rounded to sub-rounded and on average 10-20 cm in diameter, but in places they are up to 40 cm. Unit 6 is a 40 cm thick, yellow-brown, pebble rich coarse sand with rare subrounded cobbles. It is matrix-supported sand includes some horizontally bedded sand and gravel beds (approximately 10 cm thick).

The north wall and sediment sample locations can be seen in Figure 25. The grain size distribution results can be seen in Figure 17. Diatom results are shown in Table 2. Butter clam

shell casts (*Saxidomus gigantea*) were identified in the gravel and sand foreset beds as shown in Figure 26.

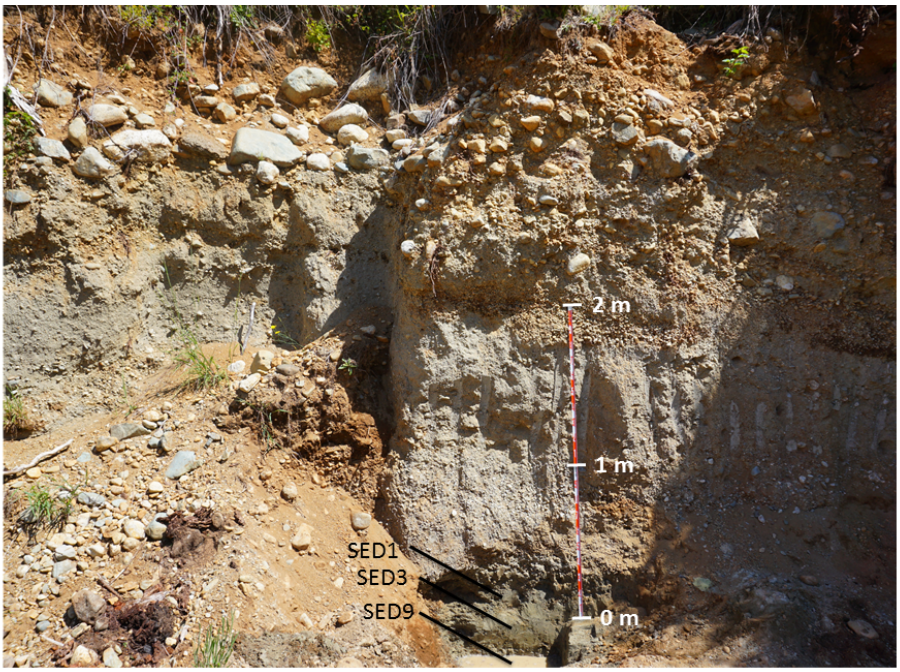

Figure 25: KGP profile of north wall showing sediment sample locations

Figure 26: KGP shell cast of a clam species

6 Discussion

6.1 Site-Specific Interpretation of Depositional Environments

The sedimentological and microfossil evidence can be interpreted in regard to relative sea level changes and landscape transitions in terms of freshwater/terrestrial, brackish/coastal or marine deposition. All of these three inland sites, CROW, KGP, and Lactarius show a basal marine signature and, in some cases, a transition from a marine to a brackish, and then to a terrestrial depositional environment.

6.1.1 CROW

The CROW site shows basal marine evidence through marine shell casts (e.g., cockles and clams at 155 cm dbs and downwards) and marine diatoms from at least 160 cm to 245 cm dbs (SED1 and S10), plus the presence of fine to very fine sand from 95 cm to 245 cm DBS (SED2 to S10). Previous studies also confirm the presence of marine diatoms at depth (Fedje et al. 2016). This corroborating evidence shows there is a marine signature at the base of the unit.

The median values for the particle size distribution for the CROW samples all fall within the 112.5 – 154.8 μm range (SED2: 129.8 μm, SED3: 144.5 μm, SED4: 121.6 μm, SED1: 154.8 μm, S10: 112.5 μm). From the similarity in grain size distribution of these sediments and marine fossil signatures, it can by hypothesized that all lower samples represent one marine unit (i.e. 170 to 245 cm dbs). Samples show slight upward coarsening from very coarse silty fine sand (S10: 245 dbs), to silty sand (SED1:170 cm dbs), to slightly gravelly, muddy sand (SED4: 120 cm dbs). It is possible that this sand might have been derived originally from the abundant regional Quadra Sands (cf. Clague 1976).

Table 4: Environment of deposition sorting classification based on standard deviation (Adapted from Friedman 1962)

Sorting Interval (ϕ)	Environment of Deposition
Medium to fine and very fine-grained sands (mean >1.0-2.0 ϕ)	
<0.35	Most coastal, barrier bar, and lake dune sands, many beach sands, many marine sands above water base, many lagoonal sands
0.35-0.50	Most beach sands, many or most marine sands above wave base, many lagoonal sands, many inland dune sands, some river sands
0.50-0.80	Most river sands, many beach sands, many lagoonal sands from restricted lagoons, most continental shelf sands below wave base, most inland dune sands
0.80-1.40	Many river sands, some lagoonal sands from restricted lagoons, some continental shelf sands below wave base, many glaciofluvial sands
1.40-2.00	Many glaciofluvial sands
2.00-2.60	Many glaciofluvial sands
>2.60	Some glaciofluvial sands
Coarse-grained sands (mean <1.00 ϕ)	
0.50-0.80	Many beach sands
0.80-1.40	Most river sands, many or most beach sands, most continental shelf sands
1.40-2.00	Some river sands, some continental shelf sands, many glaciofluvial sands
2.00-2.60	Many glaciofluvial sands
>2.60	Some glaciofluvial sands

Table 4 shows the environment of deposition for various types of sand grains based on the sorting coefficient (standard deviation of the grainsize distribution), based on research by Friedman (1962). Comparison of this table to the sorting coefficients of samples from CROW (and other sites) in Figure 17 allows for interpretation of the possible depositional environments. The samples from the lowest part of the excavation (S10, SED1, SED4, SED3) are fine sands, and with the exception of S10, all fall within the 0.80-1.40 ϕ standard deviation range. This indicates they might be river sands, lagoonal deposits, or continental shelf sands and most likely

not aeolian (windblown) sands. Given the known sea level regression on Quadra Island, it is highly likely that some of these samples represent low energy distal deltaic deposits or lagoonal deposits. S10 falls within the glaciofluvial class, but this could also result from mixing from the bioturbation of marine shell fragments that were present. The uppermost sample, SED2, has a standard deviation of 0.701 ϕ. In addition to the possible depositional environments listed above, this sample could also be beach sand or inland aeolian dunes. It should be noted that bioturbation throughout the unit may influence the degree of sorting present, so these interpretations are presented as hypothesized depositional environments. As Eamer et al. 2017a and Sevon 1966 note, single measures of grain size summary statistics should not be used alone to interpret depositional environments or sediment transport mechanisms. Further analyses (e.g., shape analysis per Eamer et al. 2017a) however, were beyond the scope of this study. The particle size distribution histograms for CROW are all fine-skewed and some are also poorly sorted (S10 and SED1), which is characteristic of intertidal environments (Parrado Roman and Achab 1999). This indicates there is a likely transition from a marine environment to an intertidal environment between 245 and 170 cm dbs.

In addition, a higher proportion of freshwater diatoms is present in the upper sand (SED3: 104 - 109 cm dbs) whereas marine diatoms that live in the pelagic and benthic ocean, such as *Thalossionema nitzchiodides* and *Plagiogramma staurophorum*, were found in lower sands (S10 in Table 2) (Campeau et al. 1999). Macrofossils in the form of marine shellfish were identified at 155 cm dbs and below. Brackish and marine diatoms are found together at around 170 cm dbs and some species are known to be dominant in tidal and nearshore locations including *Achnanthes delicatula* and *Diploneis subcinta* (Campeau et al.1999; Pientiz et al. 2003). In the

upper sand (e.g., SED3) a greater proportion of freshwater diatoms occur at around 104 cm dbs, suggesting the transition to an estuarine or terrestrial environment.

Above these primarily non-cultural deposits there appears to be a disconformity separating the darker cultural deposits. This erosive contact may represent anthropogenic digging resulting in a pithouse feature (Fedje et al. 2016). No bedding structures were present, which could be a result of shellfish bioturbation. The lack of bedding structures in the sands at both CROW and Lactarius suggest these were likely not fluvial depositional environments. Together, these results show sea level regression from 14 to 12 m amsl from marine to brackish to terrestrial environments from the sub-cultural component of the CROW site. This corresponds to the RSL curve at ca. 12 600 to 12 700 cal a BP, which is consistent with the radiocarbon age of 12 744-12 566 cal a BP from charcoal from the marine layer.

6.1.2 Lactarius

At Lactarius, the marine, brackish and freshwater diatoms, and basal shell casts also show evidence for sea level regression and stabilization. Evidence suggests this also may have been a marine location and then possibly an estuarine environment.

Marine diatoms and shellfish casts are present at depth (e.g. LRA1 – 168 cm dbs). Above there are brackish/coastal diatoms (e.g. LRA4 – 120 dbs) and above that are freshwater chrysophyte cysts and freshwater diatoms. Freshwater to upper salt marsh *Euglypha rotunda* are present in the same samples/depths (e.g. LRA7 approx. 109 dbs). While the diatom counts are low (hundreds/sample are preferable) they still provide useful information about the depositional environment as it is rare to get diatom results from sandy substrates such as those at CROW and Lactarius.

From Table 4 and Figure 17, LRA1, LRA7 and LRA8 are all medium sands and fall within the depositional environment of many river sands, some lagoonal sands, some continental shelf sands and some glaciofluvial sands (i.e., 0.80-1.40 ϕ). However, this is the upper range of river sediments and glaciofluvial sands are less probable given the timing of glacial retreat in the region. The grain size distribution results suggest that LRA4 to LRA2 (120-167 dbs) are gravelly coarse sand and consist of a larger gravel component than upper or lower samples. It may be suggested that this represents a beach berm. Two lithic artifacts were recovered from this gravel layer and likely date to ca. 12 900 from the RSL curve. The fine-skewed and poorly sorted particle size distributions from LRA2 and LRA8 are suggestive of intertidal environments (Parrado Roman and Achab 1999). These results provide evidence for a marine regression from 25 m amsl to 27 m amsl, which would have occurred around 12 900 to 12 800 cal a BP according to the RSL curve.

6.1.3 KGP

At KGP the combination of what is interpreted as a basal marine clay, the presence of shell casts in clay crossbeds interpreted to be foreset beds and bounding stratigraphy interpreted to be topset beds, suggest that this is likely a palaeo-fan delta. Porebski and Steel (2006) propose that, in terms of ancient deltas, it makes sense to also characterize them in terms of mixed energy systems, sea level change, and position on the shelf. In these terms, KGP likely represents a bayhead delta, which forms at the end of an estuary or embayment. Bayhead deltas are typically small and funnel-shaped, whereas other types like shelf-margin deltas can be 100s of meters high and up to 10 km long (Porebski and Steel 2006). During a stable or falling sea level delta movement is only progradational and is able to cross a wide area relatively quickly and without

an excessive sediment supply (Porebski and Steel 2006). A portion of the delta and, eventually all of it, may become an alluvial fan once RSL drops below the basal toe of the delta.

The presence of a palaeo-delta provides the firmest evidence of a local RSL still stand, which would have been at approximately 32-33 m amsl. This corresponds to approximately 13 000 years ago on the RSL curve (Figure 4) and the base is only 1.5 m above the elevation of the possible palaeo-delta at Lactarius (25.5 m amsl). The slightly higher position here might result from higher elevation reaches of storm surge along this much more highly exposed shoreline. This stillstand could align with the levelling out trend in RSL from 12 000 to 13 000 years ago.

6.2 Geomorphic Evidence for RSL Stillstand and Regression

The above sites may provide specific examples of palaeo-shorelines or stillstands during the late Pleistocene to early Holocene RSL regression on Quadra Island. This research confirms the presence of palaeo-coastal deposits and archaeological material at two separate terrace elevations (e.g. 8 – 14 m amsl at CROW and 26 – 32 m amsl at Lactarius and KGP). Further archaeological shovel testing showed corroborating evidence at elevations between 12 and 45 m amsl with cultural materials found most commonly at around 26 m amsl and 30 m amsl. A total of 10 sites, including Lactarius, were found within the elevational range of 26 to 34 m amsl. Handheld GPSs were used in the field with up to 5 m spatial accuracy. These positions were only used for field validation and elevation was determined using Avenza PDF Maps for position and the LIDAR DEM for elevation. Archaeological testing also uncovered three sites, including CROW within the 10 – 14 m amsl range.

Additionally, more recent fieldwork has confirmed the presence of a lower terrace at 5 – 7 m amsl, where four archaeological sites were found (Fedje et al. 2018). For example, at Yeatman Bay, the northern tip of the south LIDAR section, there is a 6 m amsl terrace with a hard packed

beach ridge layer at 5 m amsl (100 cm dbs), containing abundant archaeological material with several radiocarbon dates between 11 000 and 10 400 cal a BP (Fedje et al. 2018). The berm (i.e., a terrace that forms in the backshore) sediment consists of a placic horizon (indicating extensive soil development and environmental stability) and contains a combination of terrestrial organics and marine diatoms. Archaeological sites associated with palaeo-beach berms have been seen in other areas of the PNW coast, including Richardson Island, in southern Haida Gwaii (Fedje and Christensen 1999) and Cohoe Creek in northern Haida Gwaii (Christensen and Stafford 2005).

The three elevational ranges on Quadra Island (i.e., 5-7 m, 8-14 m, 26-32 m amsl) could indicate possible stillstands or slow phases in RSL regression in the sea level curve. The two upper elevational ranges fall within 12 500 to 13 000 years ago based on the RSL curve (Figure 4) and could possibly correspond with the Younger Dryas cooling period (12 900 – 11 500 cal a BP; Fedje et al. 2011a), when there were late Pleistocene glacial re-advances that occurred in close proximity to the Strait of Georgia study region. The Squamish valley re-advance in Howe Sound dates to 12 800 cal a BP (Friele and Clague 2002) and the Franklin Glacier at Mt. Waddington, which is visible from Quadra Island, re-advanced between 12 910 and 12 690 cal a BP (Mood and Smith 2015). The timing of such neoglacial advances along the coast of British Columbia is highly variable. For instance, in the mid-coast of BC on Calvert Island, Eamer et al., 2017b documented a glacial re-advance around 14 500 cal a BP. Another contributing phenomenon to punctuated RSL change could be meltwater pulses. Studies show that globally there have been major step-wise intervals of sea level rise during the late Pleistocene (Khanna et al. 2017). So, it is possible that perhaps these stillstands in the late Pleistocene RSL regression on

Quadra Island represent brief sea level reversals (i.e. transgressions), although there is no data to support this interpretation in this research.

6.3 Inland Prospection for Palaeo-Shoreline sites

High potential locations produced from the archaeological potential modeling include two basic geomorphic conditions. The first relates to observed breaks in slope in topography. Relatively flat terraces above these locations might have been favourable for human occupation or activities just after RSL regression from that elevation and for some time (centuries to millennia) afterwards. The second condition is the backshore portion of these terraces where people may have lived just above the palaeo-foreshore zone during a stillstand in RSL. These areas would have been relatively well-drained with a low slope and easy access for boats. We only found one very early artifact-containing deposit (deposit of waterworn artifacts in a possible ca. 12 700 cal a BP palaeo-delta at CROW), likely because of deeper burial by colluvium from the slope behind, which would have built up over the last 13 millennia. Many of these areas also have a medium coastal complexity value, meaning these areas would often be protected embayments and thus be ideal places to spend time.

From the 10 newly uncovered archaeological sites identified during the 2015 survey, four sites were dated using radiocarbon samples (Table 1). The ages of these sites are younger than would be expected based on the elevations in comparison to the Quadra Island RSL curve. While some lithic material is diagnostic of early Holocene occupation, overall it appears that most of these sites were likely not occupied at palaeo-shoreline sites, but as terraced locations after the shoreline regressed further. This means that these inland breaks-in-slope are still valuable archaeological potential map variables and considered to have high archaeological potential throughout the Holocene.

Early Holocene archaeological sites are commonly found along palaeo-shorelines (e.g., Davis 2011; Fedje et al. 2005b; Hill 2007; Mackie et al. 2011), however, most coastal archaeological surveys on the PNW coast, and on coastlines further afield, focus on the modern shoreline (Breivik 2014; Mackie et al. 2011). This is primarily driven by access and specific research foci and creates a survey bias. For example, in the Quadra Island area of this study, clam garden, fish trap and shell midden sites on the modern shoreline tend to be much better documented than other inland site types due to concentrated survey efforts and high visibility on the modern shoreline as compared to sites on forested palaeo-shorelines. Archaeological evidence on these inland palaeo-shorelines is normally limited to stone tools and charcoal concealed at depth due to long accumulation times (12 500 to 14 500 years).

Establishment of the local RSL history has proven key to archaeological prospection in coastal settings and has led to increased inland, elevated palaeo-coastal studies in suitable areas in other regions of British Columbia. For instance, in the Dundas archipelago in northern BC, many elevated sites occur between 3 and 16 m amsl, and date as early as 11,000 cal a BP (Letham et al. 2015; McLaren et al. 2011). Similarly, in nearby Haida Gwaii, the Richardson Island site (earliest date ca. 10,500 cal a BP) is on a 19 m amsl raised terrace (i.e., archaeologically-rich berm with deposits extending from 15-19 m amsl) and 50 m inland from the modern shore while in the north of the archipelago the Cohoe Creek Site (earliest date ca. 7,800 cal a BP) is located on a stranded alluvial fan more than 100 m from the modern shore and approximately 14 m amsl (Christensen and Stafford 2005). Mackie and Sumpter (2005) found that in Haida Gwaii the distributions of early Holocene to late Holocene archaeological sites were very different. For example, early Holocene sites tended to be located on more coastally complex west-facing shorelines, whereas late Holocene sites were found on more linear north-

facing shorelines (Mackie and Sumpter 2005). This suggests the recent archaeological record may be a poor proxy for locating early archaeological sites. Over 40 raised beach sites are known for other areas of Haida Gwaii, where primarily stone tools in non-shell midden deposits were identified from between 14 and 18 m amsl elevation (Fedje et al. 2005b). Such examples illustrate the high archaeological potential for inland surveys of palaeo-shorelines in areas where RSL history is well constrained.

6.4 Effectiveness and Limitations of the Archaeological Potential Model

In order to provide useful information, effective prospecting models must accurately predict high potential site locations, but also minimize the total area captured of the high potential class (Kvamme 1988). In theory, models with extensive area coverage of the high potential zone can capture all of the known site locations, demonstrating high accuracy. However, such models also capture more non-archaeological site locations and are, therefore, less accurate than models with narrower high potential zones (Kvamme 1988). A model must minimize the high potential area but maximize number of known site locations within that area to be meaningful (Kvamme 1988). For these reasons, reducing survey area was a key objective for creating the potential map here as a research tool and this was achieved through the final map, which limited areas of high archaeological potential to 0.3% of the total land survey area. This percentage was further reduced using expert knowledge to eliminate certain unsuitable survey areas that were captured by the model, such as the middle of bogs, wetlands and bedrock shorelines. Ultimately, adding additional variables could delimit the high potential targets even further, but also add more uncertainty.

This potential mapping exercise offers a methodological approach to locating early to late Holocene sites. While the field surveys following the palaeo-shorelines did result in many newly

uncovered archaeological sites, only a few were confirmed within the target age range, with ages from 7 000 to 12 700 cal a BP. However, the primary purpose of this research was to outline an integrated approach to finding early Holocene sites in a post-glacial coastal setting. The resulting potential map is a first step in archaeological inquiry and can be refined as more data becomes revealed through fieldwork.

6.4.1 Modeling Limitations

Despite becoming used increasingly in archaeological research, predictive archaeological potential modeling is not a universally agreed-upon approach in archaeology. The main criticism of predictive modeling is environmental determinism – that it might be too heavily based on environmental data (Verhagen et al. 2007; Woodman and Woodward 2002). Environmental determinism asserts that human behaviour, including habitation choices, is primarily determined by natural factors, which undermines or ignores other (e.g., cultural) factors. One of the biggest challenges in archaeological predictive modeling is the incorporation of non-environmental variables, such as intangible cultural variables, including cognitive, aesthetic, social and political factors that influence habitation choices (Maschner 1996; Verhagen et al. 2007). It is important to stress that environmental variables are only proxies for hypothesized cultural decisions in modeling attempts.

An additional drawback of predictive modeling is that environmental factors characterize the modern landscape, but are used to approximate palaeo-landscapes (Church et al. 2000). For example, while flat slopes may be a desirable living condition, modern slopes may not always be representative of slope conditions in past environments due to subsequent landscape evolution. In other words, the further into the past we attempt to prospect, the higher the uncertainty about that past landscape because of the influence of subsequent geomorphic and ecological processes

that will alter landscape configuration, deposits and visibility. The resolution of environmental data can also introduce misrepresentation because the final map product is only as accurate as the coarsest resolution data. For these reasons, we chose to limit the number of input variables from five in initial potential map trials, to three variables in the more streamlined decision tree process. Predictive modeling is primarily used to make site discovery more efficient, rather than for more detailed site interpretation or explaining the spatial distribution of sites (Verhagen and Whitley 2012).

6.4.2 Dating Limitations

There is a discrepancy between the optical and radiocarbon ages in some cases. The optical age for CROW-3 is consistent with the associated radiocarbon age, and with the RSL curve established for Quadra Island, but the optical ages for samples CROW-1 and KGP-1 are not consistent with other age information. The optical age for sample KGP-1 is 10 700 ± 1 000 at approximately 29 m amsl (Table 3). From the RSL curve (Figure 4), this elevation should produce dates of approximately 13 000 cal a BP. The optical age for sample CROW-3 is 12 400 ± 1 100 at 190 cm dbs or approximately 12 m amsl. This age aligns more closely with the ^{14}C age, which is 12 744 – 12 566 cal a BP (UCI 193684) from a sample at 105 cm dbs (approximately 13 m amsl). Due to superposition, the deeper 12 m amsl optical age should be older than the overlying 13 m amsl ^{14}C age, so it is still too young. The optical age for CROW-1, at 115 cm dbs (13 m amsl), is substantially younger at 8 900 ± 700 cal a BP.

On average, the optical ages are approximately 2 000 years younger than the associated calibrated radiocarbon ages. The discrepancy between optical and radiocarbon ages has also been seen in aeolian samples dated on nearby Savary Island, which used the same single-aliquot regenerative-dose (SAR) protocol as that which was used for the Quadra Island and Calvert

Island samples (Biln 2017). However, the assertion that this discrepancy is real depends, to a degree, on reliability of the radiocarbon ages, all of which were derived from detrital organic material. In the case of the Savary Island samples, the radiocarbon ages came from small (< 1 cm dia.) charcoal fragments dispersed in the B-horizons of palaeosols. It is possible, therefore, that the age discrepancy at this site may be a product of older organic material being re-deposited. However, in the case of Quadra Island, this is unlikely as the radiocarbon ages align with the RSL curve established for the region (Fedje et al. in press). It is, therefore, likely that there are issues with the optical age determinations.

There are also limitations associated with the RSL curve as a tool for approximating the ages of shorelines at specific elevations (Fedje et al. in press). In particular, Figure 4 shows a dashed line from approximately 13 000 to 11 000 cal a BP that signifies that the RSL curve is not well constrained for this time period, which involves significant sea level change and is a focal period for many site locations (i.e., CROW, Lactarius and KGP). From the original RSL curve with the constraining marine to freshwater diatom data points (Fedje et al. in press), there is a lack of marine data points from approximately 75 to 15 m amsl. The data between these elevations have been interpolated, so there is a higher level of uncertainty associated with these elevations, including some of focal interest to this research (i.e., 30 m amsl).

The most common source of error associated with optical ages comes from inadequate exposure of the sand grain used for dating to sunlight before burial, and there is some suggestion of this from the magnitude of the overdispersion values measured from these samples (Table 3; see discussion in Arnold and Roberts 2009). However, inadequate sunlight exposure would yield ages that are too old. Another source of error could come from the value used for the component of the total dose rate that comes from potassium that is internal to the potassium feldspar grains

being measured. Measurement of internal potassium content is difficult and therefore not practical, so Huntley and Baril (1997) suggested an estimate of 12.5 ± 0.5 % should be used. This estimate was based on direct measurement of internal potassium content of various potassium feldspar samples, and its use has become the convention of most luminescence dating practitioners. However, of the 21 samples that Huntley and Baril (1997) analyzed, two had internal potassium concentrations significantly lower than the suggested estimate. It is possible, therefore, that use of 12.5 ± 0.5 % for our samples is incorrect (C. Neudorf pers. comm. Jan. 24, 2018). Another source of error may come from the presence of Na/Ca-rich feldspar grain contamination in the samples as the luminescence from these minerals may contribute to the measured signal (e.g., Li et al. 2010; Neudorf 2011; Ollerhead et al. 1994; Spooner 1992). However, as Huntley and Baril (1997) point out, the inclusion of a blue filter, and the efficiency of the detector (photomultiplier tube) goes a long way to reducing or eliminating the luminescence wavelengths characteristic of these feldspars species, although it has been found that some Na rich feldspars have luminescence spectra similar to those typical of K-feldspar (Baril and Huntley 2003). In light of these issues, Smedley et al. (2012) suggest standards may need to be adaptive to be more conservative as their research showed actual potassium content in their samples to be between 6 and 13%, a range similar to that found by Huntley and Baril (1997). It is also known that the standard laboratory density-separation procedures are not perfect (Biln 2017). It is suggested that the mineralogy of the separated sample be investigated, as was done by Biln (2017). It is also possible that these issues could be a result of the geologic source of the feldspar. Some studies have shown that volcanically derived feldspar sediment can produce unreliable optical ages (Tsukamoto and Duller 2008). Interestingly, recent experiments on a sample from Quadra Island (LRDS-1; Lactarius site), and on another from Savary Island

(SIDS1, site 2 of Biln 2017), showed that optical ages are much closer to, or consistent with, what is expected based on radiocarbon dating and the established RSL curve, could be found using the multiple-aliquot additive-dose with thermal transfer correction (ADTT) method (e.g., Lian et al. 1995; Lian and Roberts 2006; Mathewes et al. 2015l; Neudorf et al. 2017). These results suggest that perhaps the problem does not lie with the dosimetry, but with the SAR method when applied to the K-feldspar species at these sites. Further multiple-aliquot ADTT dating, along with mineralogical investigations and analysis of luminescence emission spectra,are currently being planned for some of the other Quadra Island and Savary Island samples to help resolve these issues.

6.4.3 Diatom Limitations

Diatoms can provide indication of depositional environment, but it is important to examine the limitations of such method. There is the possibility of contamination by redeposition by aeolian or fluvial processes. Diatom, sponge and chrysophyte cysts counts ranged from 1-30, with the rare counts of 200 or 500 (Table 2). Considering the sandy substrate that was examined, these counts are useful, but recommended minimum counts are usually at least 300 specimens (Sawai et al. 2016; Serieyssol et al. 2012). Counting protocol can also bias results (Sawai et al. 2016).

6.5 Utility of LIDAR in Archaeology

LIDAR has emerged in geomorphological and archaeological research as a vital tool for mapping and interpreting landscapes. LIDAR-derived DEMs and bare-earth DTMs can be used to improve the time and efficiency, as well as effectiveness of site discovery and field surveys (e.g., Devereux et al. 2009). Typical archaeological and sedimentological field survey methods use shovel and auger testing and often rely on serendipitous occurrences of soil exposures such

as in tree-throws, road cuts and creek channels (e.g., Mackie et al. 2011). Field-testing for early Holocene sites is especially time-consuming as non-perishable artifacts such as stone tools are often the only material evidence remaining. This requires intensive shovel testing, which takes much more time and effort than simple soil probing which is very efficient in discovering the presence of shell middens, for example (Fedje and Christensen 1999). LIDAR-derived DTMs can help to identify potential palaeo-shorelines and other features at specific elevations on the landscape that represent areas considered to have highest archaeological potential, thus saving time in the field. In addition to broad scale interpretation from LIDAR DTMs, systematic sedimentological surveys should also be conducted to confirm palaeo-shoreline positions and related geomorphic interpretations, which were limited to three sites in this study. By being able to remove the vegetation layer, LIDAR-derived DTMs also reveal much more detailed information of the terrain (i.e., bare earth) than satellite or aerial imagery. The advantages of LIDAR to archaeology have been revolutionary. From revealing historic homesteads in New England to uncovering Mayan settlements in Belize, LIDAR data are highly useful to archaeologists (Johnson and Ouimet 2014). This is why LIDAR-derived DEMs, DTMs and related topographically-derived variables (e.g., slope, aspect, etc.) are often the key inputs to archaeological predictive models (Verhagen and Whitely 2012).

The availability of high-resolution archaeological and environmental data can be a limitation of archaeological potential mapping. Access to high-resolution DEMs is often a major limitation. In British Columbia, the best available digital datasets are often in tiles of 25 m horizontal resolution DEMs (GeoBC https://www2.gov.bc.ca/gov/content/data/geographic-data-services/topographic-data/terrain) often with a vertical resolution of no finer than 10 m and based on traditional aerial photogrammetry. Thus, many geomorphic features and some archaeological

sites smaller than the 25 m pixel width cannot be identified or interpreted. It is recommended that only LIDAR or data of equivalent of 1 m^2 positional resolution with a sub-metre vertical resolution be used for predictive modeling. Together, high-resolution LIDAR and a high-resolution RSL model can be used to create an archaeological potential map and accurately locating areas of high archaeological potential to excavate to uncover archaeological material.

7 Conclusions

This research enables informed archaeological prospection for late Pleistocene/early Holocene palaeo-coastal sites through integration of technology and palaeo-landscape knowledge. Prospecting for sites has always been a challenge for archaeologists. It is especially challenging in a dynamic coastal, post-glacial, rainforest setting like Quadra Island on the PNW coast. This research outlines a novel methodological approach to archaeological prospection for palaeo-coastal sites through integrating the local relative sea level history, LIDAR and derived geomorphic data, and GIS potential mapping. It provides a roadmap for future researchers to refine and modify for archaeological prospection in similar settings.

First, the local sea level history needs to be established. Then, remote terrain sensing techniques, such as satellite imagery and LIDAR-derived DTMs can help to identify potential palaeo-shorelines and specific elevations on the landscape that represent areas considered to have highest archaeological potential. Using a technique suitable to the data and project objectives, high archaeological potential landscape variables for late Pleistocene to early Holocene coastal sites are selected and combined into a potential map to be used for field survey, which can then lead to future refinements.

The 10 m and 30 m LIDAR-derived contour maps and potential maps guide researchers to locations, however the researcher must identify the terrace or break in slope in person to determine where to test. This potential map highlights high potential archaeological areas for a certain class of sites (i.e. palaeo-shoreline campsites). It is a guiding tool for field survey that incorporates multi-lines of expert archaeological knowledge into a single output.

Lastly, select geoarchaeological sites were chosen for detailed examination to confirm presence of archaeological material and RSL regression at these locations. Sites were analyzed in

terms of sedimentological make-up, stratigraphy, microfossil content and geochronology. These sites offer site-specific examples of localized RSL regression and help to nuance the RSL curve by adding potential stillstands at elevations such as 8-14 m amsl and 26-32 m amsl. Further work and data is needed to refine the elevational range of these stillstands. In conclusion, incorporating RSL history and LIDAR into a GIS-based potential model is a methodology for archaeological prospection that has many advantages. By starting archaeological investigations with this approach, field survey efforts are more effective and the site identification rate is significantly increased. This methodological approach proved an effective technique in identifying areas of high archaeological potential for late Pleistocene to early Holocene coastal sites. In 2015 several early palaeo-coastal sites were discovered using this approach. In addition, the location of several early palaeo-coastal sites discovered in 2014, based solely on sea level history and expert palaeo-coastal knowledge (prior to obtaining LIDAR), was consistent with the projections from the model described here. Research and dating is currently ongoing and there is potential to find many more late Pleistocene to early Holocene sites through further investigation. Through modification and refinement, this integrated methodology for archaeological prospection of palaeo-coastal sites can be adapted for other areas of the PNW coast and other coastal landscapes.

It is also recommended that the potential model is run for other elevations that may represent potential palaeo-shorelines. There are likely many more subtle palaeo-shorelines at elevations from 0 to 197 m amsl. Therefore, there is opportunity to employ the model at various elevations and also refine the model as future research and field surveying brings forth more site locations and more information on where early peoples may have lived. With these site locations of known inland and elevated palaeo-coastal sites, sufficient site location data may emerge in the

future to perform an inductive style potential model. This type of model is valuable as it uses known site locations as training data to create a potential model that statistically selects variables that are highly correlated with known site locations. It would also be beneficial to test more locations to better understand how the model performs in predicting high archaeological potential areas. More non-site location is needed. It should be noted that this model only captures areas of high archaeological potential and that all other areas are simply labeled not classified. This does not mean that locations not captured by the model have little or no archaeological potential, but that this model and its select variables have not captured those locations. For research and consulting archaeological purposes, all areas on the landscape should be considered as having some degree of archaeological potential.

References

Allen, K. M., Green, S. and E.B. Zubrow. (eds.). 1990. *Interpreting Space: GIS and Archaeology*. London: Taylor and Francis.

Altschul, J. 1990. Red flag models: the use of modelling in management contexts. In *Interpreting Space: GIS and Archaeology* K. Allen, S. Green, and E. Zubrow (eds.). London: Taylor and Francis: 226-238.

Arcas Consulting Ltd. 2002. *GIS Modelling of Archaeological Potential for the TFL Forest LTD.- Johnstone Strait Operation Area*.

Arcas Consulting Ltd. 2005. *TFL Forest Ltd. Johnstone Strait Operation Area Revised AOA Modelling Study Report*.

Arnold, L. J. and R. G. Roberts. 2009. Stochastic modelling of multi-grain equivalent dose (De) distributions: Implications for OSL dating of sediment mixtures. *Quaternary Geochronology* 4: 204-230.

Auclair, M., Lamothe, M., and S. Huot. 2003. Measurement of anomalous fading for feldspar IRSL using SAR. *Radiation Measurements* 37: 487-492.

Baker, R. G. V., and R. J. Haworth.1997. Further evidence from relic shellcrust sequences for a late Holocene higher sea level for eastern Australia. *Marine Geology 141*(1): 1–9.

Baril, M.R., and D. J. Huntley. 2003. Infrared stimulated luminescence spectra of irradiated feldspars. *Journal of Physics: Condensed Matter,* 15: 8029–8048.

Barrie, J. V. and K. W. Conway. 1999. Late Quaternary glaciation and postglacial stratigraphy on the Northern Pacific Margin of Canada. *Quaternary Research* 51: 113-123.

Battarbee, R.W, V. J. Jones, R.J. Flower, N.G. Cameron, H. Bennion, L. Carvalho and S. Juggins, 2006. Diatoms. In: *Tracking Environmental Change Using Lake Sediments*: Vol 3: Terrestrial, Algal, and Siliceous Indicators (J. P. Smol, H.J. Birks and W. M. Last, eds.). Kluwer Academic Publishers, Dordrecht, The Netherlands:155-202.

B.C. Ministry of Forests Lands and Natural Resource Operations 2009. *Archaeological Overview Assessments as General Land-Use Planning Tools - Provincial Standards and Guidelines*. Retrieved from https://www.for.gov.bc.ca/ftp/archaeology/external/!publish/web/professionals/FIA_AOA_Standards_2009.pdf

Bianchi, T.S. 2016. *Deltas and humans: a long relationship now threatened by global change*. New York: Oxford University Press.

Biln, L. 2017. Optical dating of stabilized parabolic dune, Savary Island, British Columbia (master's thesis). Simon Fraser University, Canada.

Blott, S. 2000. GRADISTAT version 4.0: A grain size distribution and statistics package for the analysis of unconsolidated sediments by sieving or laser granulometer. Crowthorne: Kenneth Pye Associates Ltd, Crowthorne Enterprise Centre.

Breivik, M. 2014. Palaeo-oceanographic development and human adaptive strategies in the Pleistocene–Holocene transition: A study from the Norwegian coast. *The Holocene* 24(11): 1478–1490.

Campeau, S., Pienitz, R., and A. Hequette. 1998. *Diatoms from the Beaufort Sea coast, southern Arctic Ocean (Canada): Modern analogues for reconstructing Late Quaternary environments and relative sea levels.* (Bibliotheca Diatomologica.) Gebruder Borntraeger, Stuttgart.

Canning, S. 2005. "BELIEF " in the past : Dempster-Shafer theory, GIS and archaeological predictive modelling. *Australian Archaeology* 60: 6-15.

Carlson, R. J. and J.F. Baichtal. 2015. A predictive model for locating early Holocene archaeological sites based on raised shell-bearing strata in Southeast Alaska, USA. *Geoarchaeology 30*(2): 120-138.

Carson, M. T. 2014. Paleo-terrain research: finding the first settlement sites of remote Oceania. *Geoarchaeology 29*(3): 268–275.

Challis, K., Forline, P. and M. Kincey. 2011. Automatic detection of pit structures in airborne laser scanning data. *Archaeological Prospection 18*: 279-289.

Charman, D. J. 2015. Testate Amoebae. In *Handbook of sea level research* (I. Shennnan, A.J. Long and B.P. Horton, eds.): 281-294. Hoboken, NJ: John Wiley and Sons, Ltd.

Christensen, T. and J. Stafford. 2005. Raised beach archaeology in Northern Haida Gwaii: preliminary results from the Cohoe Creek site. In *Haida Gwaii: Human History and Environment from the time of Loon to the Time of the Iron People (*D. Fedje and R. Mathewes, eds.). Vancouver: UBC Press: 245-273.

Church, T., Brandon, R. J. and G. R. Burgett. 2000. GIS applications in archaeology: method in search of theory. In *Practical Applications of GIS for Archaeologists*. (K. L. Wescott and R. J. Brandon, eds.) Philadelphia: Taylor and Francis.

Clague, J.J. 1976. Quadra Sand and its relation to the late Wisconsin glaciation of southwest British Columbia, Canadian Journal of Earth Sciences 13(6): 803-815.

Clague, J.J. 1981. Late Quaternary geology and geochronology of British Columbia. part 2: summary and discussion or radiocarbon-dated Quaternary history. *Geological Survey of Canada*. Paper 80-35.

Clague, J., Harper, J. R., Hebda, R. J. and D. E. Howes. 1982. Late Quaternary sea levels and crustal movements, coastal British Columbia. *Canadian Journal of Earth Sciences 19*(3): 597-618.

Clague, J. J. and T. S. James. 2002. History and isostatic effects of the last ice sheet in southern British Columbia. *Quaternary Science Reviews 21*: 71-87.

Colella, A. & Prior, D. B. (eds) 1990. *Coarse-Grained Deltas*. Special Publication Vol. 10 of the International Association of Sedimentologists. Oxford, London, Edinburgh, Boston, Melbourne, Paris, Berlin, Vienna: Blackwell Scientific Publications

Conolly, J. and M. Lake. 2006. *Geographical Information Systems in Archaeology*. Cambridge: Cambridge University Press.

Dalla Bona, L. 2000. Protecting cultural resources through forest management planning in Ontario using archaeological predictive modelling. In *Practical Applications of GIS for Archaeologists: A Predictive Modeling toolkit* (K. Wescott and R. J. Brandon, eds.). London: Taylor and Francis: 73-99.

Davidson-Arnott, R. 2010. *Introduction to Coastal Processes and Geomorphology*. Cambridge: Cambridge University Press.

Davis, J. C. 2002. *Statistics and data analysis in geology* (3rd ed.). New York and Chichester: Wiley.

Davis, L. G. 2011. The North American paleocoastal concept reconsidered. In *Trekking the Shore: Changing Coastlines and the Antiquity of Coastal Settlement (*N. Bicho, J. Haws, and L. Davis, eds.). New York: Springer: 3-26

Devereux, B. J., Amable, G. S. and P. Crow. 2008. Visualisation of LIDAR terrain models for archaeological feature detection. *Antiquity 82*: 470-479.

Diatoms of the United States (n.d.). Retrieved from https://westerndiatoms.colorado.edu.

Dixon, E., Heaton T., Fifield T., Hamilton T., Putnam D. and F. Grady. 1997. Late quaternary regional geoarchaeology of Southeast Alaska Karst: a progress report. *Geoarchaeology* 12: 689-712.

Duncan, R. B. and K. A. Beckman. 2000. The application of GIS predictive site location models within Pennsylvania and West Virginia. In *Practical Applications of GIS for Archaeologists* (K. L. Wescott and R. J. Brandon, eds.). Philadelphia: Taylor and Francis: 37-61.

Eamer, J., Shugar, D., Walker, I., Lian, O., and C. Neudorf. 2017a. Distinguishing depositional setting for sandy deposits in coastal landscapes using grain shape. *Journal of Sedimentary Research.* 87: 1-11.

Eamer, J., Shugar, D., Walker, I., Neudorf, C., Lian, O., Eamer, J., Bryce, J. and L. Biln. 2017b. Late Quaternary landscape evolution in a region of stable postglacial relative sea levels, British Columbia central coast, Canada. *Boreas* 83: 1-16.

Ebert, J. I. 2000. The state of the art in "inductive" predictive modeling: seven big mistakes (and lots of smaller ones). In *Practical Applications of GIS For Archaeologists. A Predictive Modeling Kit* (K. L. Wescott and R. J. Brandon, eds.). London: Taylor and Francis: 129-134.

Emery, K.O. 1968 Relict sediments on continental shelves of the world. *American Association of Petroleum Geologists* 52: 445-464

Engisch, C., Bonner, F., Russel, S., Grant, O., Nicholls, N. and D. Hall. 2004. *Final Report: Archaeological Inventory Study of Weyerhaeser TFL 39 Blocks 2 and 5 in partial fulfillment of Permit 2003-328*.

Erlandson, J., Moss, M. and M. Deslauriers. 2008. Life on the edge: early maritime cultures of the Pacific Coast of North America. *Quaternary Science Reviews 27*(23-24): 2232–2245.

Espa, G., Benedetti, R., De Meo, a., Ricci, U. and S. Espa. 2006. GIS based models and estimation methods for the probability of archaeological site location. *Journal of Cultural Heritage 7*(3): 147-155.

European Register of Marine Species. n.d. Retrieved from http://www.marbef.org/data/erms.php.

Fallu, M,. Allaire N. and R. Pientiz. 2000. *Freshwater Diatoms from Northern Quebec and Labrador (Canada)*. Bibliotheca Diatomologica 45. Gebruder Borntraeger, Stuttgart.

Fedje, D. and T. Christensen. 1999. Modeling paleoshorelines and locating early Holocene coastal sites in Haida Gwaii. *American Antiquity 64*(4): 635–652.

Fedje, D. and H. Josenhans. 2000. Drowned forests and archaeology on the continental shelf of British Columbia, Canada. *Geology 28*(2): 99.

Fedje, D., Josenhans, H., Clague, J. J., Barrie, J. V., Archer, D. J. and J.R. Southon. 2005a. Hecate Strait paleoshorelines. In *Haida Gwaii: Human History and Environment from the Time of Loon to the Time of the Iron People* (D. Fedje and R. Mathewes, eds.). Vancouver: UBC Press: 21-37.

Fedje, D. W., T. Christensen, H. Josenhans, J, Strang, and J. B. McSporran 2005b. Millennial tides and shifting shores: Archaeology on a dynamic landscape. In *Haida Gwaii, human history and environment from the time of Loon to the time of the Iron People* (D. W. Fedje and R. W. Mathewes, eds.). Vancouver: UBC Press: 163-186.

Fedje, D., Mackie, Q., Dixon, E. J. and T. Heaton. 2004. Late Wisconsin environments and archaeological visibility on the northern Northwest Coast. In *Entering America: Northeast Asia and Beringia Before the Last Glacial Maximum (*D. B. Madsen, ed.). Salt Lake City: The University of Utah Press: 97-138

Fedje, D., Mackie, Q., Lacourse, T. and D. McLaren. 2011a. Younger Dryas environments and archaeology on the Northwest Coast of North America. *Quaternary International 242*(2): 452-462.

Fedje, D., Mackie, Q., Smith, N., Mackie, A., McSporran, J., Vogelaar, C., Lausanne, A. and A. Abbott. 2016. DILA Research Report: Annual Report for 2014 Field Season. HCA Permit 2014-0046.

Fedje, D., Mackie, Q., Smith, N. F., and D. McLaren. 2011b. Function, visibility, and interpretation of archaeological assemblages at the Pleistocene-Holocene transition in Haida Gwaii. In *From the Yenisei to the Yukon: Interpreting Lithic Assemblage Variability in Late Pleistocene/Early Holocene Beringia* (T. Goebel and I. Buvit, eds.). College Station: Texas A and M University Press: 23-42

Fedje, D., McLaren, D., James, T., Mackie, Q., Smith, N., and J. Southon. In review, 2018. A revised sea level history for Quadra Island on the West coast of Canada. *Quaternary Science Reviews*.

Fernandez, J., Singhania, A., Caceres, K.C., Slatton, Starek, M. and R. Kumar. 2007. *An overview of lidar point cloud processing software*. GEM Center Report No. Rep_2007-12-001. Retrieved from http://ncalm.cive.uh.edu/sites/ncalm.cive.uh.edu/files/files/publications/reports/GEM_Rep_2007_12_001.pdf

Fladmark, K. R. 1979. Alternate migration corridors for early man in North America. *American Antiquity*, *44*(1): 55–69.

Flood, P.G. and Frankel, E. 1989. Late Holocene higher sea level indicators from eastern Australia. *Marine Geology* 90:193-195.

Folk, R.L, and W.C. W. 1957. Brazos River bar: a study in the significance of grain size parameters. *Journal of Sedimentary Petrology* 27: 3–26.

Friedman, G.M. 1962. On sorting, sorting coefficients, and the lognormality of the grain-size distribution of sandstones. *The Journal of Geology* 70(6): 737-753.

Friele, P.A. and J.J. Clague 2002. Younger Dryas readvance in Squamish river valley, southern Coast mountains, British Columbia. *Quaternary Science Reviews* 21:1925-1933

Galbraith, R.F., Roberts, R.G. 2012. Statistical aspects of equivalent dose and error calculation and display in OSL dating: An overview and some recommendations. *Quaternary Geochronology* 11: 1-27.

Gauvreau, A. and D. McLaren. 2017. Long term cultural landscape development at (EkTb-9) Triquet Island, BC, Canada. Paper presented at the *50th Annual Meeting of the Canadian Archaeological Association*, Ottawa, Canada.

Gee, G.W. and J.W. Bauder. 1986. Particle-size analysis. In *Methods of Soil Analysis, Part 1. Physical and Mineralogical Methods, Agronomy Monograph No. 9* (A. Klute, ed.). 2nd Edition. Madison, WI: American Society of Agronomy/Soil Science Society of America: 383-411.

GeoBC. n.d.. *Gridded DEMS.* Retrieved December 15, 2015, from https://www2.gov.bc.ca/gov/content/data/geographic-data-services/topographic-data/terrain

Gilbertson, D. D. 1995. Studies of lithostratigraphy and lithofacies: a selective review of research developments in the last decade and their applications to geoarchaeology. In *Archaeological Sediments and Soils: Analysis, Interpretation and Management* (A. J. Barham and R. I Macphail, eds). London: Institute of Archaeology: 99-144

Graves, D. 2011. The use of predictive modelling to target Neolithic settlement and occupation activity in mainland Scotland. *Journal of Archaeological Science 38*(3): 633–656.

Goebel, T., Waters, M. R. and D. H O'Rourke. 2008. The late Pleistocene dispersal of modern humans in the Americas. *Science 319*(5869): 1497-1502.

Guthrie, R. H. 2005. *Vancouver Island surficial Geology. Geomorphology of Vancouver Island: extended legends to nine thematic maps*. Victoria, B.C.

Harbo, R. 1997. *Shells and shellfish of the Pacific Northwest.* Madeira Park, B.C.: Harbour Publishing.

Hill, C. L. 2007. Geoarchaeology and late glacial landscapes in the western Lake Superior region, Central North America. *Geoarchaeology 22*(1): 15–47.

Hudak, G. J., Hobbs, E., Brooks, A., Sersland, C. A. and C. Phillips. 2002. *Mn/model final report phases 1-3, 2002: A predictive model of precontact archaeological site location for the state of Minnesota. St. Paul*. *Minnesota Department of Transportation*. Retrieved from http://www.dot.state.mn.us/mnmodel/P3FinalReport/final_report.html

Huntley, D. J., and M. R. Baril. 1997. The K content of the K-feldspars being measured in optical dating or in thermoluminescence dating, *Ancient TL* 15: 11–13.

Huntley, D.J., and M. Lamothe. 2001. Ubiquity of anomalous fading in K-feldspars and the measurement and correction for it in optical dating. *Canadian Journal of Earth Sciences* 38: 1093-1106.James, T., Gowan, E. J., Hutchinson, I., Clague, J. J., Barrie, J. V. and K. Conway. 2009. Sea-level change and paleogeographic reconstructions, southern Vancouver Island, British Columbia, Canada. *Quaternary Science Reviews 28*(13-14): 1200–1216.

James, T. S., Hutchinson, I., Vaughn Barrie, J., Conway, K. and D. Mathews. 2005. Relative sea-level change in Northern Strait of Georgia, British Columbia. *Géographie Physique et Quaternaire 59*(2-3):113.

Johnson, K. and W. B. Ouimet. Rediscovering the lost Archaeological landscape of southern New England using airborne light detection and ranging (LiDAR). Journal of Archaeological Science 43: 9-20

Josenhans, H.W., Fedje, D., Pientiz, R. and J. Southon. 1995. Early humans and rapidly changing Holocene sea levels in the Queen Charlotte Islands-Hecate Strait, British Columbia, Canada. *Science* 277(5322): 71-74.

Kamermans, H. 2000. Land evaluation as predictive modelling: a deductive approach. In *Beyond the Map: Archaeology and Spatial Technologies (*G. Lock, ed.). Amsterdam: IOS Press:124-146

Kamermans, H., Luesen, M. Van, and P. Verhagen. 2009. Archaeological prediction and risk management. In *Archaeological Prediction and Risk Management: Alternatives to Current Practice* (H. Kamermans, M. Van Luesen, and P. Verhagen, eds.). Netherlands: Leiden Univeristy Press: 9-19.

Kelsey, H. 2015. Geomorphological indicators of past sea levels. In *Handbook of sea level research* (Shennnan, I., Long, A.J. and B.P. Horton, eds.). Hoboken: John Wiley and Sons, Ltd.: 66-82.

Kenady, S. M., Wilson, M. C., Schalk, R. F. and R. R Mierendorf. 2010. Late Pleistocene butchered bison antiquus from Ayer Pond, Orcas Island, Pacific Northwest: Age confirmation and taphonomy. *Quaternary International 233*(2): 1-12.

Khanna, P., A.W. Droxler, J.A. Nittrouer, J.W. Tunnell and T.C. Shirley. 2017. Coralgal reef morphology records punctuated sea-level rise during the last deglaciation. *Nature Communications* 8(1046): 1-8.

Kvamme, K. 1985. Fundamentals and potential of geographic information system techniques for archaeological spatial research. In *The 50th Annual Meeting of the Society for American Archaeology*. Denver.

Kvamme, K. 1988. Development and testing of quantitative models. In *Quantifying the Present and Predicting the Past: Theory, Method, and Application of Archaeological Predictive Modeling* (J. Judge and L. Sebastian, eds.): 325-428. Denver: US Department of the Interior, Bureau of land Management Service Centre.

Kvamme, K. 2001. There and back again: views on the development of predictive location modeling in archaeology. In *Keynote address given at the conference on GIS and Archaeological Predictive Modeling: Large-scale Approaches to Establish a Baseline for Site Location Models*. Illinois.

Kvamme, K. 2006. There and back again: revisiting archaeological locational modeling. In *GIS and Archaeological Site Location Modeling (*M. Mehrer and K. Wescott, eds.). Florida: Taylor and Francis: 2-34.

Lake, M. and P. E. Woodman. 2003. Visibility studies in archaeology: A review and case study. *Environment and Planning B: Planning and Design 30*: 689–707.

Lamb, A. 2005. *Marine Life of the Pacific Northwest: A Photographic Encyclopedia of Invertebrates, Seaweeds and Selected Fishes*. Madeira Park, B.C.: Harbour Publishing.

Letham, B., Martindale, A., Macdonald, R., Guiry, E. Jones, J. and K. Ames. 2016. Postglacial relative sea-level history of the Prince Rupert area, British Columbia, Canada. *Quaternary Science Reviews* 153: 156-191.

Letham, B., Martindale, A., McLaren, D. and K. Ames. 2015. Holocene settlement history of the Dundas Islands archipelago: Northern British Columbia. *BC Studies* 187: 51-84.

Lepofsky, D., N.F. Smith, Cardinal, N., Harper, J., Morris, M., Gitla (Elroy White), Bouchard, R., Kennedy, D.I. D., Salomon, A.K., Puckett, M., Rowell, K. and E. McLay. 2015. Ancient shellfish mariculture on the Northwest Coast of North America. *American Antiquity* 80(2): 236-259.

Lian, O.B. 2013. Optical dating. In *The Encyclopedia of Quaternary Science*, vol 2 (S.A Elias, ed.): 653-666.

Lian, O.B., Hu, J., Huntley, D.J., and Hicock, S.R. 1995. Optical dating studies of Quaternary organic-rich sediments from southwestern British Columbia and northwestern Washington. *Canadian Journal of Earth Science*s, 32: 1194–1207.

Lian, O. B. and R. G. Roberts. 2006. Dating the Quaternary: progress in luminescence dating of sediments. *Quaternary Science Reviews* 25: 2449–2468.

Li, B., Li, S-H., Duller, G., and A. Wintle. 2011. Infrared stimulated luminescence measurements of single grains of K-rich feldspar for isochron dating. *Quaternary Geochronology* 6: 71-81.

Mackie, Q. 2001. *Settlement archaeology in a fjordland archipelago: network analysis, social practice, and the built environment of Western Vancouver Island, British Columbia, Canada since 2,000 BP*. Ph.D. Dissertation. Victoria: University of Victoria.

Mackie, Q., Davis, L., Fedje, D., McLaren, D., and A. Gusick. 2013. Locating Pleistocene-age submerged archaeological sites on the Northwest Coast: current status of research and future directions. In *Paleoamerican Odyssey (*K. Graf, C. Ketron, and M. Waters eds). College Station: Center for the Study of the First Americans, Texas AandM University: 133-147.

Mackie, A. P., and I. D. Sumpter. 2005. Shoreline settlement patterns in Gwaii Haanas during the early and late Holocene. In *Haida Gwaii: Human History and Environment from the Time of Loon to the Time of the Iron People (*D. Fedje and R. Mathewes, eds). Vancouver: UBC Press: 337-371.

Maschner, H. D. 1996. The politics of settlement choice on the Northwest coast: Cognition, GIS, and coastal landscapes. In *Anthropology, Space, and Geographic Information Systems* (M. Aldenderfer and H. Maschner, eds): 175-189. New York: Oxford University Press.

Maschner, H. D., and Stein, J. W. 1995. Multivariate approaches to site location on the Northwest Coast of North America. *Antiquity 69*(262): 61–73.

Mather, P. M. 2004. *Computer Processing of Remotely-Sensed images* (3rd ed.). Chichester: Wiley.

Mathewes, R.W., Lian, O.B., Clague, J.J., and Huntley, M. 2015. Early Wisconsinan (MIS 4) glaciation on Haida Gwaii, British Columbia, and implication for biological refugia. *Canadian Journal of Earth Sciences*, 52: 939–951.

McLaren, D., Fedje, D., Dyck, A., Mackie, Q., Gauvreau, A and J. Cohen. 2018. Terminal Pleistocene epoch human footprints from the Pacific coast of Canada. *PLOS ONE* 13(3): e0193522.

McLaren, D., Fedje, D., Hay, M. B., Mackie, Q., Walker, I. J., Shugar, D.H., and C. Neudorf. 2014. A post-glacial sea level hinge on the central Pacific coast of Canada. *Quaternary Science Reviews 97*:148–169.

McLaren, D., Martindale, A., Fedje, D., and Q. Mackie. 2011. Relict shorelines and shell middens of the Dundas Island Archipelago. *Canadian Journal of Archaeology 35*: 86–116.

McLaren, D., Rahemtulla, F., Gitla (White, E.) and D. Fedje. 2015. Prerogative, sea level, and the strength of persistent places: archaeological evidence for long-term occupation of the Central Coast of British Columbia. *BC Studies*. 187: 155-191.

Menard, S. 2002. *Applied Logistic Regression* (2nd ed.). Thousand Oaks, London and New Delhi: Sage.

Millennia Research Limited Research Limited. 2007. *Permit 2007-048: Campbell River Forest District Archaeological Overview Assessment*. Victoria, B.C.

Mitchell, D, 1990. Prehistory of the coasts of Southern British Columbia and Northern Washington. In The Handbook of North American Indians (W. Suttles, ed.): Vol 7: .The Northwest Coast. Washington: Smithsonian Institution, 340-358.

Mood, B.J. and D.J. Smith. 2015. Latest Pleistocene and Holocene behaviour of Franklin Glacier, Mt. Waddington area, British Columbia Coast Mountains, Canada. *The Holocene* 25: 74 – 94.

Monteleone, K. R., Dixon, E. J. and A. D. Wickert. 2012. Lost Worlds: A predictive model to locate submerged archaeological sites in SE Alaska, USA. *CAA2012 Proceedings of the 40th Conference in Computer Applications and Quantitative Methods in Archaeology,* Southampton, UK.

Moon, L. 1993. *Archaeological Predictive Modeling: an Assessment*. Retrieved from http://archive.ilmb.gov.bc.ca/risc/o_docs/culture/016/assets/016.pdf

Nemec, W. and R.J. Steel. 1988. What is a fan delta and how do we recognize it? In Fan Deltas: Sedimentology and Tectonic Settings (Nemec, W, and R.J. Steel, eds): 1-13. Glasgow: Blackie and Son.

Neudorf, C.M. 2011. Luminescence investigation into the time of final deposition of Toba volcanic ash and artefact-bearing alluvial sediments in the Middle Son Valley, Madhya Pradesh, India. PhD Dissertation. Wollongong, University of Wollongong.

Neudorf, C.M., Lian, O.B., Biln, L.C.M., Bryce, J.K., Eamer, J.B.R., Smith, N., Shugar, D.H., Walker, I.J., Fedje, D., Lausanne, A., and Clague, J.J. 2017. Optical dating sediments from coastal British Columbia: Successes, challenges, and plans for the future. GSA 2017 Annual Meeting & Exposition, October 22-25, Seattle, Washington. *Abstracts with Programs,* Vol. 49, No. 6

Neudorf, C. M., Lian, O. B., Walker, I. J., Shugar, D. H., Eamer, J. B. R., and L. C. M. Griffin. 2015. Toward a luminescence chronology for coastal dune and beach deposits on Calvert Island, British Columbia central coast, Canada. *Quaternary Geochronology* 30: 275–281.

Ollerhead, J., Huntley, D.J. and G. W. Berger. 1994. Luminescence dating of sediments from Buctouche Spit, New Brunswick. *Canadian Journal of Earth Sciences* 31: 523-531.

Otvos, E. G. 2000. Beach ridges – definitions and significance. *Geomorphology* 32: 83-108.

Owen, G., and J. A. Matthews. 2014. Alluvial Fan. In *Encyclopedia of Environmental Change* (J. A. Matthews, ed.). Vol 1, pp. 34. Thousand Oaks, Sage Publications Limited.

Parrado Roman, J.M. and J. Achab. 1999. Grain-size trends associated with sediment transport patterns in Cadiz Bay (southwest Iberian Peninsula). Boletín Instituto Español de Oceanografía 15(1-4): 269-282.

Pientiz, R.. Fedje D., and M. Poulin. 2003 *Marine and Non-Marine Diatoms from the Haida Gwaii Archipelago and Surrounding Coasts, Northeastern Pacific, Canada*. Bibliotheca Diatomologica 48. Gebruder Borntraeger, Stuttgart.

Porebski, S. J., and R. J. Steel. 2006. Deltas and Sea-Level Change. *Journal of Sedimentary Research* 76(3): 390–403.

Pratson, L. F., Nittrouer, C. A., Wiberg, P. L., Steckler, M. S., Swenson, J. B., Cacchione, D. A., Karson, J. A., Murray, A. B., Wolinsky, M. A., Gerber, T. P., Mullenbach, B. L., Spinelli, G. A., Fulthorpe, C. S., O'grady, D. B., Parker, G., Driscoll, N. W., Burger, R. L., Paola, C., Orange, D. L., Field, M. E., Friedrichs, C. T., and J.J. Fedele. 2007. Seascape Evolution on Clastic Continental Shelves and Slopes. In: *Continental Margin Sedimentation: From Sediment Transport to Sequence Stratigraphy* (Nittrouer, C. A., Austin, J. A., Field, M. E., Kravitz, J. H., Syviski, J. P. M., and P.L. Wiberg, eds): 339-380. Oxford: Blackwell Publishing Ltd

Punke, M. 2002 *Predictive Locational Modeling of the Late Pleistocene Archaeological Sites on the Southern Oregon Coast using Geographic Information System (GIS)*. M.A. Thesis. Corvallis: Oregon State University.

Roberts, R. G., Jacobs, Z., Li, B., Jankowski, N. R., Cunningham, A. C., & Rosenfeld, A. B. 2015. Optical dating in archaeology: Thirty years in retrospect and grand challenges for the future. *Journal of Archaeological Science* 56: 41–60

Rodríguez, J. G., and A. Uriarte, A. 2009. Laser diffraction and dry-sieving grain size analyses undertaken on fine- and medium-grained sandy marine sediments: a note. *Journal of Coastal Research* 25(1): 257–264.Sanders, A. 2009. Exploring the utility of computer technologies and human faculties in their spatial capacities to model the archaeological potential of lands: Holocene archaeology in northeast Graham Island, Haida Gwaii, British Columbia, Canada. M.A. Thesis. Victoria: University of Victoria.

Sawai, Y., Horton, B. P., Kemp, A. C., Hawkes, A. D., Nagumo, T., and A.R. Nelson. 2016. Relationships between diatoms and tidal environments in Oregon and Washington, USA. *Diatom Research* 31(1): 17–38

Schiffer, M. 1987. Formation processes of the archaeological record. University of New Mexico Press, Albuquerque.

Shennan, I. 1982. Interpretation of the Flandrian sea-level data from the Fenland, England. *Proceedings of the Geologists' Association* 93: 53-63.

Shennan, I. 1986. Flandrian sea-level changes in the Fenland, II: Tendencies of sea-level movement, altitudinal changes and local and regional factors. *Journal of Quaternary Science* 1: 155-179.

Schmaltz, E., Märker, M., Rosner, J. and A. Kandel. 2014. The integration of landscape processes in archaeological site prediction in the Mugello basin (Tuscany / Italy). In *Proceedings of the 42nd Annual Conference on Computer Applications and Quantitative Methods in Archaeology, CAA 2014, 21st century Archaeology* (F. Giligny, F. Djindjian, L. Costa, and P. Moscati eds.: 1-9.

Serieyssol, K. K., Cubizolle, H., Tourman, A., and C. Latour-Argant. 2012. Holocene evolution of two ponds on the Devès Plateau in the French Massif Central. *Diatom Research 27*(4): 189–211.

Sevon, W.D. 1966. Distinction of New Zealand beach, dune and river sands by their grain size distribution characteristics. New Zealand Journal of Geology and Geophysics 9(3): 212-223.

Shugar, D., Walker, I. J., Lian, O. B., Eamer, J. B. R., Neudorf, C., McLaren, D. and D. Fedje. 2014. Post-glacial sea-level change along the Pacific coast of North America. *Quaternary Science Reviews 97*: 170-192.

Smedley, G.A.T. Duller, N.J.G. Pearce, and H.M. Roberts. 2012. Determining the K-content of single-grains of feldspar for luminescence dating. *Radiation Measurements.* 47: 790-796.

Spooner, N.A. 1992. Optical dating: preliminary results on the anomalous. *Quaternary Science Reviews* 11: 139-145.

Storti, F and F. Balsamo. 2010. Particle size distributions by laser diffraction: sensitivity of granular matter strength to analytical operating procedures. *Solid Earth* 1:25–48

Stein, J. 2008. Geoarchaeology and archaeostratigraphy view from a northwest coast shell midden. In *Case Studies in Environmental Archaeology* (E. Reitz, C. Scarry, M. Scudder, and J. Sylvia, eds.) New York: Springer New York: 61-80.

Svendsen J.I. and Mangerud J. 1987. Late Weichselian and Holocene sea-level history for a cross-section of Western Norway. *Journal of Quaternary Science* 2: 113–132.

Tamura, T. 2012. Beach ridges and prograded beach deposits as palaeoenvironment records. *Earth-Science Reviews* 114(2012): 279-297.

Talling, P. J. 1998. How and where do incised valleys form if sea level remains above the shelf edge? *Geology 26*(1): 87-90.

Tsukamoto, S. and G.A.T. Duller. 2008. Anomalous fading of various luminescence signals from terrestrial basaltic samples as Martian analogues. *Radiation Measurements* 43(2–6): 721-725.

van Leusen, P. M., Millard, A. R. and B. Ducke. 2009. Dealing with uncertainty in archaeological prediction. In *Archaeological Prediction and Risk Management. Alternatives to current approaches* (H. Kamermans, M. van Leusen and P. Verhagen, eds). Leiden: Leiden University Press: 123–173.

Verhagen, P., Kamermans, H., Leusen, M. Van, Deeben, J. and D. Hallewas. 2004. First thoughts on the incorporation of cultural variables into predictive modelling. *CAA 2004 Proceedings of the 32th Conference in Computer Applications and Quantitative Methods in Archaeology*, 203–210.

Verhagen, P., Kamermans, H., van Leusen, M., Deeben, J., Hallewas, D. and P. Zootbrood. 2007. First thoughts on the incorporation of cultural variables into predictive modelling. In *Case studies in archaeological predictive modelling (*P. Verhagen, ed.). Leiden: Amsterdam University: 203-210.

Verhagen, P., and T.G. Whitley. 2012. Integrating archaeological theory and predictive modeling: a live report from the scene. *Journal of Archaeological Method and Theory* 19 (1): 49-100.

Warren, R. E. 1990. Predictive modelling in archaeology: A Primer. In *Interpreting Space: GIS and Archaeology* (K.M.S. Allen, S.W. Green, and E.B. Zubrow, eds). London: Taylor and Francis: 90-111.

Warren, R., and D. L. Asch. 2000. A predictive model of archaeological site location in the eastern Prairie Peninsula. In *Practical Applications of GIS for Archaeologists* (K. L. Wescott and R. J. Brandon eds.). London: Taylor and Francis: 5-25

Waters, M., Stafford, T. J., McDonald, H., Gustafson, C., Ramussen, M., Cappellini, E., Olsen, J., Szklarczyk, D., Jensen, L., Gilbert, M., and E. Willerslev. 2011. Pre-Clovis mastadon hunting 13,800 years ago at the Manis Site, Washington. *Science 334*, 351–354.

Weerts, H. J. T., and W.E. Westerhoff. 2007. Quaternary Stratigraphy/Lithostratigraphy. In *Encyclopedia of Quaternary Science* (S. A. Elias, ed.). pp 2826-2840. Elsevier, Oxford.

Wescott, K., and J. Kuiper, J. 2000. Using a GIS to Model Prehistoric Site Distributions in the Upper Chesapeake Bay. In *Practical Applications of GIS for Archaeologists* (K. L. Wescott and R. J. Brandon eds.). London: Taylor and Francis: 59-72.

Wheatley, D., and M. Gillings (eds). 2002. *Spatial Technology and Archaeology: the archaeological applications of GIS Title*. London: Taylor and Francis.

Wintle, A.G., 1997. Luminescence dating: laboratory procedures and protocols. *Radiation Measurements* 27: 769-817.

Wolfe, SA, Walker, IJ, Huntley, DJ. 2008. Holocene Coastal Reconstruction, Naikoon Peninsula, Queen Charlotte Islands, British Columbia. *Geological Survey of Canada, Current Research*.

Woodman, P. E. 2000. A predictive model for Mesolithic site location on Islay using logistic regression and GIS. In *Hunter-Gatherer Landscape Archaeology: The Southern Hebrides Mesolithic Project 1988-98* (S. Mithen ed.) Vol 2. Cambridge: McDonald Institute for Archaeological Research. 445–464.

Woodman, P. E. and M. Woodward 2002. The use and abuse of statistical methods in archaeological site location modeling. In *Contemporary themes in Archaeological Computing* (D. Wheatley, G. Earl, and S. Poppy eds.). Oxford: Oxbow Books: 39-43.

Zang, Y. and Y. Sawai. 2015. Diatoms. In *Handbook of sea level research* (Shennnan, I., Long, A.J. and B.P. Horton, eds.). Hoboken, NJ: John Wiley and Sons, Ltd.: 66-82.

APPENDIX A

Sediment sieving results for samples both dry sieved and by laser granulometer

Sieve (um)	LRA8 (% weight)	LRA7 (% weight)	LRA4 (% weight)	LRA2 (% weight)	LRA1 (% weight)
13200	0.0	0.0	2.0	0.0	0
11200	0.0	0.0	0.0	0.0	0
9500	0.0	0.0	0.0	0.0	0
8000	0.0	0.0	0.0	0.0	0
6700	0.0	0.0	11.0	1.5	0
5600	0.0	0.0	0.0	0.0	0
4750	0.0	0.0	0.0	0.0	0
4000	0.0	0.0	7.0	4.5	0
3350	0.0	0.0	0.0	0.0	0
2800	0.0	0.0	0.0	0.0	0
2360	0.0	0.0	0.0	0.0	0
2000	3.5	5.5	13.0	20.0	3.5
1700	1	1	3.5	9.5	1
1400	1	1.5	4.0	9.5	1
1180	1.5	1.5	4.0	10.0	1
1000	2	2	4.0	9.0	1
850	2	2	3.5	7.0	1
710	4.5	4	5.0	7.0	1.5
600	5.5	4.5	4.0	4.0	1.5
500	17.5	16	10.5	4.0	7
425	12.5	12.5	6.0	5.5	8
363.08	9.188	12.133	1.0	2.0	10.98
316.23	8.618	10.758	4.5	1.0	11.98
275.42	7.469	8.592	4.5	1.0	11.92
239.88	5.934	6.074	3.5	1.0	10.81
208.93	4.311	3.744	1.5	0.0	8.89
181.97	2.792	1.881	1.5	1.0	6.60
158.49	1.592	0.677	1.5	0.0	4.30
138.04	0.753	0.070	0.5	1.0	2.40
120.23	0.291	0.000	0.0	0.0	1.03
104.71	0.124	0.000	0.0	0.0	0.22
91.20	0.154	0.000	0.0	0.0	0.00
79.43	0.278	0.034	0.0	0.0	0.00
69.18	0.414	0.273	0.0	0.0	0.00
60.26	0.510	0.388	0.0	0.0	0.00
52.48	0.545	0.436	0.0	0.0	0.04
45.71	0.526	0.421	0.0	0.0	0.19
39.81	0.469	0.368	0.0	0.0	0.26
34.67	0.397	0.302	0.0	0.0	0.28
30.20	0.328	0.244	0.0	0.0	0.25
26.30	0.274	0.204	0.0	0.0	0.21

Sieve (um)	LRA8 (% weight)	LRA7 (% weight)	LRA4 (% weight)	LRA2 (% weight)	LRA1 (% weight)
22.91	0.239	0.187	0.0	0.0	0.16
19.95	0.223	0.186	0.0	0.0	0.11
17.38	0.218	0.196	0.0	0.0	0.09
15.14	0.218	0.208	0.0	0.0	0.09
13.18	0.219	0.217	0.0	0.0	0.09
11.48	0.216	0.219	0.0	0.0	0.11
10.00	0.209	0.214	0.0	0.0	0.12
8.71	0.197	0.203	0.0	0.0	0.13
7.586	0.182	0.188	0.0	0.0	0.13
6.607	0.167	0.172	0.0	0.0	0.13
5.754	0.151	0.157	0.0	0.0	0.12
5.012	0.137	0.145	0.0	0.0	0.11
4.365	0.125	0.134	0.0	0.0	0.10
3.802	0.115	0.125	0.0	0.0	0.10
3.311	0.105	0.117	0.0	0.0	0.08
2.884	0.096	0.108	0.0	0.0	0.05
2.512	0.086	0.100	0.0	0.0	0.05
2.188	0.076	0.089	0.0	0.0	0.02
1.905	0.066	0.055	0.0	0.0	0.00
1.660	0.044	0.049	0.0	0.0	0.00
1.445	0.026	0.007	0.0	0.0	0.00
1.259	0.000	0.000	0.0	0.0	0.00
1.096	0.000	0	0.0	0.0	0

Sediment grain size distribution results for samples only processed with the laser granulometer

Sieve (um)	CROW3 SED2 (% weight)	CROW3 SED2 (% weight)	CROW3 SED4 (% weight)	CROW3 SED1 (% weight)	CROW3 S10 (% weight)	KGP SED1 (% weight)	KGP SED9 (% weight)
2187.762	0	0	0	0	0	0	0
1905.461	0	0	0.019066	0	0	0	0
1659.587	0	0	0.029708	0	0	0	0
1445.440	0	0	0.055142	0	0	0	0
1258.925	0	0	0.06561	0	0	0	0
1096.478	0	0	0.073743	0	0	0	0
954.993	0	0	0.07575	0	0.0401	0.026103	0
831.764	0	0	0.073132	0.0796	0.2733	0.164684	0.009855
724.436	0	0	0.066177	0.29501	0.7006	0.396147	0.150476
630.957	0	0	0.084028	0.75835	1.1615	0.618603	0.417042
549.541	0	0	0.150944	1.33212	1.7235	0.872705	0.606461
478.630	0	0.071739	0.311404	2.085	2.3167	1.113105	0.801712
416.869	0.040153	0.755614	0.635778	2.9569	2.9157	1.328471	0.960261
363.078	0.593581	1.786773	1.174413	3.88493	3.4668	1.501656	1.081203
316.228	1.511688	3.197774	1.974235	4.80605	3.9402	1.634974	1.160239
275.423	2.861772	4.810059	3.018025	5.62607	4.298	1.73681	1.201292
239.883	4.578865	6.478557	4.279652	6.29575	4.5342	1.829542	1.219035
208.930	6.463738	7.94108	5.626387	6.75242	4.6459	1.932545	1.232877
181.970	8.331478	9.031158	6.9547	6.98685	4.6535	2.065971	1.264785
158.489	9.85527	9.570616	8.065609	6.99336	4.5824	2.231597	1.330635
138.038	10.831309	9.51944	8.841917	6.79144	4.4575	2.425718	1.439623
120.226	11.06927	8.918243	9.154781	6.41633	4.305	2.623208	1.585448
104.713	10.539161	7.878193	8.971145	5.89789	4.1383	2.804237	1.760366
91.201	9.347383	6.592315	8.327272	5.28951	3.9715	2.943852	1.946532
79.433	7.681697	5.222783	7.313647	4.62473	3.8061	3.031878	2.133724
69.183	5.828549	3.948209	6.087943	3.95471	3.6437	3.064151	2.308456
60.256	4.02612	2.863477	4.792717	3.30712	3.4778	3.04738	2.465908
52.481	2.491054	2.02975	3.576963	2.71437	3.3034	2.993798	2.601599
45.709	1.330019	1.441443	2.533914	2.19048	3.1132	2.917357	2.715569
39.811	0.570495	1.062509	1.718171	1.74475	2.9035	2.831098	2.808124
34.674	0.169125	0.837076	1.137105	1.37789	2.6738	2.744576	2.879986
30.200	0.012217	0.706722	0.761105	1.08321	2.4268	2.663322	2.932517
26.303	0.02242	0.624992	0.54566	0.85414	2.1714	2.59073	2.966616
22.909	0.123932	0.558884	0.435638	0.6779	1.9145	2.526171	2.983408
19.953	0.220812	0.492983	0.385281	0.54624	1.6696	2.468733	2.982734
17.378	0.270847	0.421935	0.357926	0.44695	1.4411	2.414424	2.963871
15.136	0.277062	0.350425	0.332522	0.37343	1.2398	2.360898	2.926167
13.183	0.244094	0.282896	0.298987	0.31694	1.0642	2.303706	2.867974
11.482	0.189977	0.226596	0.25783	0.27377	0.9192	2.242362	2.791508
10.000	0.130681	0.183049	0.212357	0.23898	0.7987	2.174448	2.696998
8.710	0.083649	0.154014	0.169868	0.21135	0.7034	2.103071	2.592034

Sieve (um	CROW3 SED2 (%weight)	CROW3 SED2 (% weight	CROW3 SED4 (% weight)	CROW3 SED1 (% weight)	CROW3 S10 (% weight)	KGP SED1 (% weight)	KGP SED9 (% weight)
5.012	0.006938	0.125622	0.08424	0.14432	0.4782	1.816195	2.174018
4.365	0.032158	0.125663	0.08155	0.13487	0.445	1.752548	2.094193
3.802	0.046172	0.124676	0.081409	0.12681	0.4163	1.691769	2.026858
3.311	0.049773	0.122159	0.080649	0.11926	0.3902	1.630686	1.967982
2.884	0.04767	0.118196	0.079605	0.11164	0.3658	1.566472	1.91266
2.512	0.046091	0.113198	0.073821	0.10357	0.3421	1.495514	1.854282
2.188	0.042333	0.107714	0.051388	0.09503	0.3183	1.414961	1.78641
1.905	0	0.102321	0.047513	0.0863	0.2938	1.323359	1.704132
1.660	0	0.097602	0.025873	0.0782	0.2685	1.221197	1.60578
1.445	0	0.09419	0.019996	0.07045	0.2432	1.113294	1.495724
1.259	0	0.092064	0.020264	0.0685	0.2185	1.003982	1.379177
1.096	0	0.091453	0.019579	0.05162	0.1957	0.900114	1.264464
0.955	0.019315	0.088838	0.954993	0	0.0404	0.174776	0.803194
0.832	0.021391	0.088737	0.831764	0	0.0442	0.156326	0.716145
0.724	0.012834	0.080218	0.724436	0	0.0254	0.139427	0.635457
0.631	0	0.063344	0.630957	0	0	0.123873	0.560666
0.550	0	0.013601	0.549541	0	0	0.108291	0.486266
0.479	0	0	0.47863	0	0	0.092598	0.411988
0.417	0	0	0.416869	0	0	0.076126	0.334063
0.363	0	0	0.363078	0	0	0.04795	0.252876
0.316	0	0	0.316228	0	0	0	0.175819
0.275	0	0	0.275423	0	0	0	0.08102
0.240	0	0	0.239883	0	0	0	0.018079
0.209	0	0	0.20893	0	0	0	0

APPENDIX B

Examples of Diatoms, Testate Amoebae and Sponge Spicules

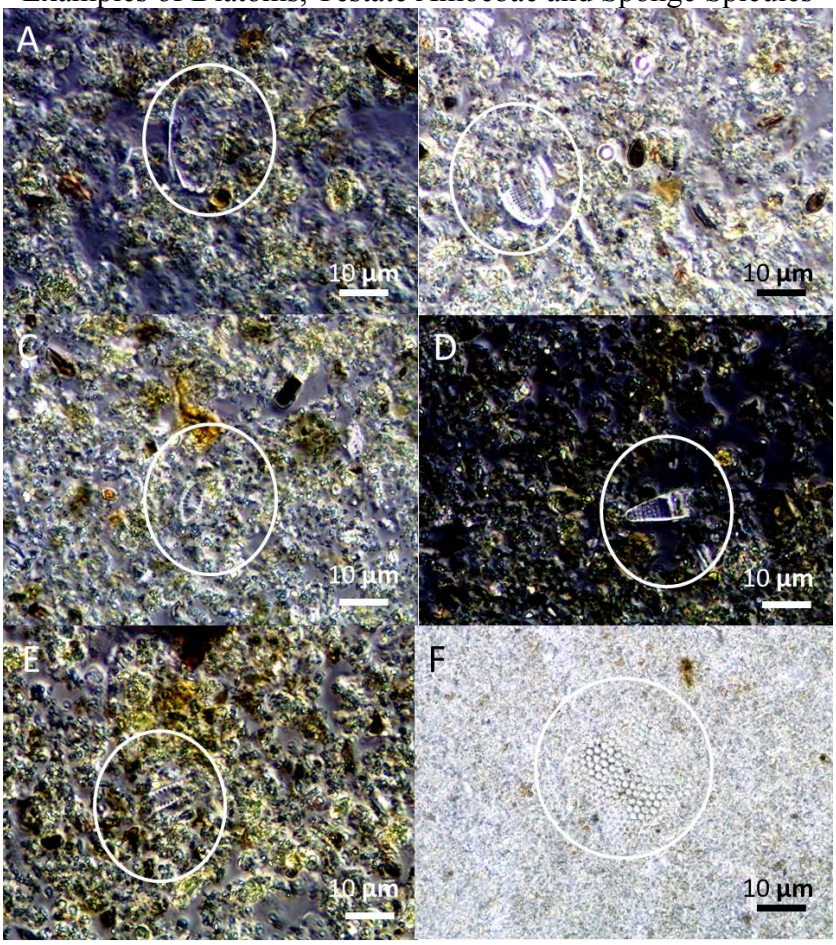

Protists from site CROW3: A) SED 1 testate Amoebae – *Euglypha rotunda*, B) SED1 diatom – *Cocconeis californica,* C) SED1 diatom - *Achnanthese delicatula*, D) SED3 diatom - *Plagiogramma staurophorum*, E) SED3 diatom – *Tabularia tabulata*, F) S10 diatom - *Coscinodiscus*

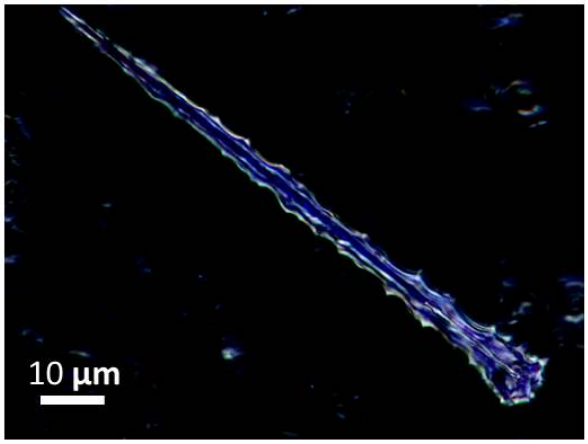

Sponge Spicule from KGP 478 cm dbd